DISSERTATION

submitted to the

Combined Faculties for the Natural Sciences and for Mathematics
of the Ruperto-Carola University of Heidelberg, Germany

for the degree of

Doctor of Natural Sciences

Put forward by

CHRISTIAN DÖRING

Born in Meschede-Eversberg

Date of oral examination: 3. November 2021

Impact Of Gravitational Waves From First-Order Phase Transitions On Structure Formation

1st Referee: Prof. Dr. Dr. h.c. Manfred Lindner

2nd Referee: Prof. Dr. Jörg Jäckel

Abstract

In this thesis we investigate the possibility that gravitational waves emitted from a first-order phase transition exhibit enough power to alter or generate fluctuations in the primordial plasma of the early universe and in turn imprint new features into the matter power spectrum. We approach this task by performing a second order perturbative expansion of two coupled non-linear equations that monitor the evolution of energy density gradients in the 1+3 covariant formulation of cosmology. As a result, we find that adiabatic density fluctuations at second order can be generated from inhomogeneities in the gravitational wave energy density on sub-horizon scales. We interpret these fluctuations as baryon acoustic oscillations seeded by gravity radiation and derive their transferfunction to study their impact on the matter power spectrum. Strength and scale of the imprinted signatures depend on three phase transition parameters, namely the latent heat, the duration and the time at which gravitational waves are released. The amplitude of the signatures is limited by the cosmic variance bound on the matter power spectrum. We use this constraint to deduce limits for these three parameters and translate them into a new exclusion region for the relic stochastic gravitational wave background today. Finally, we discuss our results in the context of first-order phase transitions occurring in particle models.

Zusammenfassung

In dieser Arbeit untersuchen wir die Möglichkeit, ob Gravitationswellen, die von Phasenübergängen erster Ordnung erzeugt wurden, stark genug sind, Fluktuationen im primordialen Plasma zu verändern oder zu erzeugen und dadurch neue Merkmale im Materie-Leistungsspektrum zu hinterlassen. Dazu führen wir an zwei gekoppelte, nichtlineare Gleichungen, welche die Entwicklung von Energiedichtegradienten in der 1+3 kovarianten Formulierung der Kosmologie beschreiben, eine störungstheoretische Rechnung in zweiter Ordnung durch. Das Ergebnis zeigt, dass adiabatische Dichtefluktuationen in zweiter Ordnung von Inhomogenitäten in der Gravitationswellenenergiedichte auf sub-Horizont Skalen erzeugt werden können. Wir interpretieren diese Fluktuationen als von Gravitationswellen hervorgerufene baryonische, akustische Oszillationen und bestimmen ihre Transferfunktion, um ihre Auswirkung auf das Materie-Leistungsspektrum zu untersuchen. Stärke und Skala der Signaturen hängt von drei Parametern des Phasenüberganges ab, nämlich der latenten Hitze, der Dauer und der Zeit, zu welcher die Gravitationswellen erzeugt wurden. Die Amplitude dieser Spuren ist beschränkt durch die kosmische Varianz des Materie-Leistungsspektrums, die wir benutzen, um Grenzwerte für die drei Parameter zu ermitteln. Anschließend werden diese neuen Ausschlussbereiche für den heutigen stochastischen Gravitationswellenhintergrund übersetzt. Schließlich diskutieren wir unsere Ergebnisse im Kontext von Phasenübergängen erster Ordnung, die in Teilchenmodellen auftreten.

Publication List

During the course of the doctoral studies the author has undertaken research in a wide variety of fields. To avoid a topical divergence, this thesis is based only on the recently uploaded paper [5], which is currently going through the peer-review process. The publication list encompasses the following works and covers the following fields:

- Two articles [1, 3] in peer reviewed journals on dark matter direct detection. One of the works was started during the author's Master thesis but completed and published in the first year of the doctoral studies.
- Investigation of a neutrino beam model for core-collapse supernovae involving all three flavors [6]; peer reviewed.
- One peer reviewed article studying an axion-dark matter model that simultaneously explains the fermion mass hierarchy [4].
- A peer-reviewed mathematical article [2] presenting an algorithm that finds an unitary matrix that simultaneously transforms a set of given unitary matrices to their given block diagonal form.

Yet unpublished work: Aside from the above mentioned papers, the author spent significant time on two ongoing research projects in collaboration with Ingolf Bischer and Andreas Trautner that are expected to be published soon, both of which concern the study of outer automorphisms as charge-parity transformations.

Each work has been done in collaboration with others.

[1] G. Arcadi, C. Döring, C. Hasterok, and S. Vogl. Inelastic dark matter nucleus scattering. *JCAP*, 12:053, 2019.

[2] Ingolf Bischer, Christian Döring, and Andreas Trautner. Simultaneous Block Diagonalization of Matrices of Finite Order. *J. Phys. A*, 54(8):085203, 2021.

[3] Riccardo Catena, Jan Conrad, Christian Döring, Alfredo Davide Ferella, and Martin B. Krauss. Dark matter spin determination with directional direct detection experiments. *Phys. Rev. D*, 97(2):023007, 2018.

[4] Salvador Centelles Chuliá, Christian Döring, Werner Rodejohann, and Ulises J. Saldaña Salazar. Natural axion model from flavour. *JHEP*, 09:137, 2020.

[5] Christian Döring, Salvador Centelles Chuliá, Manfred Lindner, Bjoern Malte Schaefer, and Matthias Bartelmann. Gravitational wave induced baryon acoustic oscillations. 7 2021.

[6] Christian Döring, Rasmus S. L. Hansen, and Manfred Lindner. Stability of three neutrino flavor conversion in supernovae. *JCAP*, 08:003, 2019.

Acknowledgments

First of all, I owe a great gratitude to my supervisor Prof. Dr. Dr. h.c. Manfred Lindner for accepting me as a PhD student although I almost hadn't had any knowledge in particle physics when I applied. His trust in my ability to learn new topics was always encouraging to me. Especially, I would also like to thank him for the possibility to take part in many summer schools and conferences where I met many remarkable people, some of whom became good friends. It has been a great pleasure to be part of his group at the Max-Planck-Institut für Kernphysik.

Furthermore, I would like to thank Prof. Dr. Jörg Jäckel for many illuminating discussions on axions and phase transitions and for agreeing to review this thesis as second referee. Likewise, I am grateful to Prof. Dr. Björn Malte Schäfer and JProf. Dr. Loredana Gastaldo for being part of my doctoral committee.

A special thank also goes to Prof. Dr. Matthias Bartelmann and Prof. Dr. Björn Malte Schäfer for their extreme expertize and incredible patience in many discussions during a crazy year of a global pandemic. Without you this work would not have been what it has become. I would like to thank Björn for the instructive time as his assistant in statistical mechanics.

Over the years I had the privileged to work with many skilled postdocs who also became good friends. I own a special thank to Rasmus Sloth Lundkvist Hansen, Stefan Vogl, Kai Schmitz and Andreas Trautner. I learned so much from you guys about good research and paper writing that I am simply very grateful for. Especially, I want to thank Kai Schmitz for the time he took in teaching me fundamentals in astro-particle physics during the initial phase of my doctoral studies. In addition I'd like to thank all my collaborators for the fruitful cooperation.

Moreover, I want to thank my friend Salva Centelles Chuliá with whom I enjoyed many summer schools, discussed the benefits of a country not being run by a government in a long time (Spain) and who is also a great collaborator.

During my time at the university I was accompanied by a group of cool people. I deeply thank my Göttinger gang for going together through hard and funny times with me over the last years and for being such good and close friends. I am looking forward to what is coming ahead of us! For insightful physics discussions a special thanks goes to Hauke and Masl.

I am also indebted to my friends Elias Most and Thorsten Hertl for many, many discussions ranging from mathematics to physics, always while enjoying a piece of cake, in cities everywhere in Germany and certainly soon elsewhere.

No PhD time would be a good time without the people you spent it with. I am very grateful for the amazing time we had together in the Party-Büro and the many hours of discussions, trips and parties! Thanks to my Sundays-walk mate Thomas Rink, my Rhine river chill mate Ingolf Bischer, my excursion mate Moritz Platscher and the always positive Oliver Scholer, Carlos Jaramillo and Thomas Hugle. I also wanna thank all the people that were part of the group during the past years, especially Susan van der Woude,

Christiane Klein, Cristina Benso, Miguel Campos, Helena Almazán Molina, Christian Roca, Veronica Pizzella, Yannick Emonds, Jackob Stegemann and Valentin Tenorth. Also I want to thank Alexei Smirnov and Evgeny Akhmedov for sharing their enormous knowledge with us students and for many funny and often historical anecdotes.

This thesis benefited from great correctors. I thank Thomas Hugle, Thomas Rink, Ingolf Bischer, Susan van der Woude, Oliver Scholer, Moritz Platscher, Philipp Saake and Carlos Jaramillo.

Finally, I want to thank my family and friends beyond physics, especially my mum Waltraud Döring and my sister Nicola Döring for their love and incredible life-long support in any situation. Lastly, I want to thank my late father Dr. Wolfgang Döring who paved the way for me into natural science.

In Gedenken an meinen Vater
Dr. rer. nat. Wolfgang Döring (25.1.1951-31.8.2009)

Contents

List of Figures

List of Tables

Acronyms

ΛCDM Cosmological Standard Model.

2dfGRS 2-degree Field Galaxy Redshift Survey.

BAO Baryon Acoustic Oscillations.

BBN Big Beng Nucleosynthesis.

CMB Cosmic Microwave Background.

DM Dark Matter.

EW Electroweak.

FLRW Friedman-Lemaître-Robertson-Walker.

FOPT First-Order Phase Transition.

GR General Relativity.

GW Gravitational Wave.

LHC Large Hadron Collider.

QCD Quantum Chromo Dynamics.

SDSS Sloan Digital Sky Survey.

SM Standard Model of Particle Physics.

SSB Spontaneous Symmetry Breaking.

SUSY Super Symmetry.

VEV Vacuum Expectation Value.

Chapter 1

Introduction

"The Starry Night" by Vincent van Gogh.
From [7] - ©Public Domain.

"Ich betrachtete nur das, was mir das Universum zeigte."— Claude Monet[a]

[a]*14.11.1840-†5.12.1926 [8].

The painting "The Starry Night" by Vincent van Gogh[1] is one of the most famous examples for the inspiring nature of the night sky to humankind. Certainly, one reason for the remarkable effect of the picture is caused by the structures created from the brush work that complements the arrangement of objects like clouds, the moon and stars. While van Gogh could only observe these small scale structures on the sky, today the objects we can describe range from galaxies to nebula's and quasars. With an ever deeper gaze into space, we have gained an ever deeper insight into the nature of these objects but also an understanding of their distribution. Remarkably, as sky surveys have measured, most of the matter is organized in a web-like structure where galaxies and

[1]*30.3.1853-†29.7.1890 [9].

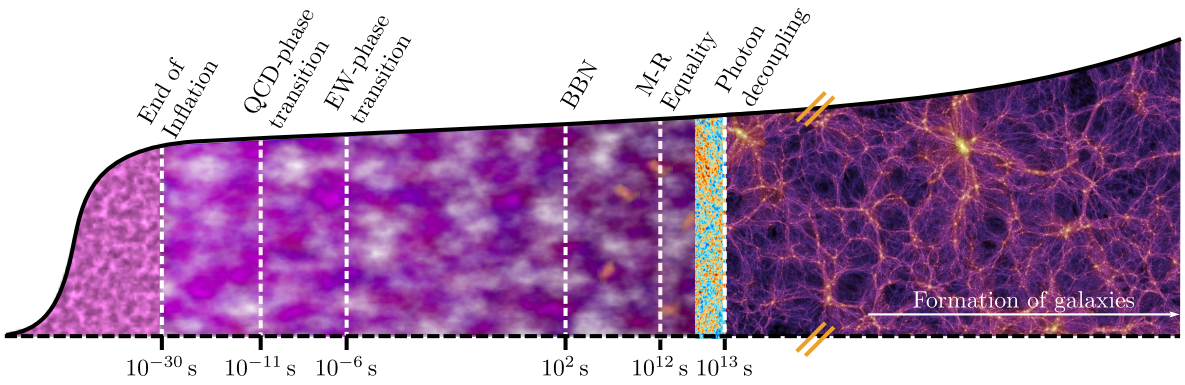

Figure 1.1.: The history of the universe according to current theory. Shown are some of the most important events with a special focus on the two phase transitions. The graphic is inspired by [13, 14] and uses parts of pictures from Planck [15] and the Millennium Simulation [16, 17].

clusters of galaxies are arranged in huge halos and filaments enclosing large empty voids [10–12] and therefore draw a very different picture of the night sky, see right part of Fig. 1.1. The origin of the structure relies on the two pillars of fundamental physics today, namely the Standard Model of Particle Physics (SM) and the Cosmological Standard Model (ΛCDM). With the detection of the Higgs particle [18] by the Large Hadron Collider (LHC) [18–20] the particle family of the SM [21–23] is very much complete. The rise of the ΛCDM on the other hand began with the measurement of the Cosmic Microwave Background (CMB) [24–26] and its capability to explain this earliest snapshot of the universe drawn from temperature fluctuations in the oldest photons to a very high accuracy [15, 27]. These two pillars allow us to reconstruct the history of the universe (Fig. 1.1) and reproduce the emergence and evolution of the large scale structure we observe today [28, 29] from small initial perturbations in the primordial soup.

However, tests from new (observational) perspectives of these two concepts are in dire need, as until now both theories still evaded any attempt to unfold some of their greatest remaining mysteries by our classical methods: Despite many experimental efforts (see e.g. [30]) the origin of Dark Matter (DM) [31] still remains unrevealed though it is an essential ingredients of the ΛCDM and its existence is supported by many observational hints including galaxy rotation curves [32], gravitational lensing [33] and the synthesis of light elements during Big Beng Nucleosynthesis (BBN) [34, 35]. The nature of dark energy poses a similar puzzle [36] which makes up 70% [15, 27] of the energy budged of our universe and has been found to cause the accelerated expansion of the cosmos [37, 38]. Due to these and many other open issues, physicists opened the hunt for physics beyond the SM to tackle the intertwined challenges both fundamental theories still flaw.

From the experimental side an ever increasing arsenal of technical instruments and methods has been developed to circle the secrets of the universe from new perspectives. Most prominently, the newest of them are Gravitational Wave (GW) interferometers such as the LIGO-VIRGO collaboration [39, 40] which in 2015, for the first time, directly measured a GW signal from a black hole binary merger [41]. Until then only indirect

hints for the existence of GWs had been found [42]. Not only do these detectors provide a new channel to the cosmos but they also complement our present instruments based on electromagnetic signals as the famous observation of merging neutron stars [43, 44] in both channels has proven.

Beyond the astrophysical sources that have been explored so far the aim for the future is to extend GW searches also to signals potentially arising from the birth and early childhood of the cosmos. This offers the possibility to look beyond the CMB and therefore opens a new window to explore fundamental physics. A number of earth- and space based experiments are under consideration to tackle this challenge, such as LISA [45], ETH [46, 47], DECIGO [48] and BBO [49]. Meanwhile, efforts are also invested to detect indirect effects caused by the stochastic waves in the pulsation period of pulsars [50–53] which recently attracted some attention when one of the timing pulsar arrays – NANOGrav – reported deviations from background [54]. By their ability to look beyond the current limits GW experiments have the potential to probe the fundamentals of physics and draw a renewed picture of the cosmos.

One of the earliest possible process that is capable to generate a relic stochastic background of gravitational radiation is inflation, see e.g. Refs. [55–58] where they arise from vacuum fluctuations of the gravitational field. In recent years, however, the possible occurrence of a First-Order Phase Transition (FOPT) during the evolution of the universe and its potential as a seed for gravity radiation has gained rising attention. FOPTs are a special type of phase transitions in which the phase changes discontinuously and is initially taken on at random locations by the formation of vacuum bubbles instead of a smooth transition. The motion through the plasma and their collision emits GWs. In cosmology these transitions can occur when particles acquire non-zero masses by Spontaneous Symmetry Breaking (SSB). However, to current knowledge neither the Electroweak (EW) [19, 20] nor the Quantum Chromo Dynamics (QCD) phase transition [59] in the SM are of first order (see Fig. 1.1 for chronological context). Therefore, one extensively investigates the nature of transition in models beyond the SM, see e.g. [60–69]. While these models primarily seek to provide explanations for DM, the masses of neutrinos and other SM puzzles, the possibility of GW production offers a promising and complementary way to test if the involved symmetry breaking occurs via a FOPT. Beyond the measurement of GWs as messengers from early exotic physics the presence of bubbles can also have direct effects. For example, the environment close to the bubble walls can fulfill the Sakharov conditions [70] and thus lead to the generation of a baryon-asymmetry in the universe [71, 72]. Since a FOPT would constitute a violent event in the life of our universe it potentially may effect further processes directly. This brings us back to the beginning of this paragraph and the question how the structures we observe in the sky today have formed. In our current understanding, the structures emerged from small perturbations in the cosmic fluid seeded by inflation and then evolved according to the laws of the ΛCDM. However, adding events like a FOPT might have affected the formation of structure and therefore might have left imprints in it today. In this work we will address this question using second order cosmological perturbation theory. We will focus on effects induced by GWs emitted from the bubble collisions. If these are strong enough, fluctuations in the early plasma might gain or loose power. In Fig.

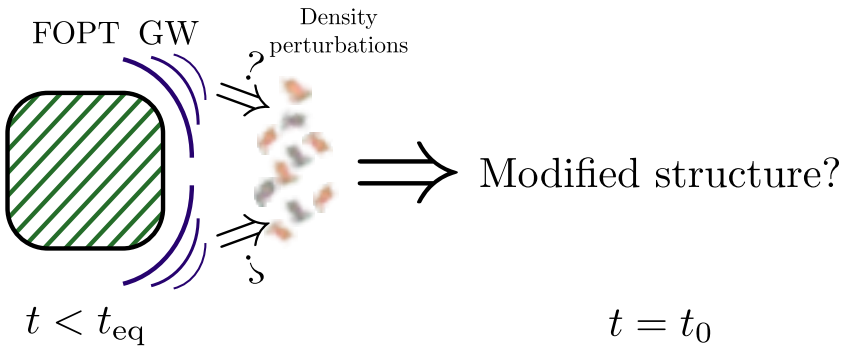

Figure 1.2.: Sketch of the process that is under investigation in this thesis. If a FOPT is triggered by some particle model (hatched box) during the radiation dominated epoch, this results in the generation of GW (blue curved lines). Can these be strong enough to disturb the present plasma fluctuations or even creat additional ones? If yes, how would the formation of structure be affected?

1.2 we have summarized the system that we want to investigate graphically. It should be noted that there had been similar efforts in the literature in the past. For example, Schmid et al. [73–75] pointed out that the QCD phase transition can lead to significant decrease in the speed of sound of preexisting perturbations and hence make them gaining strength as they freely fall. However, in beyond the SM theories it is more likely that the sound speed remains almost constant as long as not too many fermions are involved in the transition [76]. Another example is Ref. [77] in which direct effects on the collapse time of perturbations have been considered but also effects due to GWs are discussed. However, in both references the transition occurs during the matter dominated era.

The thesis is structured into three segments each containing two chapters: In the first part we discuss and summarize the foundations upon which our work is built. In chapter 2 we review two different approaches to cosmological perturbation theory, namely the standard Bardeen formalism based on space-time slicing and the 1+3 covariant viewpoint originating from space-time threads. Chapter 3 then addresses the dynamics of FOPTs in the early universe triggered in particle models and the succeeding generation of GWs. If and how these two processes interact is the quest we pursue in the second part of this work. Therefore, we perform in chapter 4 a perturbative expansion to second order of the non-linear equations of motions for density gradients obtained in the 1+3 covariant framework. In chapter 5 the resulting equation is adapted to the environment of generic FOPTs such that we eventually can draw conclusions about the consequences for the formation of structure induced by the generated GWs. With our findings we constrain the strength and duration of FOPTs which should not be in conflict with the cosmic variance limit of the linear matter power spectrum. In the next part the first chapter 6 is devoted to the evaluation of the obtained results and includes a critical discussion of the assumptions made as well as an outlook about potentially future work. Finally, in chapter 7 we summarize and conclude. Additional information and subsidiary material are listed in the appendix.

Tools: In this work we used Python [78] Mathematica [79] and Inkscape [80].

Part I

Foundations

Chapter 2

Cosmological Perturbation Theory

Linear perturbation theory is the standard tool to investigate the formation of structure in the early life time of the universe. In the first part of this chapter we present the formalism developed by Bardeen [81] upon which most works in the recent years are based on. Thereby, we follow closely Refs. [82, 83]. The variance of perturbations as a function of length scale is measured by the matter power spectrum and we are guided by Refs. [82, 84] to review it's definition and main features. At the end of this chapter we introduce the 1+3 covariant approach to linear perturbation theory, which provides geometrical quantities that are naturally gauge invariant at linear order. The discussion is tightly aligned with two reviews on the topic and the present author's recent paper [5, 85, 86].

Looking at the world surrounding us, at the first glance it seems pretty oversimplified and even presumptuous to claim a *homogeneous*[1] and *isotropic*[2] Universe. No one would do so for the solar system nor for our local group. Nonetheless, this so called *Cosmological principle* [88] is a long-standing pillar of cosmology and for most of the time was based on the *Copernican principle*, which was developed in the 1960's when the cosmologist Hermann Bondi initiated the idea that the Earth and our solar system is not a special, not a distinct place from any other in the Universe. Today, a number of surveys like the Sloan Digital Sky Survey (SDSS) [89], the 2-degree Field Galaxy Redshift Survey (2dfGRS) [10] and the measurement of the CMB by COBE [24] have concluded that on scales of $\sim 100\,\mathrm{Mpc}$ and bigger, which roughly corresponds to the sice of superclusters[3], the assumptions of isotropy and homogeneity are reasonably well fulfilled [90, 91].

On these large scales gravity is certainly the by far dominating force and thus Albert Einstein's theory of General Relativity (GR) is the tool to develope a cosmological model. For reasons that will become apparent later, let us review some details of the construction of cosmology. Consider spacetime $(\mathcal{M}, g)$ as a four-dimensional, pseudo-Riemannian manifold $\mathcal{M}$ accompanied by a metric $g_{\mu\nu}$. To form the spacetime $(\mathcal{M}, g)$ to a cosmological model, it must obey the two symmetries discussed in the previous paragraph. The translation of homogeneity to the language of Riemannian differential geometry slices the manifold into 3-dimensional layers that are threaded along the time line. The time t, called cosmic time, is a parameter that lables each hypersurfaces $\Sigma_t = \{\mathbf{x}|(t, \mathbf{x}) \in \mathcal{M}\}$ and we call the orientation of the vector u^μ that is tangent to the world line of a fundamental observer the direction of time [83, 92]. Isotropy then implies that these spacelike hypersurfaces are maximally symmetric and for each time-point t the respective spacelike hypersurface is also perpendicular to the world lines' tangent vector u^μ [83]. These properties fix the form of the spacetime manifold to $\mathbb{R} \times \Sigma_t$. In comoving spherical coordinates $x^\mu = (x^0, x^1, x^2, x^3) = (t, r, \Theta, \phi)$ on the spatial hypersurfaces the metric $g_{\mu\nu}$ takes the form [93]

$$\mathrm{d}s^2 := g_{\mu\nu}\mathrm{d}x^\mu \mathrm{d}x^\nu = -\mathrm{d}t^2 + a^2(t)\left[\frac{\mathrm{d}r^2}{1 - Kr^2} + r^2\mathrm{d}\Omega^2(\phi, \Theta)\right], \tag{2.1}$$

which is the well-known Friedman-Lemaître-Robertson-Walker (FLRW) [94–97] metric, named after A. Friedmann, G. Lemaître, H. P. Robertson and A. Walker. The curvature constant of the spacelike hypersurface K is usually normalized such that it takes the values $K = -1$ for an *open* universe with hyperbolic spatial geometry, $K = 0$ for a *flat* universe with Euclidian spatial geometry and $K = +1$ for a *closed* universe with the geometry of the three-sphere. All time dependence of the spatial part of the metric is condensed in the scale factor $a(t)$. The concrete form of this function depends on the

[1] Homogeneity means, that their is no prominent position in the Universe at any given time.

[2] Isotropy means, that there is no outstanding direction in the Universe. Or as S. Weinbergs [87] states it a bit more precise:

"[...] the Universe seems the same in all directions to a family of "typical" freely falling observers."

[3] See, e.g. the very nice introductory discussion in Barbara Ryden's book [84].

last ingredients needed, namely the field content of the universe. The equations that determine the dynamics of the universe by an interplay of geometry and physical fields are Einstein's field equations [98, 99]

$$R_{\mu\nu} - \frac{1}{2}Rg_{\mu\nu} = 8\pi G T_{\mu\nu} + \Lambda g_{\mu\nu}\,. \tag{2.2}$$

Here $R_{\mu\nu}$ is the Ricci tensor and R is the Ricci scalar which are both derived from the metric tensor $g_{\mu\nu}$. On the right hand side we have the cosmological constant Λ and the energy-momentum tensor $T_{\mu\nu}$. Due to the space-time symmetries the latter takes on the form of the energy-momentum tensor of a perfect fluid with energy density $\rho(t)$ and pressure $p(t)$ [100], namely

$$T_{\mu\nu} = (\rho + p)\, u_\mu u_\nu + p g_{\mu\nu}. \tag{2.3}$$

Plugging this energy-momentum tensor into Einstein's field equations Eq. (2.2) leads to equations that govern the dynamics of the scale factor - the *Friedmann equations* [94, 101] (see e.g. Ref. [102])

$$\dot{H} = -H^2 - \frac{8\pi G}{6}(\rho + 3p) + \frac{1}{3}\Lambda\,, \tag{2.4}$$

$$H^2 = \frac{8\pi G}{3}\rho - \frac{K}{a^2} + \frac{1}{3}\Lambda\,, \tag{2.5}$$

where $H(t) := \dot{a}/a$ is the Hubble parameter. Additionally, momentum energy conservation $\nabla^\nu T_{\mu\nu} = 0$ demands

$$\dot{\rho} = -3H(\rho + p). \tag{2.6}$$

The fluid type is specified by the *equation of state* $\rho(t) = \omega\, p(t)$ where $\omega = 1/3$ stands for radiation, $w = 0$ for (dark) matter and $w = -1$ for dark energy. The expansion rate at any time can then be determined from Friedmann Eqs. (2.4) and (2.5) and the composition of the total cosmic fluid via

$$H^2(a) = H_0^2 \sqrt{\sum_i \frac{\Omega_i(t_0)}{a^{3(1+\omega_i)}}}\,, \tag{2.7}$$

where $\Omega_i(t) := \rho_i/\rho_{\rm crit}$ is the dimensionless density parameter of the $i^{\rm th}$ species and $\rho_{\rm crit}(t) := \frac{3H^2(t)}{8\pi G}$ is the cirtical density.

2.1. Linear perturbation theory

The emergence of structure in the universe requires a departure from a perfectly homogeneous and isotropic universe. Therefore, one studies small perturbations on this background [103] which evolve after being seeded during inflation. The "standard" for-

malism used today was introduced by Bardeen [81] but in this work we will make use of a different approach mainly developed by Marco Bruni, George F. R. Ellis, Peter K. S. Dunsby and different coauthors [104]. In the standard relativistic treatment of perturbations it has become common to work in conformal time η and express the time derivative $f' := \mathrm{d}f/\mathrm{d}\eta = a\,\mathrm{d}f/\mathrm{d}t$ with respect to it. In contrast, the literature using the "Bruni-Ellis-Dunsby" approach prefers to use the cosmic time derivative $\dot{f}$. Throughout this work we will stick to the respective convention of the literature.

2.1.1. Bardeen formalism

Perturbation theory requires two space-time manifolds. The first one is called the background manifold $\mathcal{M}_b$. It is homogeneous and isotropic and therefore equipped with the FLRW metric $g^{(0)}_{\mu\nu}$. The other space-time manifold $\mathcal{M}_p$ carries the metric $g_{\mu\nu}$ and is slightly perturbed compared to the latter one. If the deviation from the background is small, then we can decompose the metric $g_{\mu\nu}$ into the background and a small perturbation $g^{(1)}_{\mu\nu} =: \delta g_{\mu\nu}$, such that[4]

$$g_{\mu\nu} = g^{(0)}_{\mu\nu} + \delta g_{\mu\nu}\,. \tag{2.8}$$

On the perturbed space-time the decomposition is adopted by the Einstein tensor $G_{\mu\nu} := R_{\mu\nu} - \frac{1}{2}Rg_{\mu\nu}$ and the energy momentum tensor $T_{\mu\nu}$ whose small perturbations $\delta G_{\mu\nu}$ and $\delta T_{\mu\nu}$ linearize the Einstein field equations

$$\delta G_{\mu\nu} = 8\pi G \delta T_{\mu\nu}\,. \tag{2.9}$$

Famously, this equation can be solved in an elegant way by using a parametrization of the two tensors proposed by James M. Bardeen in 1980 [81] and elaborated on by Ref. [105]. In this approach, the metric is decomposed into two scalar variables $A(\eta, x^i)$ (lapse function) and $D(\eta, x^i) = -1/6 \cdot \delta^{ij}\delta g_{ij}$, a vector $\mathbf{B}(\eta, x^i)$ and a tensor $E_{ij}(\eta, x^i)$ with $\delta^{ij}E_{ij} = 0$ and reads for the spatially flat case $K = 0$ [81]

$$\begin{aligned} &\mathrm{d}s^2 = a^2(\eta)\left\{-(1+2A)\,\mathrm{d}\eta^2 - B_i\,\mathrm{d}\eta\,\mathrm{d}x^i + [(1-2D)\delta_{ij} + 2E_{ij}]\,\mathrm{d}x^i\mathrm{d}x^j\right\}, \\ &\text{or}: \quad g_{\mu\nu} = g^{(0)}_{\mu\nu} + \delta g_{\mu\nu} = a^2\left[\eta_{\mu\nu} + \begin{pmatrix} -2A & -B_i \\ -B_i & -2D\delta_{ij} + 2E_{ij}, \end{pmatrix}\right], \end{aligned} \tag{2.10}$$

where $\eta_{\mu\nu}$ is the Minkowski metric. On the other side of Einstein's equation, the cosmic ingredients in the energy momentum tensor behave like a fluid, but it doesn't necessarily has to be a perfect fluid. With respect to the fluid four velocity u_μ the energy momentum tensor is written in terms of the fluid energy density ρ, pressure p and anisotropic stress $\Pi_{\mu\nu}$ and reads $T_{\mu\nu} = (\rho + p)u_\mu u_\nu + pg_{\mu\nu} + \Pi_{\mu\nu}$. Inserting into this equation the first

[4] As emphasized before we closely follow Refs. [82, 83] in this subsection.

order expansion of these quantities, i.e.

$$\begin{aligned} \rho(\mathbf{x},t) &= \rho^{(0)}(t) + \delta\rho(\mathbf{x},t)\,, \quad p = p^{(0)}(t) + \delta p(\mathbf{x},t), \\ u_\mu(\mathbf{x},t) &= u^{(0)}_\mu + \delta u^\mu(\mathbf{x},t) \quad \text{and} \quad \Pi_{\mu\nu}(\mathbf{x},t) = \underbrace{\Pi^{(0)}_{\mu\nu}}_{=0} + \Pi_{\mu\nu}(\mathbf{x},t)\,, \end{aligned} \tag{2.11}$$

the linear perturbation $\delta T^\mu{}_\nu$ becomes [81, 105]

$$\delta T^\mu{}_\nu = \begin{pmatrix} -\delta\rho & (\rho^{(0)} + p^{(0)})(v_i - B_i) \\ -(\rho^{(0)} + p^{(0)})v_i & \delta p\,\delta^i{}_j + \Pi^i{}_j \end{pmatrix}. \tag{2.12}$$

Here $v_i := a\,\delta u^i$ denotes the peculiar velocity. Note that the anisotropic stress is absent at zero order and thus we omit the label to mark the linear perturbation. Also note that due to $g_{\mu\nu}u^\mu u^\nu = -1$ the perturbed energy momentum tensor picks up a $\mathbf{B}$ contribution from the parametrization of the perturbed metric. Also, due to the orthogonality of the anisotropic stress tensor to the fluid flow $\Pi_{\mu\nu}u^\mu = 0$ we only need to consider its spatial part.

Isotropy and homogeneity of the background enable us to isolate the scalar, vector and tensor degrees of freedom by splitting the vector $\mathbf{B}$ and the tensor E_{ij} into their $SO(3)$ irreducible components according to the Helmoltz theorem [92, 103]. The vector $\mathbf{B} = \mathbf{B}^\perp + \mathbf{B}^{||}$ divides into a transverse $\nabla\cdot\mathbf{B}^\perp = 0$ part and a longitudinal $\nabla\times\mathbf{B}^{||} = 0$ part that originates from a scalar potential $\mathbf{B}^{||} = -\nabla B$. The tensor E_{ij} splits into three components $E_{ij} = E^\perp_{ij} + E^{||}_{ij} + E^T_{ij}$. The first one can be derived from a vector potential $\mathbf{E}$, the second one from a scalar E and the last one is traceless and transverse.

$$E^{||}_{ij} = (\partial_i\partial_j - \frac{1}{3}\delta_{ij}\nabla^2)E\,, \tag{2.13}$$

$$E^\perp_{ij} = -\frac{1}{2}(\partial_j E_i + \partial_i E_j) \quad \text{with} \quad \nabla\cdot\mathbf{E} = 0\,, \tag{2.14}$$

$$\delta^{il}\partial_l E^T_{ij} = 0 \quad \text{and} \quad \delta^{ij}E^T_{ij} = 0\,. \tag{2.15}$$

In this way tensor, vector and scalar perturbations can be discussed separately. In the following, we will do so by focusing on the scalar ones only.

However, the decomposition into background and small perturbations suffers from the well known *gauge issue*. It states that this decomposition is not unique due to various choosable diffeomorphisms that send a point on the background space-time to some close by point on the perturbed space-time (see, e.g. [82]). To see how such gauge transformations (coordinates transformation) act on tensors like the metric[5] one has to compare a diffeomorphism $f : \mathcal{M}_b \to \mathcal{M}_p$ with a family of diffeomorphisms defined by a vector field ξ^μ and a small parameter ϵ that map $h_\epsilon : \mathcal{M}_b \to \mathcal{M}_b$ such that $x^\mu \to x^\mu + \epsilon\xi^\mu$. Imposing that f and its pullback f^* respect the smallness of the perturbation $\delta g_{\mu\nu} = (f^*g)_{\mu\nu} - g^{(0)}_{\mu\nu}$, i.e. $|\delta g_{\mu\nu}| \ll 1$, the metric transforms under the

[5] This discussion is adapted from [93].

coordinate transformations h_ϵ as

$$\delta g^{[\epsilon]}_{\mu\nu} = [h^*_\epsilon(f^* g)]_{\mu\nu}] - g^{(0)}_{\mu\nu} = h^*_\epsilon(\delta g_{\mu\nu}) + h^*_\epsilon(g^{(0)}_{\mu\nu}) - g^{(0)}_{\mu\nu}\,. \tag{2.16}$$

For infinitesimal $\epsilon < 1$ gauge transformations we have $h^*_\epsilon(\delta g_{\mu\nu}) \approx \delta g_{\mu\nu}$ and the last two terms merge into the Lie derivative

$$\delta g_{\mu\nu} \to \delta g^{[\epsilon]}_{\mu\nu} = \delta g_{\mu\nu} + \epsilon \mathscr{L}_\xi g^{(0)}_{\mu\nu}\,. \tag{2.17}$$

This transformation behavior generalizes to any tensor and causes statements about the perturbations to be dependent on the coordinate frame. However, it also allows to built gauge invariant variables. For later use in the second part of this work we will state them here for adiabatic $\delta s = 0$ (no entropy perturbations), scalar perturbations. To do so, we define the overdensity and the sound speed

$$\delta := \frac{\delta\rho}{\rho^{(0)}} \quad \text{and} \quad \delta p = c_s^2 \delta\rho + \sigma\delta s \equiv c_s^2 \delta\rho\,, \tag{2.18}$$

respectively, with $\sigma := (\partial p/\partial s)$. All scalar quantities in the perturbed metric (Eq. (2.10)) transform non trivial under a gauge transformation, e.g. $A \to A - \xi^{0\prime} - a'/a\,\xi^0$. However, famously, the four scalars A, B, D and E can be combined to two gauge invariant quantities – the Bardeen potentials [81]

$$\Phi := A + \mathcal{H}(B - E') + (B + E')'\,, \tag{2.19}$$
$$\Psi := \psi - \mathcal{H}(B - E')\,, \tag{2.20}$$

where $\psi = D + \frac{1}{3}\nabla^2 E$ is the curvature perturbation and $\mathcal{H} := Ha$. The scalar of the energy momentum tensor δ, the scalars inferred from the longitudinal parts of the velocity vector $\mathbf{v}^{||} =: -\nabla v$ and the anisotropic stress tensor $\Pi^{||}_{ij} =: (\partial_i\partial_j - \frac{1}{3}\delta_{ij}\nabla^2)\Pi$ change as

$$\delta \to \tilde{\delta} := \delta + 3\mathcal{H}(1+\omega)\xi^0\,, \tag{2.21}$$
$$v \to \tilde{v} := v + \xi'\,, \tag{2.22}$$
$$\Pi \to \Pi\,, \tag{2.23}$$

where $\boldsymbol{\xi}^{||} =: -\nabla\xi$. Note that the background fluid is perfect $\Pi^{(0)} = 0$, thus its Lie derivative $\mathscr{L}_\xi \Pi^{(0)} = 0$ and Π is gauge invariant. However, solving the perturbed Einstein equation Eq. (2.9) requires us to chose a gauge. A typical and insightful gauge is the Newtonian or Poisson gauge. It demands that $\xi^0 = -B + E'$ and $\xi = -E$ where B can be set to zero. In this gauge, the two constraining and two evolution field equations in Fourier space $f(\mathbf{x}) = \int f_\mathbf{k}\, e^{-i\mathbf{k}\cdot\mathbf{x}} \mathrm{d}k^3$ ($\mathbf{k}$ is the spatial comoving wave number) deduced

from Einstein's equations read [82]

$$\left(\frac{k}{\mathcal{H}}\right)^2 \Psi_k = -\frac{3}{2}\left[\delta_k + 3(1+\omega)\frac{\mathcal{H}}{k}v_k\right], \tag{2.24}$$

$$\left(\frac{k}{\mathcal{H}}\right)^2 (\Psi_k - \Phi_k) = 3\omega\Pi_k\,, \tag{2.25}$$

$$\mathcal{H}^{-1}\Phi_k' + \Phi_k = \frac{3}{2}(1+\omega)\frac{\mathcal{H}}{k}v_k\,, \tag{2.26}$$

$$\mathcal{H}^{-2}\Psi_k'' + \mathcal{H}^{-1}(\Phi_k' + 2\Psi_k') + \left(1 + \frac{2\mathcal{H}'}{\mathcal{H}^2}\right)\Phi_k - \frac{1}{3}\left(\frac{k}{\mathcal{H}}\right)^2(\Phi_k - \Psi_k) = \frac{3}{2}c_s^2\,, \tag{2.27}$$

where $k = |\mathbf{k}|$. The equations of motion for pressure and energy density arise from the energy-momentum conservation equation $\nabla^\nu T_{\mu\nu} = 0$ and read

$$\delta\rho_k' + 3\mathcal{H}(\delta\rho_k + \delta p_k) = -(\rho^{(0)} + p^{(0)})\left(kv_k - 3\Psi_k'\right), \tag{2.28}$$

$$(\partial_\eta + 4\mathcal{H})\left[\frac{v_k}{k}(\rho^{(0)} + p^{(0)})\right] = \delta p_k - \frac{2}{3}\Pi_k + (\rho^{(0)} + p^{(0)})\Phi_k\,. \tag{2.29}$$

In the case of a perfect fluid $\Pi_k \equiv 0 \Rightarrow \Psi = \Phi$ such that the equation of motion for the Bardeen potential obeys

$$\Phi_k'' + 3(1+c_s^2)\mathcal{H}\Phi_k' + 3(c_s^2 - \omega)\mathcal{H}^2\Phi_k + (c_s k)^2\Phi_k = 0\,. \tag{2.30}$$

Furthermore, Eq. (2.24) becomes the Poisson equation ($4\pi G a^2\rho^{(0)} = \frac{3}{2}\mathcal{H}^2$)

$$-k^2\Phi_k = 4\pi G a^2\delta\rho_k\,. \tag{2.31}$$

Thus, we are back to an ordinary Newtonian treatment where the gravitational potential arises from an inhomogeneous density distribution. Consequently, we obtain the wave equation for an adiabatic instability under the influence of Newtonian gravity in an expanding universe:

$$\delta_k'' + 2\mathcal{H}\delta_k' + \left(c_s^2k^2 - 4\pi G a^2\rho^{(0)}\right)\delta_k = 0\,. \tag{2.32}$$

2.1.2. Matter power spectrum

With the differential equations for the perturbations, in principle, the evolution of the universe could be fully determined to first order if the initial conditions for each dynamical variable would be known. This is, however, not the case. Instead the initial overdensity $\delta(\mathbf{x}, t) = \int \mathrm{d}k^3\delta(\mathbf{k}, t)e^{-i\mathbf{k}\cdot\mathbf{x}}$ is generated by quantum fluctuations of the inflaton field which constitutes a statistically homogeneous and isotropic random process[6] [82]. Therefore, we should rather see $\delta(\mathbf{x}, t)$ as a random field. Statistical homogeneity implies that Fourier

[6] For original work on statistics of random fields see e.g. Refs. [106, 107].

modes $\delta(\mathbf{k}) = |\delta(\mathbf{k})|e^{i\phi_\mathbf{k}}$ are uncorrelated to each other [83, 84]

$$\langle\delta(\mathbf{k})\delta^*(\mathbf{k}')\rangle = (2\pi)^3\delta^\mathrm{D}(\mathbf{k}-\mathbf{k}')\mathcal{P}(\mathbf{k}) \quad \text{with} \quad \mathcal{P}(\mathbf{k}) = \int \xi(x)e^{-i\mathbf{k}\cdot\mathbf{x}}\mathrm{d}x^3\,, \tag{2.33}$$

where δ^D denotes the Dirac delta, $\xi(x)$ is the autocorrelation function $\xi(\mathbf{x},\mathbf{x}') = \langle\delta(\mathbf{x})\delta(\mathbf{x}')\rangle$ and $\langle\bullet\rangle$ denotes the expectation value. Gaussianity means that the random fields are normally distributed with width $\sigma_\mathbf{k}$[7] [82]

$$p(\delta(\mathbf{k})) = \frac{1}{2\pi\sigma_\mathbf{k}^2}\exp\left(-\frac{|\delta(\mathbf{k})|^2}{2\sigma_\mathbf{k}^2}\right) \tag{2.34}$$

and thus all information about the random field is fully encoded in the variance (2nd moment) [82]

$$\langle\delta(\mathbf{k})\delta(\mathbf{k}')\rangle = \int p(\delta)\delta^2\mathrm{d}\delta = 2\sigma_\mathbf{k}^2\delta^\mathrm{K}_{\mathbf{k}\mathbf{k}'} \equiv \mathcal{P}(\mathbf{k})\delta^\mathrm{K}_{\mathbf{k}\mathbf{k}'}\,, \tag{2.35}$$

where δ^K denote the Dirac and Kronecker delta, respectively. We call $\mathcal{P}(\mathbf{k})$ the power spectrum and in the case of matter fields, the *matter power spectrum*. Thanks to isotropy the direction of $\mathbf{k}$ is irrelevant such that only the magnitude k plays a role and the power spectrum becomes $\mathcal{P}(\mathbf{k}) = \mathcal{P}(k)$.

The linear matter power spectrum today can be described by the fitting formula (BBKS) [108]

$$\mathcal{P}_0(k) = A_0\,k\cdot\frac{\ln(1+c_1q)}{c_1q}\cdot\left(1+(c_2q)+(c_3q)^2+(c_4q)^3+(c_5q)^4\right)^{-\frac{1}{4}}\,, \tag{2.36}$$

with

$$q := \frac{k}{\Omega_{m_0}h\cdot\exp\left(-\Omega_{\mathrm{baryon}_0}-\sqrt{2h}\cdot\frac{\Omega_{\mathrm{baryon}_0}}{\Omega_{m_0}}\right)} \approx 0.073\frac{k}{k_\mathrm{eq}}\,, \tag{2.37}$$

where $c_1 = 2.34, c_2 = 3.89, c_3 = 16.1, c_4 = 5.46$ and $c_5 = 6.71$. Here k_eq denotes the comoving wave number at matter-radiation equality and $\Omega_{m_0} = 0.3$ is the abundance of matter today which partitions into the DM abundance and baryon abundance $\Omega_{\mathrm{baryon}_0} = 0.05$ [109]. The shape of the matter power spectrum is caused by the different growth behavior of matter modes inside and outside the Hubble horizon. While the amplitude of modes outside of the horizon increases linearly with time, once they enter the horizon their amplitudes remain almost constant (grow only logarithmically) during the radiation dominated era. For this reason modes that entered the horizon before equality are suppressed with regards to the primordial spectrum $\mathcal{P}_\mathrm{prim} \sim k$. After matter-radiation

[7] Here we follow Ref. [82] and choose the normalization such that real and imaginary part of the overdensity are distributed each with normalization $1/\sqrt{2\pi\sigma_\mathbf{k}^2}$ and hence the distribution of the full complex variable is normalized according to Eq. (2.34).

equality the magnitude of the matter power spectrum grows in the same way for all modes and therefore the shape is not altered anymore.

The amplitude A_0 of $\mathcal{P}_0(k)$ is calibrated to the total variance, which is measured to be [109]

$$0.8^2 = \sigma_8^2 = \int_0^\infty \mathrm{d}\tilde{k} \frac{\tilde{k}^2}{2\pi^2} \mathcal{P}_0(\tilde{k}) \times \left(\frac{3 j_1(\tilde{k}R)}{\tilde{k}R} \right)^2 . \tag{2.38}$$

Here $j_1(x) := \sin(x)/x^2 - \cos(x)/x$ and $R = 8\,\mathrm{Mpc}/h$ is the typical top hat filter radius. Any effects by additional physical processes during the propagation of the modes is captured by the *transferfunction* $\delta(\mathbf{k}, t_{\mathrm{out}}) = T(k)\delta(\mathbf{k}, t_{\mathrm{in}})$.

Let us briefly summerize here the two most important effects on the matter power spectrum.

Baryon Acoustic Oscillations: The first one is of special importance for this work. It concerns the propagation of baryon δ_b and photon δ_γ perturbations on sub-horizon scales. At high temperatures photons and baryons scatter on each other and hence their momenta are not independent $v_b' = -\mathcal{H}v_b - k\Phi + a\sigma_T n_e / R_{b\gamma}(v_\gamma - v_b)$ and vice versa for v_γ'. Here $\sigma_T = 6.65 \times 10^{-25}\,\mathrm{cm}^2$ is the Thomson cross section [110], n_e the number density of free electrons and $R_{b\gamma} := 3\rho_b^{(0)}/(4\rho_\gamma^{(0)})$ is the baryon-to-photon energy density ratio. The coupling is even so tight that their velocities almost coincide $v_b \approx v_\gamma - R_{b\gamma}(a\sigma_T n_e)^{-1}(v_\gamma' + \mathcal{H}v_\gamma - k\Phi)$. Together with the equations for energy and momentum conservation Eqs. (2.28) and (2.29) and the Poisson Eq. (2.32) on sub-horizon scales this yields a wave equation for both, the photon and the baryon overdensity[8] [111, 112]

$$\delta_\gamma'' + \frac{R_{b\gamma}'}{1 + R_{b\gamma}} \delta_\gamma' + c_s^2 k^2 \delta_\gamma = \frac{4}{3} 4\pi G \left(\rho_d^{(0)} \delta_d + \rho_b^{(0)} \delta_b \right) , \tag{2.39}$$

where the sound speed is $c_s^2 := (3(1 + R_{b\gamma}))^{-1}$. This collective oscillation of baryons and photons is imprinted in the CMB via the photons and also in the matter power spectrum via the baryons. It is known as baryon accoustic oscillations [113] and imposes a wavy pattern upon the spectrum. The oscillation ends when photons and baryons decouple at t_{dec} which defines the *sound horizon*, the biggest distance that a mode can travel before contraction [15, 114]

$$r_s := \int_0^{t_{\mathrm{dec}}} \mathrm{d}t \, \frac{c_s(a)}{a} \approx 147\,\mathrm{Mpc} . \tag{2.40}$$

Neutrino Free Streaming: Secondly, the matter power spectrum can experience suppression on small scales due to *neutrino free streaming* [115, 116]. When the neutrino velocity transitions from the relativistic to the non-relativistic regime their thermal velocity is controlled by their mass m_ν and neutrino perturbations on scales smaller than

[8] One can approximately interchange δ_γ and δ_b here.

the free streaming length $k > k_{\rm fs}$

$$k_{\rm fs}(z) \approx 0.81 \frac{\sqrt{\Omega_\Lambda + \Omega_{m_0}(1+z)^3}}{(1+z)^2} \left(\frac{m_\nu}{1\,\mathrm{eV}}\right) h\,\mathrm{Mpc}^{-1}\,, \tag{2.41}$$

are damped. This in turn reduces the depth of the potential Φ and as a consequence dark matter perturbations grow slower. Depending on the neutrino mass small scales in the matter power spectrum therefore experience suppression.

2.2. The 1+3-covariant formulation

2.2.1. Threading of the space-time manifold

In the preluding words to this chapter we repeated the observation that the symmetries *homogeneity* and *isotropy* allow for a 3+1 slicing of the space-time manifold into a one parameter family of spacelike hypersurfaces Σ_t.

However, the symmetries also allow for the dual approach[9]. Instead of slicing space-time we can also *thread* it by introducing a family of observers whose world lines we denote in local coordinates as $L_{x^\alpha}(t) = x^a(\tau)$ and use as affine parameter the proper time τ. In our labeling of space-time indices we follow the standard literature [86] and use Latin variables for a four-vector $a \in \{0,1,2,3\}$ and Greek ones $\alpha, \beta, \gamma = 1,2,3$ for three-vectors to emphasize the duality between threading and slicing. How do these two approaches differ concretely? In the 3+1 decomposition time t was just a label of spacelike slices Σ_t with space coordinates x^i. In contrast, in the 1+3 splitting, the time like world lines $L_{x^\alpha}(t)$ have coordinate t and are labeled by x^α. This has two important implications [117]

a) In the case of threading the distance of two points is defined by the distance of nearby fundamental observers L_{x^α} and $L_{x^\alpha + \Delta x^\alpha}$ and the spatial metric $h_{\alpha\beta}\Delta x^\alpha \Delta x^\beta$. While for slicing two close by points differ by the gap between the space like hypersurfaces Σ_t and $\Sigma_{\Delta t}$ where the distance is given by a lapse function $N(x^\alpha, t)\Delta t$ (see Fig. 2.1).

b) In the 3+1 formulation the construction only required space like hypersurfaces but did not demand causality of the time curves. Vice versa, in the 1+3 approach, we considered time like curves but did say nothing about the causality conditions on the spatial distances.

Though the two approaches provide different points of view, it has been shown that they are equivalent [117]. For us, in this work, the benefit of the 1+3 approach originates from a different point. As it turns out, it provides a very transparent way of constructing gauge invariant quantities in cosmological perturbation theory that allow for much easier

[9] This paragraph is based upon the very nice Ref. [117] which we encourage the reader to have a look at.

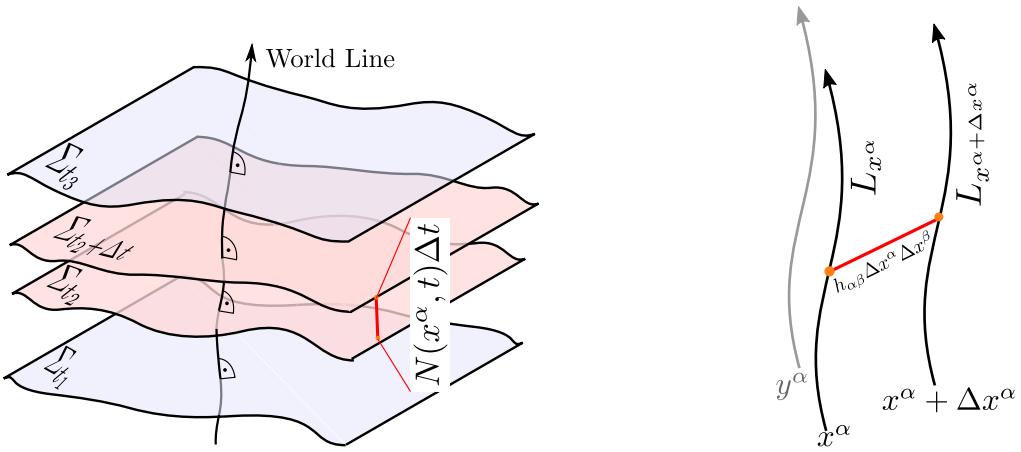

Figure 2.1.: *Left:* Sketch that shows how distances are calculated when space-time is sliced in the 3+1 point of view. The world line intersects the hypersurfaces orthogonally if they are homogeneous. Both sketches reproduced and modified from [117]. *Right:* Sketch that shows the dual approach to the previous one. Distances are calculated between the time like curves of fundamental observers.

geometrical and physical interpretation, in contrast to Bardeen's formulation, cf. Sec. 2.1.1. These variables are constructed with regards to the four-velocity - the time direction - of the world lines of the comoving, fundamental observers

$$u^a = \frac{\mathrm{d}x^a}{\mathrm{d}\tau}\,, \tag{2.42}$$

with the usual normalization $u^a u_a = -1$. In a cosmic setup the world lines are just the fluid flow lines. The orthogonal projector at fixed t that measures the distance between such lines mentioned in **a)** projects at each point (event) each tensor onto the instantaneous rest space of u^a and reads [86]

$$h_{ab} := g_{ab} + u_a u_b\,, \tag{2.43}$$

where g_{ab} denotes the metric tensor with signature $(-+++)$. It is easy to see that h_{ab} is indeed orthogonal to the four velocity

$$h_{ab}u^b = g_{ab}u^b + u_a u_b u^b = u_a - u_a = 0\,. \tag{2.44}$$

Both u^a and h_{ab} can therefore be used to uniquely split space-time quantities into time and space components. As an important example, consider the covariant derivative ∇_a. Projecting it onto the flow lines yields the time derivative, while the spatial gradient can be obtained from projecting with h_{ab}, which gives

$$\dot{S}_{ab\ldots}{}^{cd\ldots} := u^e \nabla_e S_{ab\ldots}{}^{cd\ldots} \quad \text{and} \quad \mathrm{D}_e S_{ab\ldots}{}^{cd\ldots} := h_e{}^s h_a{}^f h_q{}^c \cdots \nabla_s S_{f\ldots}{}^{q\cdots}\,, \tag{2.45}$$

for a general tensor $S_{ab\ldots}{}^{cd\ldots}$. In the literature it is common to stick within this framework

to cosmic time and hence so we do here too.

2.2.2. Kinematic variables and gauge invariance in the 1+3 covariant formulation

Looking at cosmology from the 1+3 standpoint was first done in the pioneering papers by Heckmann and Schücking (Ehlers) [118, 119], Raychaudhuri [120] and Hawking [121]. The variables that determine the motion of a test particle emerge from applying the covariant derivative to the four-velocity vector yielding the following irreducible decomposition

$$\nabla_b u_a = \sigma_{ab} + \omega_{ab} + \frac{1}{3}\Theta h_{ab} - A_a u_b \,. \tag{2.46}$$

Here $\sigma_{ab} := \mathrm{D}_{\langle b} u_{a\rangle}$ denotes the tracefree *shear* tensor, $\omega_{ab} := \mathrm{D}_{[b} u_{a]}$ is the antisymmetric (hence tracefree) *vorticity* tensor, the scalar $\Theta := \mathrm{D}^a u_a$ describes *volume expansion* and finally $A_a = \dot{u}_a = u^b \nabla_b u_a$ is the four-*acceleration*. The shear tells us how the shape of a volume is distorted while vorticity corresponds to spinning and twisting of it. The brackets used in the definitions above are defined for a tensor S_{ab} in the following way

$$S_{(ab)} := \frac{1}{2}\left(S_{ab} + S_{ba}\right), \quad S_{[ab]} := \frac{1}{2}\left(S_{ab} - S_{ba}\right), \tag{2.47}$$

$$S_{\langle ab\rangle} := h_a{}^c h_b{}^d S_{cd} - \frac{1}{3} h^{cd} S_{cd} h_{ab}, \quad V_{\langle a\rangle} := h_a{}^b V_b \,. \tag{2.48}$$

A list of frequently used identities for this brackets can be found in Appendix B.1.

The shear, the vorticity and the four-acceleration are quantities orthogonal to the fluid velocity $u^a \sigma_{ab} = u^a \omega_{ab} = u^a A_a = 0$ and identically zero in a pure FLRW universe (the volume expansion is in this case just the Hubble function $\Theta(t) = 3H(t)$). They only start to play a role once we consider perturbations. A little bit more intuition for these variables can be gained by recalling that the distance between two time like curves can be measured using h_{ab}. With the help of the shear, the vorticity and the volume expansion scalar we can derive the relative motion of two such world lines $v_{ab} = \mathrm{D}_b u_a = \sigma_{ab} + \omega_{ab} + \Theta/3\, h_{ab}$. Note that in FLRW this simply reduces to $v_{ab} = \mathrm{D}_b u_a = H(t)\, h_{ab}$ as expected and hence the relative velocity for world lines with distance ξ_a is $v_a := H(t) h_{ab} \xi^b = H(t)\xi_a$, restoring Hubble's law [122].

The absence of shear, vorticity and acceleration in a perfectly homogeneous and isotropic universe makes them automatically gauge invariant to first order[10]. As for the metric tensor in Eq. (2.17), an arbitrary tensor field S when expanded to first order[11] $S = S^{(0)} + \epsilon\, S^{(1)}$ transforms under an infinitesimal change of coordinates $\tilde{x}^\mu = x^\mu + \epsilon\, \xi^\mu$ as (see also [92, 123, p.59])

$$S^{(1)} \to S^{(1)} + \epsilon \mathscr{L}_\xi S^{(0)} \,, \tag{2.49}$$

[10] We will often refer to the term "gauge invariant" and mean by that gauge invariant to first order.
[11] The notations $\delta S \equiv \epsilon\, S^{(1)}$ are equivalent and interchangeably used when suitable.

where $\mathscr{L}_\xi$ denotes the Lie-derivative of the background term $S^{(0)}$ along ξ^μ. Building upon this rule, the conditions for gauge invariance are condensed in the Stewart & Walker Lemma [123, 124].

Stewart & Walker Lemma:
A tensor is gauge invariant if and only if it either vanishes in the background, is a constant scalar in the background or can be written as a sum of products of Kronecker-deltas with constant coefficients.

Based on this Lemma, Marco Bruni, George F. R. Ellis, Peter K. S. Dunsby and coauthors substantially extended the 1+3 covariant description of space-time to a gauge invariant cosmological perturbation theory [104, 125–128], which we review in the following paragraphs. We use the short hand $\kappa := 8\pi G$, where G is the gravitational constant.

2.2.3. Space-time geometry and matter fields

The behavior of the kinematic variables under the influence of matter fields is deduced from Einstein's equation. In contrast to the approach by Bardeen this is done with the curvature variables directly rather than the gravitational potentials [126]. The total information about the curvature of a space-time manifold is encoded in the Riemann tensor that measures how much a parallel transported vector is altered with regard to its original orientation. The tensor can be split into a tracefree part and a part with trace. The tracefree part is the Weyl tensor[12] C_{abcd} that depicts the propagating degrees of freedom (e.g. GWs). Volume changes due to a local matter source and hence the local deviation of the curvature from flat space is reflected by the Ricci tensor R_{ab} and its trace, the Ricci scalar R. The splitting of the Riemann tensor then reads

$$R_{abcd} = C_{abcd} + \frac{1}{2}(g_{ac}R_{bd} + g_{bd}R_{ac} - g_{bc}R_{ad} - g_{ad}R_{bc}) - \frac{1}{6}R(g_{ac}g_{bd} - g_{ad}g_{bc})\,. \tag{2.50}$$

In a homogeneous background the Weyl tensor is identically zero and therefore according to the Stewar & Walker Lemma gauge invariant. Consequently, so are the electric and magnetic part in which the Weyl tensor can be split [129, 130]

$$E_{ab} = C_{acbd}u^c u^d \quad \text{and} \quad H_{ab} = \frac{1}{2}\epsilon_a^{cd}C_{cdbe}u^e\,. \tag{2.51}$$

Physically, the electric tensor E_{ab} describes tidal forces while the magnetic part H_{ab} is essential for the description of GWs.

Let us now turn to the right hand side of Einstein's equation. In the 1+3 framework we adopt the decomposition of the energy momentum tensor as before, but with respect

[12] The Weyl tensor and the Riemann tensor obey the same symmetries $R_{abcd} = R_{cdcb}$, $R_{abcd} = R_{[ab][cd]}$ and $R_{a[bcd]} = 0$.

to the four velocity field u_a and the orthogonal projection h_{ab}:

$$T_{ab} = \rho u_a u_b + 2u_{(a}q_{b)} + p h_{ab} + \pi_{ab}\,. \tag{2.52}$$

In terms of the four velocity the energy density and the pressure are given as $\rho := T^{ab}u_a u_b$ and $p := T_{ab}h^{ab}/3$, the traceless, symmetric anisotropic stress is labeled with a small letter in the literature $\pi_{ab} = T_{\langle ab\rangle}$ and $q_a := h_a^{\ b}T_{bc}u^c$ denotes the energy current density. The latter two, as they vanish in the background, are gauge invariant quantities while ρ and p are gauge dependent. Plugging the energy momentum tensor Eq. (2.52) into Einstein's field equations $R_{ab}u^a u^b = T_{ab} - \frac{1}{2}T_{ab} + \Lambda g_{ab}$ yields three equations that connect curvature to cosmic fluid [86]

$$R_{ab}u^a u^b = \kappa\frac{1}{2}(\rho + 3p) - \Lambda\,, \tag{2.53}$$

$$h_a^{\ b}R_{bc}u^c = -\kappa q_a \quad \text{and} \tag{2.54}$$

$$h_a^{\ c}h_b^{\ d}R_{cd} = \kappa\frac{1}{2}(\rho - p)h_{ab} + \kappa\pi_{ab} + \Lambda h_{ab}\,. \tag{2.55}$$

These relations between the Ricci tensor and the fluid content form the basis to derive the evolution and constraint equations of the involved variables from Bianchi- and Ricci identities in the next sections.

2.2.4. Constraint and evolution equations

We have now collected a set of dynamical variables upon which a description of cosmological perturbation theory can be based. What remains to be done is to derive for each of them the equation of motion and the constraint equations as we have done before for the gravitational potentials in the Bardeen formalism. To do so, we make use of the *Bianchi* and *Ricci* identities and combine them with Eqs. (2.53), (2.54) and (2.55) deduced from Einstein's field equations. For details of this calculation see [86] which has originally been done by Refs. [85, 131]. In the following equations we denote by $\omega_a := \epsilon_{abc}\omega^{bc}/2$ the vorticity vector that in the Newtonian limit corresponds to $\boldsymbol{\omega} = -\nabla \times \boldsymbol{v}/2$, where the orthogonal projected tensor ϵ_{abc} is the contraction $\epsilon_{abc} := \eta_{abcd}u^d$ of u^d with the totally antisymmetric pseudotensor η_{abcd} depicting the space-time volume element. The Bianchi identities for the Weyl tensor

$$\nabla^d C_{abcd} = \nabla_{[b}R_{a]c} + \frac{1}{6}g_{c[b}\nabla_{a]}R \tag{2.56}$$

together with Eq. (2.55) lead to the evolution equations for the electric and magnetic components of the Weyl tensor

$$\dot{E}_{\langle ab\rangle} = -\Theta E_{ab} - \frac{1}{2}\kappa\,(\rho+p)\sigma_{ab} + \operatorname{curl} H_{ab} - \frac{1}{2}\kappa\,\dot{\pi}_{ab} - \frac{1}{6}\kappa\,\Theta\pi_{ab} - \frac{1}{2}\kappa\,\mathrm{D}_{\langle a}q_{b\rangle} - \kappa A_{\langle a}q_{b\rangle} + 3\sigma_{\langle a}{}^{c}\left(E_{b\rangle c} - \frac{1}{6}\kappa\,\pi_{b\rangle c}\right) + \varepsilon_{cd\langle a}\left[2A^{c}H_{b\rangle}{}^{d} - \omega^{c}\left(E_{b\rangle}{}^{d} + \frac{1}{2}\kappa\,\pi_{b\rangle}{}^{d}\right)\right], \tag{2.57}$$

$$\dot{H}_{\langle ab\rangle} = -\Theta H_{ab} - \operatorname{curl} E_{ab} + \frac{1}{2}\kappa\,\operatorname{curl}\pi_{ab} + 3\sigma_{\langle a}{}^{c}H_{b\rangle c} - \frac{3}{2}\kappa\,\omega_{\langle a}q_{b\rangle} - \varepsilon_{cd\langle a}\left(2A^{c}E_{b\rangle}{}^{d} - \frac{1}{2}\kappa\,\sigma^{c}{}_{b\rangle}q^{d} + \omega^{c}H_{b\rangle}{}^{d}\right). \tag{2.58}$$

and to a constraint equation for each of them

$$\mathrm{D}^{b}E_{ab} = \kappa\left[\frac{1}{3}\,\mathrm{D}_{a}\rho - \frac{1}{2}\mathrm{D}^{b}\pi_{ab} - \frac{1}{3}\,\Theta q_{a} + \frac{1}{2}\,\sigma_{ab}q^{b}\right] - 3H_{ab}\omega^{b} + \varepsilon_{abc}\left(\sigma^{b}{}_{d}H^{cd} - \frac{3}{2}\kappa\,\omega^{b}q^{c}\right), \tag{2.59}$$

$$\mathrm{D}^{b}H_{ab} = \kappa(\rho+p)\omega_{a} - \frac{1}{2}\kappa\,\operatorname{curl} q_{a} + 3E_{ab}\omega^{b} - \frac{1}{2}\kappa\,\pi_{ab}\omega^{b} - \varepsilon_{abc}\sigma^{b}{}_{d}\left(E^{cd} + \frac{1}{2}\kappa\,\pi^{cd}\right). \tag{2.60}$$

Here, the operator curl on a four-vector v_a is defined as $\operatorname{curl} v_a := \epsilon_{abc}\mathrm{D}^{b}v^{c}$. Like we have done in the previous section, we find the equation of motion for the energy density from $\nabla^{a}T_{ab} = 0$, which demands the conservation of energy

$$\dot{\rho} = -\Theta(\rho+p) - \mathrm{D}^{a}q_{a} - 2A^{a}q_{a} - \sigma^{ab}\pi_{ab}\,. \tag{2.61}$$

The same equation leads also to the propagation equation of the energy current density

$$\dot{q}_{\langle a\rangle} = -\mathrm{D}_{a}p - (\rho+p)A_{a} - \frac{4}{3}\,\Theta q_{a} - (\sigma_{ab}+\omega_{ab})q^{b} - \mathrm{D}^{b}\pi_{ab} - \pi_{ab}A^{b}\,. \tag{2.62}$$

In order to obtain the evolution equations for the three covariant kinematical quantities that we inferred from the decomposition of the four-velocity, we apply the separated Riemann tensor Eq. (2.50) to the Ricci-identities $2\nabla_{[a}\nabla_{b]}u_{c} = R_{abcd}u^{d}$. In combination with Eqs. (2.53), (2.54) and (2.55) the purely geometric kinematics relate to the matter fields via

$$\dot{\Theta} = -\frac{1}{3}\,\Theta^{2} - \frac{1}{2}\kappa\,(\rho+3p) - 2(\sigma^{2}-\omega^{2}) + \mathrm{D}^{a}A_{a} + A_{a}A^{a} + \Lambda, \tag{2.63}$$

$$\dot{\sigma}_{\langle ab\rangle} = -\frac{2}{3}\,\Theta\sigma_{ab} - \sigma_{c\langle a}\sigma^{c}{}_{b\rangle} - \omega_{\langle a}\omega_{b\rangle} + \mathrm{D}_{\langle a}A_{b\rangle} + A_{\langle a}A_{b\rangle} - E_{ab} + \frac{1}{2}\kappa\,\pi_{ab}, \tag{2.64}$$

$$\dot{\omega}_{\langle a\rangle} = -\frac{2}{3}\,\Theta\omega_{a} - \frac{1}{2}\,\operatorname{curl} A_{a} + \sigma_{ab}\omega^{b}\,. \tag{2.65}$$

Here $\sigma^2 := \frac{1}{2}\sigma_{ab}\sigma^{ab}$ and $\omega^2 := \frac{1}{2}\omega_{ab}\omega^{ab}$ denote the magnitudes of the shear and the vorticity, respectively. Observe that in the first line we have rediscovered the *Raychaudhuri equation*, which measures the rate by which the volume expansion changes due to the cosmic ingredients. At zeroth order ($\sigma^2 = \omega^2 = A_a = 0$) it is just the Friedman equation. Additionally, the spacelike part forces the kinematics to satisfy the conditions

$$\mathrm{D}^b\sigma_{ab} = \frac{2}{3}\mathrm{D}_a\Theta + \operatorname{curl}\omega_a + 2\varepsilon_{abc}A^b\omega^c - \kappa q_a, \quad \mathrm{D}^a\omega_a = A_a\omega^a, \tag{2.66}$$

$$\mathrm{D}^a\omega_a = A_a\omega^a\,, \tag{2.67}$$

$$H_{ab} = \operatorname{curl}\sigma_{ab} + \mathrm{D}_{\langle a}\omega_{b\rangle} + 2A_{\langle a}\omega_{b\rangle}\,. \tag{2.68}$$

With this, we have all needed tools to develop a gauge invariant perturbation theory based on the 1+3 covariant framework. However, the only quantity in our discussion escaping from a gauge invariant dual version until now is the energy density ρ. We shall see in the next subsection how this issue can be solved.

2.2.5. Linear density perturbations

In the background of a FLRW universe, all discussed quantities vanish except for the volume expansion Θ and the energy density $\rho(p)$. In fact in the background both variables are functions solely depending on time. This, however, implies that their spatially projected gradients are zero $\mathrm{D}_a\rho(t) = \mathrm{D}_a\Theta(t) = 0$ and thus provide gauge invariant variables for inhomogeneities in matter and space. The resulting comoving fractional gradient of the energy density and the comoving expansion gradient therefore become central to our discussion [104]

$$\Delta_a := \frac{a}{\rho}\mathrm{D}_a\rho\,, \tag{2.69}$$

$$Z_a := a\mathrm{D}_a\Theta\,. \tag{2.70}$$

It is tempting to think of the former as the density contrast $\delta := \delta\rho/\rho$ at first order, but it should be kept in mind that it is rather the Laplacian of δ. All information about scalar, vector and tensor perturbations are combined in the comoving fractional density gradient and thus it can be decomposed into these three irreducible parts: The density distortion $\Delta_{\langle ab\rangle} := a\mathrm{D}_{\langle b}\Delta_{a\rangle}$ measures shape changes of a clump of matter, the vorticity perturbation $\Delta_{[ab]} := a\mathrm{D}_{[b}\Delta_{a]}$ determines rotational variations and $\Delta := a\mathrm{D}^a\Delta_a$ denotes scalar over- and under densities . They emerge from the splitting

$$a\mathrm{D}_b\Delta_a = \frac{1}{3}\Delta h_{ab} + \Delta_{\langle ab\rangle} + \Delta_{[ab]}\,. \tag{2.71}$$

Their propagation equations can be determined from the propagation equation for Δ_a. To find the latter, we simply have to take the spatial derivative D_a of the energy conservation law Eq. (2.61), multiply with the scale factor $a(t)$ and divide by ρ in order to convert all ρ-terms to Δ_a-terms and finally apply this and Eq. (2.62) to $\dot{\Delta}$. Together with

Raychaudhuri's equation (2.63) this culminates in two coupled, non-linear equations that dictate the evolution of spatial inhomogeneities and the volume expansion gradient [86]

$$\begin{aligned}\dot{\Delta}_{\langle a\rangle} =& \frac{p}{\rho}\,\Theta\Delta_a - \left(1+\frac{p}{\rho}\right) Z_a + a\frac{\Theta}{\rho}\left(\dot{q}_{\langle a\rangle} + \frac{4}{3}\,\Theta q_a\right) - \frac{a}{\rho}\,\mathrm{D}_a\mathrm{D}^b q_b + a\frac{\Theta}{\rho}\,\mathrm{D}^b\pi_{ab}\\ &- \left(\sigma^b{}_a + \omega^b{}_a\right)\Delta_b - \frac{a}{\rho}\,\mathrm{D}_a\left(2A^b q_b + \sigma^{bc}\pi_{bc}\right) + a\frac{\Theta}{\rho}\left(\sigma_{ab}+\omega_{ab}\right)q^b + a\frac{\Theta}{\rho}\,\pi_{ab}A^b\\ &+ \frac{1}{\rho}\left(\mathrm{D}^b q_b + 2A^b q_b + \sigma^{bc}\pi_{bc}\right)\left(\Delta_a - aA_a\right)\,, \end{aligned} \tag{2.72}$$

and

$$\begin{aligned}\dot{Z}_{\langle a\rangle} =& -\frac{2}{3}\,\Theta Z_a - \frac{1}{2}\,\kappa\rho\Delta_a - \frac{3}{2}\,\kappa a\mathrm{D}_a p - a\left[\frac{1}{3}\,\Theta^2 + \frac{1}{2}\,\kappa(\rho+3p) - \Lambda\right]A_a + a\mathrm{D}_a\mathrm{D}^b A_b\\ &- \left(\sigma^b{}_a + \omega^b{}_a\right)Z_b - 2a\mathrm{D}_a\left(\sigma^2-\omega^2\right) + 2aA^b\mathrm{D}_a A_b\\ &- a\left[2\left(\sigma^2-\omega^2\right) - \mathrm{D}^b A_b - A^b A_b\right]A_a\,. \end{aligned} \tag{2.73}$$

To show how these equations work, we seek to recover the equation of motion of linear density variations. We choose the same assumptions as before: a FLRW background, $\Theta = 3H(t)$, and a barotropic, $p = \omega\rho$, perfect, $q_a = \pi_{ab} = 0$, fluid without any shear and vorticity currents, $\omega_{ab} = \sigma_{ab} = 0$. Setting all these variables to zero reduces Eqs. (2.72) and (2.73) to (we follow here again Ref. [86])

$$\dot{\Delta}_a = 3\omega H\Delta_a - (1+\omega)Z_a, \tag{2.74}$$

$$\dot{Z}_a = -2HZ_a - \frac{1}{2}\kappa\rho\Delta_a - \frac{3}{2}\kappa a\mathrm{D}_a p \tag{2.75}$$

$$- a\left[3H^2 + \frac{1}{2}\kappa\rho(1+3\omega) - \Lambda\right]A_a + a\mathrm{D}_a\mathrm{D}^b A_b\,. \tag{2.76}$$

To linear order the four-acceleration is determined from Eq. (2.62) and $\mathrm{D}_a p = \frac{\rho}{a}c_s^2\Delta_a$ by $-c_s^2\Delta_a = a(1+\omega)A_a$. Taking the orthogonal projected gradients of these equations and applying the Friedman equations simplifies the system to

$$\dot{\Delta} = 3\omega H\Delta - (1+\omega)Z, \tag{2.77}$$

$$\dot{Z} = -2HZ - \left[\frac{1}{2}\kappa\rho + \frac{3Kc_s^2}{a^2(1+\omega)}\right]\Delta - \frac{c_s^2}{1+\omega}\mathrm{D}^2\Delta\,, \tag{2.78}$$

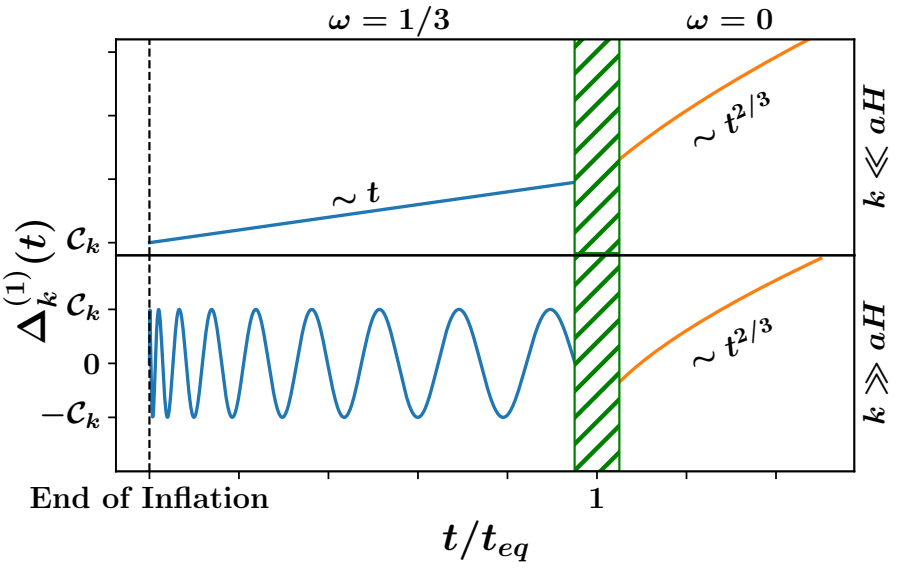

Figure 2.2.: Time dependence of the linear comoving fractional gradient modes as a function of cosmic time during radiation- and matter domination for super- and sub-horizon scales. The green shaded region symbolizes the transition zone between radiation and matter domination.

which can be combined to (recall K is the curvature scalar) [125]

$$\begin{aligned}\ddot{\Delta} =& -2\left(1-3\omega+\frac{3}{2}c_s^2\right)H\dot{\Delta}\\ &+\kappa\left[\left(\frac{1}{2}+4\omega-3c_s^2-\frac{3}{2}\omega^2\right)\rho+(5\omega-3c_s^2)\Lambda-\frac{12(\omega-c_s^2)K}{a^2}\right]\Delta\\ &+c_s^2\mathrm{D}^2\Delta\,.\end{aligned} \tag{2.79}$$

Recall that $\Delta \equiv \Delta^{(1)}$, $Z \equiv Z^{(1)}$ due to a vanishing zeroth order and that we must have $\rho \equiv \rho^{(0)}$ in order to preserve the first order perturbation. To find the solution of this equation for different scales, we transform the expression into k-space. Therefore, we decompose Δ into spherical harmonics $\mathcal{Q}_k$ which obey the conditions $\mathrm{D}_a\mathcal{Q}_k = 0$, $\dot{\mathcal{Q}}_k = 0$ and $\mathrm{D}^2\mathcal{Q}_k = -\frac{k^2}{a^2}\mathcal{Q}_k$. These spherical harmonics are a generalized versions of the standard Fourier basis e^{-ikx} (see appendix B.2). In a flat, $K = 0$, universe without cosmological constant, $\Lambda = 0$, filled with DM, $\omega = 0$, and DM perturbations, $c_s^2 = 0$, we rediscover Eq. (2.32)

$$\ddot{\Delta}_k + 2H\dot{\Delta}_k + 4\pi G\rho\Delta_k = 0\,. \tag{2.80}$$

In a matter dominated universe we have $H = 2/(3t)$ and $\rho = 4/(3t^2)$ the solution of Eq. (2.80) has a growing and a decaying mode $\Delta_k \sim \Delta_{1,k}t^{2/3} + \Delta_{2,k}t^{-1}$. In contrast, the

Variable	Symbol	Perturbative Expansion $S = S^{(0)} + \epsilon\, S^{(1)}$	First order GI
Energy density	ρ	$\rho(t) + \rho(\mathbf{x}, t)$	$\mathrm{D}_a\rho(\mathbf{x}, t)$
Pressure	p	$p(t) + p(\mathbf{x}, t)$	$\mathrm{D}_a p(\mathbf{x}, t)$
Anisotropic stress	π	$0 + \pi(\mathbf{x}, t)$	$\pi(\mathbf{x}, t)$
Energy density current	q	$0 + q(\mathbf{x}, t)$	$q(\mathbf{x}, t)$
Volume expansion	Θ	$\Theta(t) + \Theta(\mathbf{x}, t)$	$\mathrm{D}_a\Theta(\mathbf{x}, t)$
Shear	σ	$0 + \sigma(\mathbf{x}, t)$	$\sigma(\mathbf{x}, t)$
Vorticity	ω	$0 + \omega(\mathbf{x}, t)$	$\omega(\mathbf{x}, t)$
Acceleration	A	$0 + A(\mathbf{x}, t)$	$A(\mathbf{x}, t)$
Long range grav. field (Weyl tensor)	C	$0 + C_{abcd}(\mathbf{x}, t)$	$C_{abcd}(\mathbf{x}, t)$

Table 2.1.: The central variables in the 1+3 covariant approach, their perturbative decomposition and their gauge invariant version. Taken from [5].

equation for radiation fluctuations in a radiation dominated universe, $c_s^2 = \omega = 1/3$, with $H = 1/(2t)$ and $\kappa\rho = 3/(4t^2)$ leads to the equation

$$\frac{\mathrm{d}^2\Delta_k}{\mathrm{d}t^2} + \frac{1}{2t}\frac{\mathrm{d}\Delta_k}{\mathrm{d}t} - \frac{1}{2t^2}\left[1 - \frac{1}{6}\left(\frac{k}{a(t)H(t)}\right)^2\right]\Delta_k = 0\,. \tag{2.81}$$

This yields an oscillatory solution for sub-horizon modes $k/aH \gg 1$ [86]

$$\Delta_k^{(1)} = \mathcal{C}_{1,k}^{(1)} \sin\left[\frac{1}{\sqrt{3}}\frac{k}{a_0 H_0}\left(\frac{t}{t_0}\right)^{1/2}\right] + \mathcal{C}_{2,k}^{(1)} \cos\left[\frac{1}{\sqrt{3}}\frac{k}{a_0 H_0}\left(\frac{t}{t_0}\right)^{1/2}\right], \tag{2.82}$$

where t_0, a_0 and H_0 denote initial values and $\mathcal{C}_{1/2,k}^{(1)}$ are given by the initial conditions. Hence, during radiation domination density perturbations on sub-horizon scales do not grow but rather oscillate with respect to time and scale. Instead for super-horizon scales, $k/aH \ll 1$, the amplitude of the growing mode increases linearly with time $\Delta_k \sim t$. In Fig. 2.2 the solutions of Eq. (2.79) in different regimes are sketched. Conclusively, for this section we give a summary of the main variables in the 1+3 covariant framework in Tab. 2.1 including their first order gauge invariant version.

2.2.6. Gravitational waves

The evolution of GWs is mainly dictated by the magnetic part of the Weyl tensor while the electric part resembles tensors in Newtonian gravity that monitor tidal forces [132]. Neglecting all quadratic terms of gauge invariant variables linearizes the propagation Eqs. (2.57), (2.58) and the constraint Eqs. (2.59), (2.60) automatically. Note again that gauge invariant variables in the following are of first order and hence we omit the label

for sake of shortness. As a result, we have [133, 134]

$$\dot{E}_{ab} = -\Theta^{(0)} E_{ab} + \operatorname{curl} H_{ab} - \frac{1}{2}\kappa \left[(\rho^{(0)} + p^{(0)})\sigma_{ab} - \mathrm{D}_{\langle a} q_{b\rangle} + \dot{\pi}_{ab} + \frac{1}{3}\Theta^{(0)}\pi_{ab} \right] , \quad (2.83)$$

$$\dot{H}_{ab} = -\Theta^{(0)} H_{ab} - \operatorname{curl} E_{ab} - \frac{1}{2}\kappa\pi_{ab} , \quad (2.84)$$

$$\mathrm{D}^b E_{ab} = \kappa \left(\frac{1}{3}\Theta^{(0)} q_b + \frac{1}{3}\mathrm{D}_a \rho^{(1)} + \frac{1}{2}\mathrm{D}^a \pi_{ab} \right) , \quad (2.85)$$

$$\mathrm{D}^b H_{ab} = \frac{1}{2}\kappa \left[2(\rho^{(0)} + p^{(0)})\omega_a + \operatorname{curl} q_b \right] . \quad (2.86)$$

In order to describe GWs we need to isolate the transverse part of the tensors. As the two latter constraint equations show, electric and magnetic part of the Weyl tensor are transverse if and only if they do not originating from gradients of density variations $\mathrm{D}_a\rho = 0$, non transverse parts of anisotropic stresses $\mathrm{D}^a\pi_{ab} = 0$, energy density currents in the fluid $q_a = 0$ and vorticity $\omega_a = 0$. If this is the case these two fields are transverse, $\mathrm{D}^a E_{ab} = 0$ and $\mathrm{D}^a H_{ab} = 0$. The same is true for the shear tensor, $\mathrm{D}^a\sigma_{ab} = 0$ and together with the linearized version of Eq. (2.64) we arrive at

$$\dot{\sigma}_{ab} = -\frac{2}{3}\Theta\sigma_{ab} - E_{ab} - \frac{1}{2}\kappa\pi_{ab} . \quad (2.87)$$

Now we can remove H_{ab} and E_{ab} completely from the discussion and merge all information into an equation of motion for the shear tensor [132, 135]

$$\ddot{\sigma}_{ab} + 5H(t)\dot{\sigma}_{ab} + \frac{1}{2}\kappa\rho(1 - 3\omega)\sigma_{ab} - \mathrm{D}^2\sigma_{ab} = 0 . \quad (2.88)$$

Again we assumed a perfect fluid, $q_a = \pi_{ab} = 0$, on a FLRW background $\Theta = 3H(t)$ without spatial curvature, $K = 0$. This shows that the shear tensor is the appropriate quantity in the 1+3 covariant framework to describe GWs. This will become important later in the next part of this thesis.

2.2.7. Comparing the formalisms

As we noted before, slicing and threading are two equivalent approaches to cosmology. Consequently, it is also possible to find equations that relate quantities in the 1+3 covariant formalism to quantities in the Bardeen formulation. These equations have been worked out by Goode [136] and Bruni et al. in Ref. [123] for all types of perturbations from which we will quote here a limited selection of relations that are of later use. The spatial comoving density variations Δ relate to the density contrast δ in a flat space-time $K = 0$ via

$$\Delta(\mathbf{x}, t) = \nabla^2 \left(\delta + 3\mathcal{H}(1 + \omega)\xi^0 \right) = \nabla^2 \tilde{\delta}(\mathbf{x}, t) , \quad (2.89)$$

where we have used that the Laplace-Beltrami operator $\mathrm{D}^a\mathrm{D}_a$ corresponds to the Laplacian in a spatially flat space space-time

$$\mathrm{D}^a\mathrm{D}_a = \frac{\nabla^2}{a^2}\,. \tag{2.90}$$

If $\Delta(\mathbf{x},t) \equiv \Delta^{(1)}(\mathbf{x},t)$ constitutes a linear perturbation then $\tilde{\delta}^{(1)} := \delta + 3H(1+\omega)\xi^0$ is Bardeen's gauge invariant version of δ [123, 136]. We will need this connection in the next part of this work. The second interesting relation for our purposes is between the spatial part of the shear tensor $\sigma_{\alpha\beta}$ and the transverse, traceless linear tensor perturbations $E^T_{\alpha\beta}$. It is given by

$$\sigma_{\alpha\beta} = a(\nabla_{\alpha\beta}\tilde{v} + \nabla_{(\alpha}\tilde{v}_{\beta)} + E^{T\prime}_{\alpha\beta})\,, \tag{2.91}$$

where $\Delta_{\alpha\beta} := \nabla_\alpha\nabla_\beta - \frac{1}{3}\delta_{\alpha\beta}\nabla^2$. By $\tilde{v} = v + \xi'$ we denote the gauge invariant version of the scalar velocity v and by $\tilde{v}_\alpha = v^\perp_\alpha + \xi'_\alpha$ the gauge invariant version of the spatial component of the solenoid velocity vector. With this, we are equipped with all necessary tools for the perturbative analysis in the result part of this work. However, before moving on, we briefly review FOPTs in particle physics.

Chapter 3

Gravitational Waves from First-Order Phase Transitions

This chapter is devoted to the study of first-order phase transitions in particle physics and cosmology and their presumably most famous byproduct: Gravitational waves. After briefly discussing phase transitions in the context of the early universe and the standard model we review the major building blocks to derive the effective, temperature-dependent potential for a given particle model and how to investigate its phase structure from it. Then we illustrate how the nucleation temperature, the duration and the strength of a first-order phase transition can be deduced from the bubble nucleation rate. In this first part we closely follow Ref. [137]. These three parameters determine the energy spectrum of gravitational waves from bubble collisions. In order to see how the collision of bubbles and the generation of gravity waves is linked, we present the major steps of such a deviation in a two-bubble model, based on Refs. [138, 139]. Then we proceed with the presentation of an analytical model of the gravitational wave energy density spectrum [140] which we will use in the next part of this work.

Be it the conversion from liquid water to ice, the transition from paramagnetism to ferrormagnetism or the generation of a non-zero Vacuum Expectation Value (VEV) of the Higgs particle – phase transitions occur in many types of physical systems from the macroscopic scale to the quantum world. Characteristic for the different phases is the degree of order (associated with a symmetry) that they exhibit which is typically represented by an order parameter ϕ that is zero in the disordered phase (symmetric phase) and non-zero in the ordered one (asymmetric phase). A transition between the old phase ϕ_{old} and the new phase ϕ_{new} occurs when - with changing temperature T - the configuration of the new phase begins to minimize the system's free energy density instead of the old phase [141]

$$f(\phi, T) = -\frac{T}{V} \ln Z(\phi, T). \tag{3.1}$$

Here V is the system volume and $Z(\phi, T)$ the partition function. The change in the value of the order parameter implies a change in the symmetry that the free energy density obeys. In the case that the system converts from a high temperature phase to a low temperature phase the symmetry is reduced, while the opposite transition restores the full symmetry of the system.

One distinguishes between different types of phase transitions. According to the classification by Paul Ehrenfest [142] a phase transition is of second order when the second derivative of the energy density $\frac{\partial^2 f}{\partial T^2}$ is discontinuous at the critical temperature T_c at which the two minima are degenerate $f(\phi_{\text{old}}, T_c) = f(\phi_{\text{new}}, T_c)$, while it is of first-order when the entropy density $s = -\frac{\partial f}{\partial T}$ is discontinuous at T_c. Especially, this is the case when the two minima are separated by a barrier which hinders the order parameter to take on the value of the forming global minimum. The state in which the system is kept in the old phase while the new phase would be energetically preferred is called supercooling. In order to end the supercooling phase the barrier must be overcome. Classically, this requires either sufficiently large temperature fluctuations, impurities or external energy [141]. In quantum systems however, there exists also the possibility for the field ϕ to reach the new phase by tunneling through the barrier. This process is of special importance for particle models in which particle masses are generated by a FOPT driven by a scalar field in the early universe that involves the spontaneous breaking of the model symmetry (SSB). As a consequence of this discontinuous process in real space the system does not convert smoothly to the new phase (like it does in a second order phase transition) but rather experiences the nucleation of bubbles that contain the new VEV of ϕ and expand in space until the new phase is reached everywhere. In case of cosmological FOPTs this process has a striking consequence. While expanding, the bubbles collide and thereby produce GWs [143, 144], which remain as relics in the universe and thus offer today a potentially measurable window to the past.

In our current understanding, cosmological phase transitions have happened at least twice during the history of the universe. The first one is the EW phase transition (see e.g. [145–148]) which was driven by the Higgs field and occurred around $T_{\text{EW}} \approx 159.5 \pm 1.5\,\text{GeV}$ [149]. In this transition the EW symmetry of the standard model was

spontaneously broke $SU(2)_L \times U(1)_Y \to U(1)_{QED}$ when the Higgs acquired a VEV of $v_{\text{EW}} = 246\,\text{GeV}$ [19, 20, 150] resulting in masses for all fields that are coupled to it, especially the gauge bosons $W^{\pm}$ and Z^0. If the Higgs mass had been smaller than $\sim 80\,\text{GeV}$, the EW phase transition would have been of first-order [151, 152]. However, as the value of the Higgs mass has been measured by the LHC to be $m_H \approx 125\,\text{GeV}$ [19, 20, 150], the EW phase transition turns out to be a crossover. In these transitions all derivatives of the free energy density with respect to temperature are continuous, leading to smooth conversion between the phases.

The second phase transition in the SM took place at the QCD scale $\Lambda_{\text{QCD}} \approx 100\,\text{MeV}$ [153] which corresponds roughly to $10^{-5}\,\text{s}$ after the big bang (e.g. in a recent calculation the authors find $T_c = 132^{+3}_{-6}\,\text{MeV}$ [154]). The QCD phase transition is subject to extensive current research and many important questions about its nature are still not understood [59], which is mainly due to its non-perturbative nature at these scales. It separates the deconfined and confined phases of quarks and gluons and features the SSB of chiral symmetry when the chiral condensate $\langle\bar{\Psi}\Psi\rangle = \langle\bar{\Psi}_R\Psi_L + \bar{\Psi}_L\Psi_R\rangle$, which serves as the order parameter, becomes non-zero [155]. Here R and L refer to right- and left handed fields. In Tab. 3.1 we give an overview of the two transitions.

However, it has been shown by many authors that extensions of the SM can make the EW as well as the QCD phase transition a FOPT, see e.g. [72, 156]. Moreover, it is very likely that there have been even more phase transitions in the history of the universe. Investigating these beyond the SM theories especially for FOPTs has become a lively field, especially those offering explanations for DM, neutrino masses and the matter-antimatter asymmetry of the universe [60–64, 68, 69]. For recent reviews see [72, 157–160].

The aim of this section is to review the standard procedure from building the effective temperature-dependent potential, inferring the phase transition parameters up to the calculation of the GW energy density from them. We start with the effective potential in the next section.

PT	driving field	SSB	type	critical temperature	features
EW	Higgs field H	EW symmetry	crossover	$\sim 160\,\text{GeV}$	generation of masses for gauge bosons and fermions
QCD	chiral condensate $\langle\bar{\Psi}\Psi\rangle$	chiral symmetry	unknown	$\sim 130\,\text{MeV}$	confinement of quarks and gluons

Table 3.1.: Comparison of the SM phase transitions.

3.1. First-order phase transition in particle physics

3.1.1. The effective temperature-dependent potential

Typically in particle models a phase transition occurs when the VEV of a scalar field changes due to the formation of a new minimum in the free energy density with decreasing temperature. For scalar fields the free energy density coincides with the scalar potential (see e.g. [161]) and hence studying the phase structure of a model requires knowledge about the temperature evolution of the potentials of all involved scalar fields that acquire a VEV. However, the essentials of the mechanism can be understood from a phase transition driven by a single field at which we want to look in the following. The discussion is partially based on appendix A in [162]. Consider a particle model with a scalar field ϕ that is coupled to a set of vector fields (gauge bosons) V , Weyl fermions F and real scalar fields S with $\langle s\rangle(T) = 0\,\forall\, s \in S$ at all temperatures T. The model Lagrangian is denoted $\mathcal{L}(\phi)$ and the tree-level potential[1] $V^{(0)}(\phi) \subset \mathcal{L}(\phi)$ has a non-zero minimum at $T = 0$ such that the VEV is $\langle\phi\rangle\big|_{T=0} =: v_\phi \neq 0$. Most phenomenological studied models are weakly coupled and hence temperature effects can be added to the zero order potential using thermal perturbation theory. In that case the first-order, finite-temperature effective potential of the (classical) field ϕ is given as the following sum

$$V_{\text{eff}}(\phi, T) = V^{(0)}(\phi) + V^{(1)}(\phi) + V_T^{(1)}(\phi, T) + V_{\text{c.t.}}\,. \tag{3.2}$$

In this sum the tree-level potential (zeroth order) is given by the Lagrangian $V^{(0)}(\phi) \subset \mathcal{L}(\phi)$ and the second term is given by the Coleman-Weinberg potential [163] in the $\overline{\text{MS}}$ renormalization scheme at scale μ and degrees of freedom $n_{\{V,F,S\}}$. It reads

$$\begin{aligned} V^{(1)}(\phi) = \frac{1}{64\pi^2}\Bigg\{ &\sum_{v\in V}(m_v^2)^2 \cdot n_v \left[\ln\frac{m_v^2}{\mu^2} - \frac{5}{6}\right] + \sum_{s\in S}(m_s^2)^2 \cdot n_s \left[\ln\frac{m_s^2}{\mu^2} - \frac{3}{2}\right] \\ &- \sum_{f\in F}(m_f^2)^2 \cdot n_f \left[\ln\frac{m_f^2}{\mu^2} - \frac{3}{2}\right]\Bigg\}\,, \end{aligned} \tag{3.3}$$

where $m_i^2 \equiv m_i^2(\phi)$ are the squared field-dependent masses of the particles. The next term denotes the one-loop temperature contributions [137]

$$V_T^{(1)}(\phi) = \frac{T^4}{2\pi^2}\left[\sum_{b\in B} n_b\, J_T^B(m_b(\phi)) - \sum_{f\in F} n_f\, J_T^F(m_f(\phi))\right]\,, \tag{3.4}$$

[1] The tree-level potential depends also on the scalar fields s. For brevity we omit writing this dependence explicitly. In cases where more than one scalar field acquire a VEV multistep phase transitions can occur.

where we have introduced the set of bosons $B := \{V, S\}$ and the thermal functions $J_T^B(m_b)$ and $J_T^F(m_f)$ which are respectively given by

$$J_T^{B/F}(m_{b/f}) := \int_0^\infty \mathrm{d}q\, q^2 \ln\left(1 \mp \exp\left(-\sqrt{q^2 + \frac{m_{b/f}^2}{T^2}}\right)\right). \tag{3.5}$$

If the particle mass is larger than the temperature, $m^2 \gg T^2$, the thermal functions can be expanded as [137]

$$J_T^{B/F}(m_{b/f} \gg T) = \mp\left(\frac{m}{2\pi T}\right)^{\frac{3}{2}} e^{-\frac{m}{T}}\left[1 + \mathcal{O}\left(\frac{T}{m}\right) + \mathcal{O}\left(e^{-\frac{m}{T}}\right)\right] \tag{3.6}$$

and thus thermal effects experience exponential suppression in this regime. In the relativistic regime $m^2 \ll T^2$ on the other hand the expansion reads [137, 164]

$$J_T^B(m_b \ll T) = -\frac{\pi^2}{90} + \frac{m^2}{24T^2} - \frac{m^3}{12\pi T} + \mathcal{O}(m^4), \tag{3.7}$$

$$J_T^F(m_f \ll T) = \frac{7\pi^2}{720} - \frac{m^2}{48T^2} + \mathcal{O}(m^4)\,. \tag{3.8}$$

The interesting observation in this limit is the occurrence of a cubic term for bosons $m^3(\phi)/T$ which is essential for the emergence of a barrier in the effective potential. Obviously, if the critical temperature is much higher than the particle masses at that temperature one can benefit from Eq. (3.7) and Eq. (3.8) and avoid using Eq. (3.5).

Due to the one-loop corrections the minimum of the effective potential at zero temperature does not coincide with the minimum of the tree-level potential. It is useful, however, to have the zero temperature VEV at the tree-level position. To ensure this one shifts the effective potential by the constant counter term $V_{\text{c.t.}}$ upon which one imposes the conditions

$$\left.\frac{\partial(V^{(1)}(\phi) + V_{\text{c.t.}}(\phi))}{\partial\phi}\right|_{\phi=v_\phi} = 0 \quad \text{and} \quad \left.\frac{\partial^2(V^{(1)}(\phi) + V_{\text{c.t.}}(\phi))}{\partial\phi^2}\right|_{\phi=v_\phi} = 0\,. \tag{3.9}$$

and thus the minimum position $\langle\phi\rangle\big|_{T=0} = v_\phi$ and the tree-level mass remain untouched. Depending on the model one may also impose further counter term conditions [165]. With these formulae the first-order potential can be derived for any weakly coupled particle model. There is, however, one important last issue that has to be taken into account before the discussion is complete. It turns out that the thermal perturbation of the free energy density suffers from an infrared divergence which occurs in the limit of massless bosonic fields $m_b \to 0$ [137]. The reason for this are the terms with odd powers of mass which originate from the Matsubara zero mode that is zero, in contrast

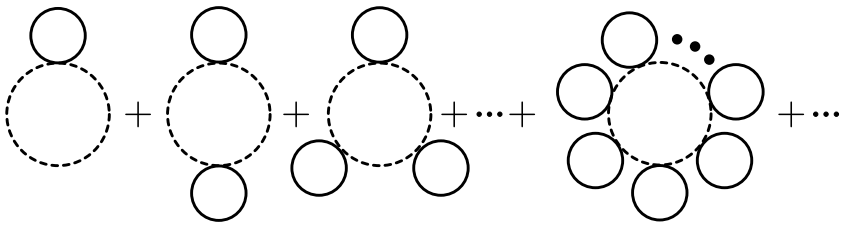

Figure 3.1.: Daisy diagrams showing the zero mode dressed by non-zero modes. While each diagram by in itself is infrared divergent, summing over all diagrams with $N-1$ rings attached yields a finite result (see e.g. Eq. (3.91) in [137])).

to fermions[2] and thus mimics a massless degree of freedom at high temperatures [166]. This obstacle can be solved by resumming Daisy-diagrams, see Fig. 3.1, which reflect the thermal self energy at high temperatures. As a result each boson mass acquires a thermal contribution[3], called the Debye mass

$$m_b^2(\phi) \to m_b^2(\phi) + \Pi_b(T)\,. \tag{3.10}$$

The Debye mass must be calculated for each boson and receives contributions from all couplings of this boson to other fields. It is therefore a sum of terms of the form $\Pi_b(T) \sim g_i T^2$, where g_i depicts the coupling constant to the i^{th} field. The replacement of the boson masses can be rewritten by means of an additional contribution to the effective potential which reads [166–168]

$$\Delta V_{\text{Daisy}}(\phi, T) = \sum_{b\in B} \frac{n_b T}{12\pi}\left[(m_b^2(\phi))^{3/2} - (m_b^2(\phi) + \Pi_b(T))^{3/2}\right] \tag{3.11}$$

and has to be added to the effective potential [169]. Overall the temperature evolution of the effective potential and the VEV is illustrated in Fig. 3.2. The finite temperature contributions lead to a restoration of the unordered vacuum $\langle\phi\rangle(T \gg m_\phi) = 0$ and the full symmetry of the Lagrangian at high temperatures.

If the effective potential in Eq. (3.2) possesses a barrier for a certain set of coupling parameters in $\mathcal{L}(\phi)$ and thus allows for a FOPT the old vacuum may decay into the new vacuum via the nucleation of bubbles. These bubbles enclose the new vacuum and are surrounded by the old one. The probability that the field tunnels into the new minimum is given by the bubble nucleation rate per unit time and unit volume Γ and is of the form [170–172]

$$\Gamma = A(t)\exp(-S_{4\text{E}}(\bar{\phi}, t))\,, \tag{3.12}$$

[2] In thermal quantum field theory the field is Fourier decomposed with respect to imaginary frequencies ω_n, called Matsubara frequencies, in the domain $0 \le \tau \le \hbar/(k_B T)$. For bosons $\omega_n^b \sim 2\pi n T = 0$ for $n = 0$ while $\omega_n^f = (2n+1)\pi T \neq 0$ for all n. The frequencies enter into the partition function and are summed over, leading to the thermal functions $J_T^{B/F}(m_{b/f})$.

[3] More precisely, one has to add the thermal mass matrix to the tree-level boson mass matrix.

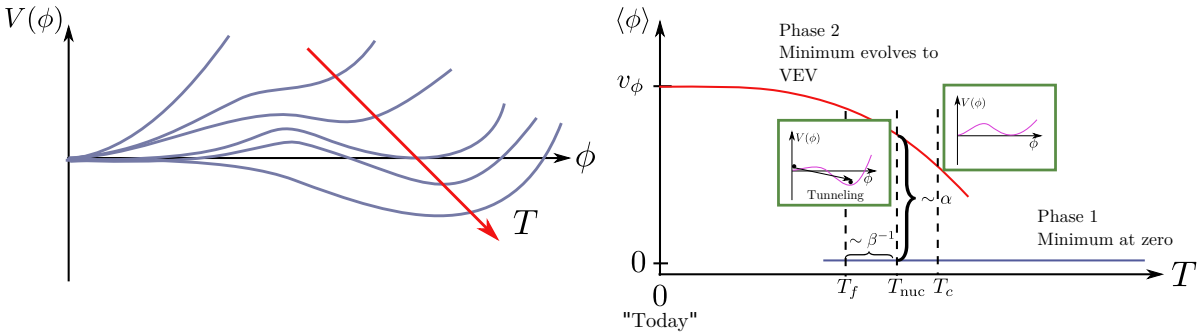

Figure 3.2.: *Left:* Sketch of the thermal evolution of the effective potential $V_{\rm eff}(\phi, T)$ as function of the field value ϕ for a FOPT. *Right:* General temperature-dependent behavior of the VEV $\langle\phi\rangle$ for a FOPT. Highlighted are the most important temperatures. Adapted from Ref. [5].

where $A(t)$ is the amplitude and $S_{4\rm E}(\bar{\phi}, t)$ is the $O(4)$ symmetric Euclidean action of a spherical, critical bubble $\bar{\phi}$ (the instanton solution) which is especially important for vacuum transitions [159]. In most applications the temperature is relatively large, such that the time integration in the action can be carried out and one can replace $S_{4\rm E}$ by the $O(3)$ symmetric action $S_{3\rm E}/T$ which reads

$$S_3 = 4\pi \int_0^\infty r^2 {\rm d}r \left(\frac{1}{2} \left(\frac{{\rm d}\phi}{{\rm d}r} \right)^2 + V_{\rm eff}(\phi, T) \right) . \tag{3.13}$$

The action is minimized by the field configuration that solves the equation of motion

$$\frac{{\rm d}^2\phi}{{\rm d}r^2} + \frac{2}{r}\frac{{\rm d}\phi}{{\rm d}r} = \frac{\partial V_{\rm eff}(\phi)}{\partial\phi} , \tag{3.14}$$

with boundary conditions

$$\phi(r \to \infty) = 0, \quad \left.\frac{{\rm d}\phi}{{\rm d}r}\right|_0 = 0 . \tag{3.15}$$

The form of the instanton solutions at different temperatures are shown in in Fig. 3.3. At low temperature the solution is $O(4)$ symmetric and then gets constantly compressed as temperature increases. One can gain some intuition for the form of the action in the *thin wall limit*. We denote the region of the bubble where the derivative ${\rm d}\phi/{\rm d}r$ is large as bubble wall [173]. The wall is called thin, when the width $|V(0,T) - V(v_\phi, T)| = \Delta p$ (pressure difference between the phases) is smaller than the hight of the barrier. For large enough bubbles, the second term in Eq. (3.14) can be neglected since $2/r{\rm d}\phi/{\rm d}r \ll 1$ and the action becomes [137, 173, 174]

$$S_3(r) = -\frac{4}{3}\pi r^3 \Delta p + 4\pi r^2 S_1(T) \equiv 4\pi r^2 \sigma - \frac{4}{3}\pi r^3 \Delta p , \tag{3.16}$$

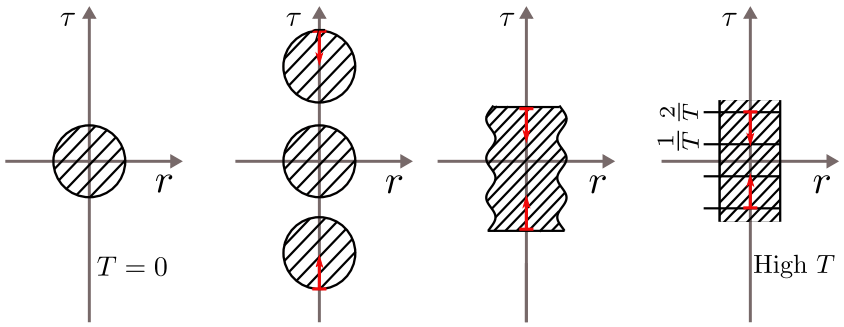

Figure 3.3.: Typical form of instanton solutions as functions of "time" $\tau := 1/T$ and radius $r(T)$. For $T = 0$ the instanton solution of S_{4E} respects 4D rotational symmetry whereas for high temperatures much bigger than the inverse bubble radius the solution get squeezed such that it ultimately respects only a spatial 3D rotational symmetry (last picture) and one uses S_3/T. Plot has been reproduced from [137] and [173].

where $\sigma := S_1 = \int_0^{v_\phi} \mathrm{d}\phi \sqrt{2V(\phi, T)}$ is the surface tension. Extremizing this action with respect to the radius, one finds $r_{\mathrm{ex}} = 2\sigma/\Delta p$, such that the action becomes[4] [137]

$$S_3(r_{\mathrm{ex}}) = \frac{16\pi}{3} \frac{\sigma^3}{(\Delta p)^2} \,. \tag{3.17}$$

For the purpose of this work there are three important parameters that are deduced from the previous discussion so far. The first one is the nucleation temperature T_{nuc} (or time t_{nuc}) which is defined as the temperature at which the probablity $\Gamma(t)$ to nucleate one bubble per Hubble volume is unity [159]. For example, for phase transitions around the EW scale the three-dimensional action has to fulfill the condition[5] $S_3/T_{\mathrm{nuc}} \approx 100$ [174, 177].

Another important parameter is the duration of the phase transition β^{-1}. It can be inferred from the action and is defined as [173, 178]

$$\beta := - \left. \frac{\mathrm{d}S(t)}{\mathrm{d}t} \right|_{t_{\mathrm{nuc}}} \tag{3.18}$$

under the assumption that time-dependent changes in the nucleation rate are mainly due to the action. For practical applications this is reformulated by means of the temperature and relative to the Hubble time at t_{nuc} [179]

$$\frac{\beta}{H_{\mathrm{nuc}}} = T_{\mathrm{nuc}} \left. \frac{\mathrm{d}S}{\mathrm{d}T} \right|_{T_{\mathrm{nuc}}} \,. \tag{3.19}$$

[4] Note that the derivation requries $\Delta p \neq 0$ and thus at least a small phase of supercooling.

[5] A more general condition for the three-dimensional action for phase transitions in a radiation dominated universe can be found in [175] and [176].

With this definition the nucleation rate can also be rephrased

$$\Gamma = \Gamma_{\rm nuc}\, e^{\beta(t-t_{\rm nuc})}\,, \tag{3.20}$$

where β plays the role of the decay rate.

Finally, the third parameter is the strength α of the transition and is closely related to the *latent heat*. The latter describes the energy density difference $\Delta\rho$ at the transition that appears due to the discontinuous behavior of the entropy density and therefore is inherent to any FOPT. From the energy density $\rho = Ts - p$ and the continuity of the pressure at T_c one finds [137]

$$L := -\delta\rho = -T_c\Delta s = -T_c\frac{{\rm d}\Delta p}{{\rm d}T}\,. \tag{3.21}$$

However, it has become conventional to define α as the ratio of the stored energy in the vacuum and the radiation energy density at the nucleation temperature

$$\alpha := \frac{\rho_{\rm vac}}{\rho_{\rm rad}(T_{\rm nuc})}\,, \tag{3.22}$$

where $\rho_{\rm vac} \sim \Delta p(T_{\rm nuc})$. In cases of a strong transition where the derivative ${\rm d}\Delta p/{\rm d}T \sim \Delta p/T_c$ the definitions coincide for $T_c = T_{\rm nuc}$. In the right plot of Fig. 3.2 we have illustrated the meaning of α and the other transition parameters by reference to the temperature evolution of the order parameter. If $\alpha > 1$, then the phase transition is subject to a lot of supercooling and the expansion of bubbles proceeds into a universe dominated by vacuum energy[6]. A FOPT is called strongly first-order if the value of the VEV exceeds the critical temperature $\langle\phi\rangle(T_c)/T_c > 1$ [175] which is for example a necessary condition for successful baryogenesis [71, 180–183].

We have seen in this section how one determines the *nucleation temperature* (time), the duration and the strength of a FOPT from a particle theory. Next, we will discuss how these parameters translate into the released energy density of GWs by a FOPT. To do so, we first have to recall how anisotropic stresses actually produce gravitational radiation.

3.2. Gravitational wave production

The creation of bubbles during a FOPT has a striking consequence. After nucleation the bubbles expand due to the pressure difference Δp between the symmetric and asymmetric phase and eventually collide until the whole space acquired the new VEV. The expansion into the surrounding plasma and the collisions, however, leads to anisotropic stresses in the fluid which serve as seeds of GWs. These in turn provide a potentially observable relic signal today from a FOPT in the early universe. It is this feature which makes the study of FOPTs in particle models so interesting and prominent and has experienced

[6] As we will see later this is the relevant regime for the purpose of this work.

increasing attention due to the advent of GW astrophysics. This section is devoted to summarizing the literature on this topic with a special focus on on GW production in a supercooled phase transition.

Let us denote by t_* the percolation time when GWs are produced. The treatment of GWs inherits two important simplifications from the nature of phase transitions ($H_* = H(t_*)$ is the Hubble time at t_*):

- Phase transitions occur on **sub horizon scales** $k > H_*$.
- Phase transitions complete in **less than a Hubble time** $\beta^{-1} \ll H_*^{-1}$.

Thus the background metric is well described by the Minkowsikian one and any friction and damping due to the expansion of the universe $\sim H\,\dot{f}(t)$ can be neglected. For a Minkowsikian background metric $g^{(0)}_{\mu\nu} = \eta_{\mu\nu}$ the line element that feels a linear perturbation by a traceless ${E^T}^i{}_i = 0$ and transverse $\partial^j E^T_{ij} = 0$ tensor reads

$$\mathrm{d}s^2 = -\mathrm{d}t^2 + (\delta_{ij} + 2E^T_{ij})\mathrm{d}x^i\mathrm{d}x^j\,, \tag{3.23}$$

where δ_{ij} is the Kronecker delta and latin indices denote spatial coordinates. From Einstein's equations one deduces that the tensor $E^T_{ij}(\mathbf{x}, t)$ obeys the wave equation [184, 185] which is driven by the transverse and tracefree component of the anisotropic stress tensor $\Pi^T_{ij}(\mathbf{x}, t)$. Transforming the latter and the tensor $E^T_{ij}(\mathbf{x}, t)$ into Fourier space, yields the equation of motion

$$\ddot{E}^T_{ij}(\mathbf{k}, t) + k^2 E^T_{ij}(\mathbf{k}, t) = 16\pi G\,\Pi^T_{ij}(\mathbf{k}, t)\,, \tag{3.24}$$

where $k := |\mathbf{k}|$. Suppose the source is active for a time interval $[t_*, t_f]$, then the solution can be expressed by means of a Green's function and matched on the boundaries to the homogeneous solution. This results in a wave function [140, 186, 187]

$$E^T_{ij}(\mathbf{k}, t) = A_{ij}(\mathbf{k})\sin(k(t - t_f)) + B_{ij}(\mathbf{k})\cos(k(t - t_f))\,, \tag{3.25}$$

with source-dependent coefficients

$$\begin{aligned} A_{ij}(\mathbf{k}) &= \frac{8\pi G}{k}\int_{t_*}^{t_f} \mathrm{d}t\cos(k(t_f - t))\Pi^T_{ij}(\mathbf{k}, t) \quad \text{and} \\ B_{ij}(\mathbf{k}) &= \frac{8\pi G}{k}\int_{t_*}^{t_f} \mathrm{d}t\sin(k(t_f - t))\Pi^T_{ij}(\mathbf{k}, t)\,. \end{aligned} \tag{3.26}$$

For observational purposes the interesting quantity is the energy density $\rho_{\mathrm{GW}}(t)$ which is deduced from Eq.'s (3.25) and (3.26) using

$$\rho_{\mathrm{GW}}(t) := \frac{\langle \dot{E}^T_{ij}\dot{E}^T_{ij}\rangle}{8\pi G} = \int_0^\infty \frac{k^3}{2\pi}|\dot{E}^T(k, t)|^2\mathrm{d}\ln k\,, \tag{3.27}$$

where we have used the isotropy of the system. The stochastic backgrounds of GWs that could be detected by future interferrometer experiments is given in terms of the GW

abundance per logarithmic frequency interval and follows from the total energy density Eq. (3.27) to be

$$\Omega_{\mathrm{GW}}^{\log}(k,t) := \frac{1}{\rho_{\mathrm{tot}}}\frac{\mathrm{d}\rho_{\mathrm{GW}}}{\mathrm{d}\ln k} = \kappa_{\mathrm{eff}}^2\left(\frac{H_*}{\beta}\right)^2\left(\frac{\alpha}{1+\alpha}\right)^2\Delta(k,\beta,t,v_w)\,. \tag{3.28}$$

Hereby is $\Delta(k,\beta,t,v_w)$ the dimensionless GW power spectrum which depends on the wave number k, the bubble wall velocity v_w and the decay rate β and is determined from $\Pi_{ij}^T(k,t)$. The efficiency factor κ_{eff} only plays a role when the bubbles expand into a radiation dominated universe and accounts for the loss of energy to the surrounding plasma [188, 189].

From Eqs. (3.27) and (3.26), it becomes clear that the energy density is of the form $\rho_{\mathrm{GW}}(t_f) \sim \Pi^{T\,2}$ [160] and therefore the challenge lies in an accurate modeling of the anisotropic stress. In the case of transitions into the radiation plasma of the early universe it is additionally necessary to acquire a deep understanding of the bubble wall velocity and dynamics. In this case also magnetohydrodynamic effects and the formation of sound waves play an essential and in some regimes even dominant role [159]. The total anisotropic stress in a realistic study of the GW spectrum from a FOPT accounts for all these sources and therefore the total GW spectrum includes a contribution from bubble collision $\Omega_{\mathrm{BC}}(k)$, sound waves produced by bulk fluid motion $\Omega_{\mathrm{SW}}(k)$ [190–192] and magnetic and hydrodynamical effects $\Omega_{\text{MHD-turb}}(k)$ [193, 194] such that

$$\Omega_{\mathrm{GW}}(k) = \Omega_{\mathrm{BC}}(k) + \Omega_{\mathrm{SW}}(k) + \Omega_{\text{MHD-turb}}(k)\,. \tag{3.29}$$

Which of these sources dominates the spectrum highly depends on the bubble wall dynamics which is commonly divided into the following categories [159]:

- **Weak supercooling:** In a surrounding plasma, bubbles can either reach a terminal velocity or keep accelerating and run away $\gamma := (1-v_w^2)^{-1/2} \gg 1$ [195]. In the first case the $\Omega_{\mathrm{BC}}(k)$ can be neglected while in the latter all contributions matter. In all cases the efficiency factor κ_{eff} has to be taken into account. To good approximation, one can assume that the nucleation temperature and the temperature at which the GWs are released, called *percolation temperature*, are approximately equal $T_* \approx T_{\mathrm{nuc}}$.

- **Strong supercooling:** If the supercooling is strong enough to have $\alpha > 1$, the universe turns temporarily into vacuum domination. In that case all plasma-related contributions as well as the efficiency factor is unity. In this case it will take some time after bubble nucleation until GWs are released $T_{\mathrm{nuc}} \ll T_* \approx T_{\mathrm{reh}}$ and the universe is reheated. However, it still holds $H_* \approx H_{\mathrm{nuc}}$. The only relevant term in Eq. (3.29) is Ω_{BC}, since the vacuum energy dominates and thus plasma effects vanish.

In this work we focus on the latter case in which bubbles expand into a vacuum dominated universe. The reason will become clear in the next part of this thesis. Therefore, we are interested in the calculation of $\Omega_{\mathrm{GW}} \equiv \Omega_{\mathrm{BC}}$. In order to show, how we come from

the collision of bubbles to the generation of anisotropic stress and in turn to GWs, we present in the following subsection the result for a simplified model for two colliding bubbles from the beginning of the 1990s. This model, however, only provides a rough idea. Over the last decades, more and more elaborated studies have been performed with ever refined modeling of the anisotropic stress and the dimensionless power spectrum $\Delta(k, \beta, t, v_w)$, both numerically [196–198] and analytically [186, 187, 199–201] .

3.2.1. Vacuum collision of two bubbles

In order to gain some intuition how bubble collisions produce anisotropic stress and in turn source GWs we show here a simplyfied derivation of $\Pi_{ij}^T(t, k)$ first presented in Refs. [138, 139] which we closely follow. When talking about the generation of gravitational radiation, in the first thought that is immediately triggered one would ask for the occurrence of a time varying quadrupole moment. To reflect this, we will single out the quadrupole term in the energy momentum tensor and use it to derive the GW energy density.

The energy momentum tensor of a spherically symmetric bubble is given by

$$T_{\mu\nu} = \partial_\mu\phi\partial_\nu\phi - g_{\mu\nu}\mathcal{L}(\phi)\,. \tag{3.30}$$

However, the second term does not possess any spatial anisotropy and is thus irrelevant for the generation of gravitational radiation. Therefore, it is sufficient to look at

$$T_{ij} = \partial_i\phi\partial_j\phi\,. \tag{3.31}$$

Transforming the energy momentum tensor Eq. (3.31) to Fourier space both in time and space one obtains (we follow here the convention used in the literature for the Fourier transforms.)

$$T_{ij}(\mathbf{k}, \omega) = \frac{1}{2\pi}\int \mathrm{d}t\, e^{i\omega t}\int \mathrm{d}^3x\, \partial_i\phi\partial_j\phi\, e^{-i\mathbf{k}\cdot\mathbf{x}}\,, \tag{3.32}$$

where frequency ω and wave number k_μ are related via the null-condition $k_\mu k^\mu = |\mathbf{k}|^2 - \omega^2 = 0$. Next, we apply two approximations to the energy momentum tensor. First, we employ the quadrupole approximation which states $e^{ikx} \to 1$. Second, we assume that the contribution to the GW energy density of already collided bubble wall segments is negligible. This is called *envelope approximation* and allows us to separate the surface integration from the integration over the bubble radius. Imposing also spherical symmetry on the uncollided bubbles, ϕ and its derivatives are purely radial. Applying these assumption to the energy momentum tensor leads to

$$T_{ij}^Q = \frac{1}{2\pi}\int \mathrm{d}t\, e^{i\omega t}\int_{\mathcal{S}} \mathrm{d}\Omega \int \mathrm{d}r\, r^2(\mathbf{e}_i \otimes \mathbf{e}_j)\left(\frac{\partial\phi}{\partial r}\right)^2\,, \tag{3.33}$$

where $\mathbf{e}_i$ is the unit vector ($(\mathbf{e}_i \otimes \mathbf{e}_j) \equiv \mathbf{e}_i\mathbf{e}_j$) in the i^{th} direction and $\mathcal{S}$ is the bubble

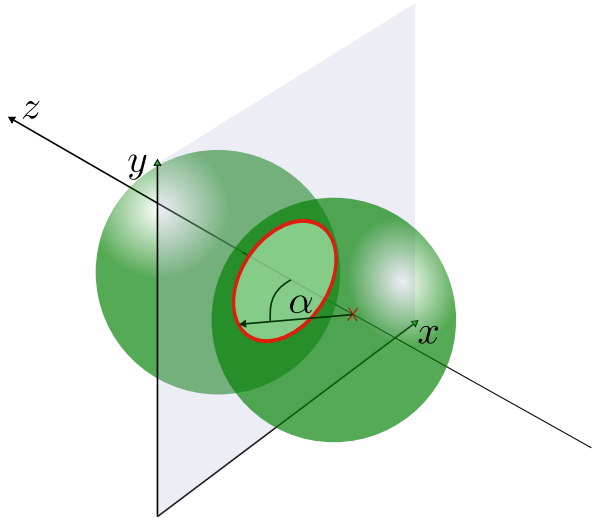

Figure 3.4.: Schematic illustration of two colliding bubbles with equidistant centers from the origin aligned on the z-axis. The right bubble has a hole in its north pole measured by the angle α. From the point of view of the other bubble the hole is at its south pole.

surface. Next, we have to deal with the radial derivative of ϕ. To this end, let us have a look to the zero-zero component of the energy momentum tensor

$$T_{00}(x,t) = \frac{1}{2}\left[\left(\frac{\partial\phi}{\partial t}\right)^2 + \left(\frac{\partial\phi}{\partial r}\right)^2\right] + V(\phi,t)\,. \tag{3.34}$$

It has been shown in Ref. [139] that the gradient energy of the field roughly corresponds to the kinetic energy of the system and also that the potential becomes successively irrelevant once the bubble radius becomes bigger and the bubble wall thinner (*thin wall approximation*). Consequently the energy $E(t)$ of the bubble is

$$E(t) = \frac{4\pi}{3} r(t)^3 \rho_{\text{vac}} \approx 4\pi \int \mathrm{d}r\, r^2 \left[\frac{1}{2}\left(\frac{\partial\phi}{\partial t}\right)^2 + \frac{1}{2}\left(\frac{\partial\phi}{\partial r}\right)^2\right] \approx 4\pi \int \mathrm{d}r\, r^2 \left(\frac{\partial\phi}{\partial r}\right)^2 , \tag{3.35}$$

where $r(t)$ is the time-dependent bubble radius and ρ_{vac} is the energy density difference between disordered and ordered vacuum. Replacing the radial derivative using Eq. (3.35) we observe that we have isolated a quadrupole moment like term of the energy momentum tensor of a collided bubble

$$T^Q_{ij} = \frac{1}{6\pi}\int \mathrm{d}t\, e^{i\omega t} \int_{\mathcal{S}} \mathrm{d}\Omega \int \mathrm{d}r\, r^2\, \mathrm{e}_i \mathrm{e}_j \underbrace{T_{00}}_{E(t)} = \frac{\rho_{\text{vac}}}{6\pi}\int \mathrm{d}t\, r^3(t)\, e^{i\omega t} \int_{\mathcal{S}} \mathrm{d}\Omega\, \mathbf{e}_i \mathbf{e}_j\,. \tag{3.36}$$

For vacuum transitions, the bubbles are expected to expand with the speed of light,

$r(t) = ct$, and thus it remains to solve the spherical integration. The latter is the origin of the breaking of spherical symmetry and hence the source of anisotropy: due to the collision with another bubble, in the envelope approximation, our probe bubble can be viewed as a sphere with a circular hole in it which expands with time. To account for this consider the following configuration: The center of two bubbles nucleated at $t = 0$ are separated by the distance d and aligned along the z-axis. When the bubbles touch at $t = d/2$ at $z = 0$ the bubble at $z = +d/2$ obtains a hole at its south pole and the bubble placed at $z = -d/2$ develops a hole at the north pole. The polar angle of the hole shall be denoted by α and changes with time like $\cos\alpha(t) = d/(2t)$ for $t > d/2$ (see Fig. 3.4). For the two bubble system the energy momentum tensor becomes

$$T_{ij}^{Q} = \frac{\rho_{\text{vac}}}{6\pi}\int_0^\infty \mathrm{d}t\, e^{i\omega t}t^3\left[\underbrace{\int_0^{\pi-\alpha(t)}\mathrm{d}\theta\sin\theta\int_0^{2\pi}\mathrm{d}\phi\,\mathbf{e}_i\mathbf{e}_j}_{\text{Bubble at}-d/2} + \underbrace{\int_{\alpha(t)}^{\pi}\mathrm{d}\theta\sin\theta\int_0^{2\pi}\mathrm{d}\phi\,\mathbf{e}_i\mathbf{e}_j}_{\text{Bubble at}+d/2}\right]. \tag{3.37}$$

Expressing the normed basis vectors $\mathbf{e}_i$ in terms of spherical coordinates and performing the integration over ϕ and θ gives

$$T_{xx} = T_{yy} = \frac{\rho_{\text{vac}}}{3}\int_{d/2}^\infty \mathrm{d}t\, e^{i\omega t}\left[\frac{2}{3}t^3 + \frac{d}{2}t^2 - \frac{d^3}{24}\right]C(t)\,, \tag{3.38}$$

$$T_{zz} = \frac{2\rho_{\text{vac}}}{9}\int_{d/2}^\infty \mathrm{d}t\, e^{i\omega t}\left(t^3 + \frac{d^3}{8}\right)C(t)\,, \tag{3.39}$$

where the function $C(t)$ is a time cutoff that accounts for the finite duration of the phase transition and is non-zero between t_{nuc} (here $= 0$) and $t_f = \beta^{-1}$ (see Ref. [188] for an example). Finally, with this we are ready to calculate the total energy released in form of GWs. Within our approximations the total GW energy per frequency interval is simply the contraction of the anisotropic stresses which emerge from the traceless and transverse projector $\Lambda_{ij,lm}(\mathbf{k})$ of the energy momentum tensor

$$\frac{\mathrm{d}E}{\mathrm{d}\omega\mathrm{d}\Omega} = 2G\omega^2\underbrace{\Lambda_{ij,lm}(\mathbf{k})T_{ij}^*(\mathbf{k},\omega)T_{lm}(\mathbf{k},\omega)}_{\sim\Pi^2(\mathbf{k},\omega)}\,, \tag{3.40}$$

where $\Lambda_{ij,lm}(\mathbf{k}) = P_{ik}P_{jl} - 1/2P_{ij}P_{kl}$ and $P_{ij} := \delta_{ij} - k_ik_j$ and $\Pi_{ij}(\mathbf{k},\omega) = \Lambda_{ij,lm}T_{lm}(\mathbf{k},\omega)$. From this the GW energy liberated from the collision of two bubbles in the envelope and quadrupole approximation is $T_{ij} = \Delta(\omega)\delta_{iz}\delta_{jz}$

$$\frac{\mathrm{d}E}{\mathrm{d}\omega} = \frac{32\pi}{15}G\omega^2|\Delta(\omega)|^2\,, \quad \text{with} \quad \Delta(\omega) := T_{zz} - \frac{1}{2}(T_{xx} - T_{yy})\,. \tag{3.41}$$

Let us emphasize that it turns out that the quadrupole approximation overestimates the result of the full linearized gravity calculation, see appendix B in Ref. [138]. According to

the same Ref. this is due to the fact that we have not performed a far field approximation, distance $\gg$ wavelength (and hence also the result does *not* exactly coincide with the quadrupole moment, see Ref. [202]). In this section we have closed the gap between the collision of bubbles and the appearance of anisotropic stresses in a simple model. We close the discussion with Eq. (3.41) that estimates the energy liberated into GWs from the transverse parts of the anisotropic stress tensor.

3.2.2. Model of the gravitational wave spectrum in vacuum transitions

An appropriate analytic model of the GW dimensionless power spectrum $\Delta(k, \beta, t, v_w)$ was given by Caprini et. al. in Ref. [140]. It especially applies to the case of bubbles expanding into a vacuum dominated universe, which as we discussed, is related to a phase transition with a substantial amount of supercooling. As it will turn out this most suitable for the purpose of this work [5]. In Ref. [140] the dimensionless power spectrum for a phase transition starting at time t_* and lasting until $t_f := t_* + \beta^{-1}$ producing bubbles with velocity v_w is modeled by a broken rational function $f(k,t)$ of the form

$$f(k,t)^2 = L(t)^2 \left(\frac{v_w \epsilon}{\beta}\right) \left(\frac{1 + (\frac{kL}{3})^2}{1 + (\frac{kL}{2})^2 + (\frac{kL}{3})^6}\right) , \tag{3.42}$$

where ϵ is a small parameter and $L(t)$ is the characteristic length scale of the transition

$$L(t) = \frac{v_w}{\beta} g(t). \tag{3.43}$$

The function $g(t)$ incorporates all time dependencies

$$g(t) = 4\beta^2 (t - t_*) \left(\frac{1}{\beta} - (t - t_*)\right) \left[\Theta_{\mathrm{Hv}}\left(t - t_*\right) \cdot \Theta_{\mathrm{Hv}}\left(\frac{1}{\beta} - t_*\right)\right] , \tag{3.44}$$

where Θ_{Hv} denotes the Heaviside step function. Then the dimensionless power spectrum at a time $t \leq t_f$ is given by

$$\Delta(k, \beta, t, v_w) = \beta^2 k^3 \left| \int_{t_*}^{t} f(k, \tilde{t}) e^{i\tilde{t}k} \mathrm{d}\tilde{t} \right|^2 \approx k^3 \beta^2 (t - t_*)^2 f^2(k, (t + t_*)/2) , \tag{3.45}$$

where in the last step we have approximated the integral by its mean value. The functions above use the fact that phase transitions are taking place on sub-horizon scales and that they proceed within a Hubble time $\beta \gg H_*$. This allows to omit the scale factor from the calculation and work in Minkowsiki space. However, for transparency reasons we will keep the scale factor in our calculations in the next part of this work and therefore we replace $k \to k/a_*$ here. Also it is convenient to rescale the time and the wave number variables by means of the Hubble constant H_* at the transition (note that also for vacuum

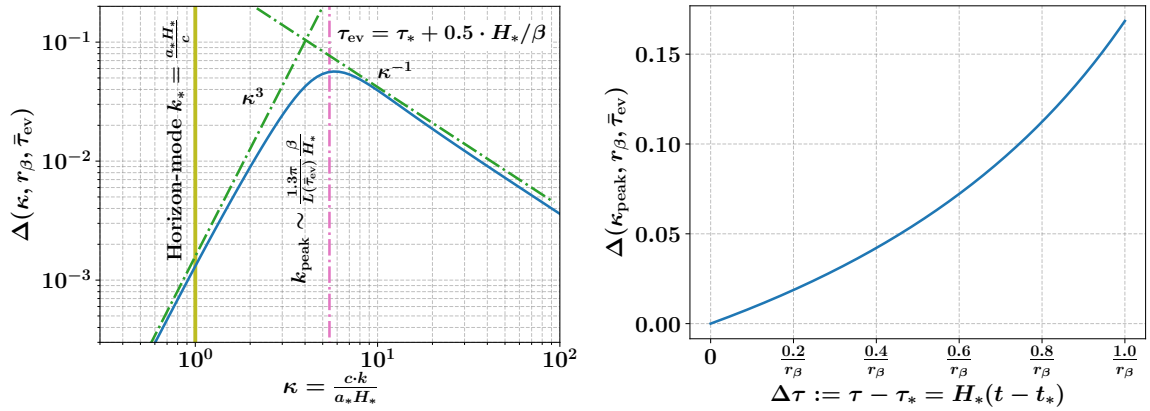

Figure 3.5.: *Left:* Approximated form of the dimensionless power spectrum in the middle of the phase transition $\tau = \tau_* + 0.5 \cdot H_*/\beta$ and its small and high κ behavior. *Right:* The peak of the dimensionless power spectrum as a function of rescaled time. The mean time is $\bar{\tau}_{\rm ev} := \frac{\tau_{\rm ev}+\tau_*}{2}$ and $\Delta\tau_{\rm ev} := \tau_{\rm ev} - \tau_*$ is the time difference. Adopted from [5].

transitions $H_* \approx H_{\rm nuc}$ holds [159]). Introducing also the dimensionless, inverse duration ratio r_β, we have

$$\tau := H_* \cdot t\,, \quad \kappa := \frac{ck}{a_* H_*} \quad \text{and} \quad r_\beta := \frac{\beta}{H_*}\,. \tag{3.46}$$

We have also reintroduced the speed of light c for better readability. Obviously, the length scale $L(t)$ times the wave number is a scale invariant product which we can easily rescale:

$$k/a_* \cdot L(t) = \frac{k}{a_* H_*} \cdot H_* \cdot \frac{c}{\beta} \left(\frac{v_w}{c}\right) g(t) = \kappa \left(\frac{v_w}{c}\right) \left(\frac{H_*}{\beta}\right) \tilde{g}(\tau) = \kappa L(\tau)\,. \tag{3.47}$$

The rescaled version of the time dependence $\tilde{g}(\tau)$ reads

$$\tilde{g}(\tau) = 4 r_\beta^2 (\tau - \tau_*) \left(\frac{1}{r_\beta} - (\tau - \tau_*)\right) \Theta_{\rm Hv}(\tau_*, \tau_* + r_\beta^{-1})\,, \tag{3.48}$$

and the broken rational function $f(\kappa, \tau)$ yields

$$k^3 f(k,t) = \kappa^3 f^2(\kappa, \tau) = \big(\kappa L(\tau)\big)^2 \left(\kappa \frac{v_w}{c} \frac{\epsilon}{r_\beta}\right) \left(\frac{1 + \left(\frac{\kappa L(\tau)}{3}\right)^2}{1 + \left(\frac{\kappa L(\tau)}{2}\right)^2 + \left(\frac{\kappa L(\tau)}{3}\right)^6}\right)\,. \tag{3.49}$$

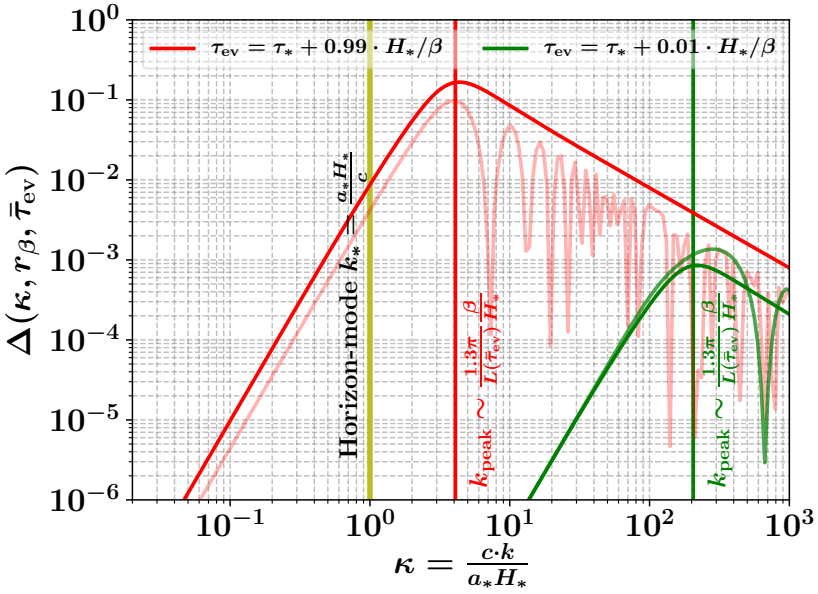

Figure 3.6.: The dimensionless power spectrum with and without the approximation of the time integration (bold and light lines) in Eq. (3.45) almost at the end and the beginning of the phase transition (red and green). The horizon mode is indicated by the yellow line. Adopted from [5].

With this we obtain the rescaled GW energy density fraction at time τ from the energy density fraction per logarithmic frequencies interval Eq. (3.28) and find

$$\Omega_{\mathrm{GW}}(\kappa, \tau) = \kappa_{\mathrm{eff}}^2 (\tau - \tau_*)^2 \left(\frac{\alpha}{1+\alpha}\right)^2 \int_1^\kappa \mathrm{d}\tilde{\kappa} \tilde{\kappa}^2 f^2 \left(\tilde{\kappa}, \frac{(\tau + \tau_*)}{2}\right) , \tag{3.50}$$

where $k_* := a_* H_*/c$ is the mode entering the horizon at t_* and thus $\kappa_* = 1$. Note, that for vacuum transitions $v_w = c$ and $\kappa_{\mathrm{eff}} = 1$ as mentioned earlier.

Comparing this model with more elaborated works like [187] suggests that $\epsilon = 0.01$ is a good choice. This results in the dimensionless power spectrum shown in the left plot in Fig. 3.5 in the middle of the transition $\tau_{\mathrm{ev}} = \tau_* + 0.5\, r_\beta^{-1}$. We have highlighted the three major features that GW spectra typically appreciate. Namely,

- The peak of the spectrum is approximately around $\sim k_{\mathrm{peak}}(\tau_*) = \frac{1.3\,\pi\,\beta}{c \cdot L(\tau_{(\mathrm{ev}} + \tau_*)/2)}$ and approaches $\frac{2\,\pi\,\beta}{c}$ at the end of the transition.
- The spectrum behaves as k^3 for small wave numbers.
- For large wave numbers the spectrum decreases as k^{-1}.

The progression of the maximum $\Delta(\kappa_{\mathrm{peak}}(\tau), \tau)$ is presented in the right plot in Fig. 3.5 and reflects the growth of GW energy density towards the end of the FOPT. Finally, in Fig. 3.6 we have plotted the resulting $\Delta(\kappa, \tau)$ from the approximation of the time-integral

used in Eq. (3.45) against the full solution. Apart from an overall oscillation pattern which is also not found in numerical calculations [187], the approximation we propose here resembles the full solution to a satisfying degree.

Part II

Results

Chapter 4

Density Perturbations at Second Order

The goal of this chapter is to derive an equation of motion for density perturbations related to gravitational waves. Since at linear order density fluctuations and tensor perturbations do not interact with each other, we need to go to second order in perturbation theory. Therefore, we perform a second order expansion in perturbation theory using the non-linear Eqs. (2.72) and (2.73), which drive the evolution of the density gradient in the 1+3 covariant approach. To do so, we first introduce our fluid model and adapted the non-linear equations to the two essential quantities we are interested in, namely the comoving density gradient and the transverse shear tensor, which corresponds to GWs. Then, we carry out the perturbation and finally find a wave equation for second order density perturbations driven by various types of couplings between the shear tensor and first order density perturbations. On a FLRW background, we investigate the equation in the matter dominant regime and the radiation dominant regime. In the former case we compare our results with existing literature Ref. [135] in which a similar calculation was performed. The equation found for a radiation dominated universe, however, is the relation which we will use in the next chapter to analyze the impact of gravitational radiation from a first-order phase transition on structure formation. This chapter is built upon chapter 3 in Ref. [5].

From inflationary models we are familiar with the concept that GWs are sourced by density perturbations, e.g. Ref. [57, 203–205]. In this context, Einstein's equations are expanded to second order in perturbation theory and, under certain assumptions, one derives a wave equation for the second order transverse tensor $E_{ij}^{T\,(2)}$, sourced by linear perturbations of the Bardeen potentials. Conversely, in this work, we seek for an equation in which second order density perturbations $\delta^{(2)}$ are directly connected to GWs.

We chose to tackle this task by using the 1+3 covariant formulation of cosmological perturbation theory, which we introduced in Sec. 2.2.5. There we discovered that the role of GWs is played by the shear tensor σ_{ab} while the comoving density contrast Δ resembles what we usually denote as density fraction δ. By a first observation of the non-linear Eqs. (2.72) and (2.73) we notice that they feature several promising terms like $\sigma^b{}_a\Delta_b$ or $-2a\mathrm{D}_a\sigma^2$ (recall the magnitude of the shear $\sigma^2 = 1/2\sigma^{ab}\sigma_{ab}$). Potentially, if these terms survive the perturbative calculation, they could serve as the desired coupling. Thus we aim to isolate the shear together with the density gradient and derive an equation that connects both such that the evolution of the latter is affected by the presence of the former[1]. However, we need to expand the equation to second order to make more concrete statements. To do so, we employ the following strategy: First we outline our model by introducing several requirements that are chosen such that they can also apply for the typical situation of a phase transition in the early universe. Then we expand the remaining quantities to second order. By doing so, we lose the property of gauge invariance[2] (see Ref. [207, 208] for a discussion of gauge invariant perturbation theory at second order). The resulting equation is given in most possible generality (we neither specify the background nor neglect the cosmological constant Λ at first) before we fix the background to a FLRW space-time and investigate the radiation and matter dominated regime. For brevity we set $\kappa = 8\pi G = 1$ in this chapter.

4.1. Second order expansion of the comoving density gradient

For better clarity, in this first part of the calculation we condense the zeroth, first and second order series elements of a variable f into one label,

$$f = \underbrace{f^{(0)} + f^{(1)} + f^{(2)}}_{\equiv f} + \mathcal{O}(\epsilon^3)\,. \tag{4.1}$$

If the variable f is gauge invariant to first order in our cases this implies $f^{(0)} = 0$ and thus triple combinations of these variables are at least of third order $f^3 \leq \mathcal{O}(\epsilon^3)$. Therefore, such terms can already be excluded in the following without explicitly carrying out the expansion of the variables.

We impose to our fluid the following conditions [5]:

[1] For a relation between the density gradient and the vorticity tensor, see Ref. [206].
[2] We will comment on this in the next chapter.

Assumption 1 The background fluid is perfect and to the relevant perturbative orders the contributions of the current density and the anisotropic stress are negligible $q_a = \pi_{ab} = 0$.

Assumption 2 There is no vorticity $\omega_{ab} = \omega_a = 0$.

Assumption 3 The fluid is barotropic, which means the equation of state can be written in the form $p = \omega\rho$.

Assumption 4 The density perturbations are adiabatic $\delta p/\delta\rho = c_s^2$ and we demand that derivatives vanish $\mathrm{D}_a\omega = \dot{\omega} = \mathrm{D}_a c_s^2 = \dot{c}_s^2 = 0$.

Assumption 5 The background is FLRW.

From **Assumption 1** - **Assumption 4** we draw the immediate and important consequence from the conservation Eq. (2.62) that the four-acceleration is

$$A_a^{(i)} = -\frac{c_s^2 \Delta_a^{(i)}}{a(1+\omega)} \quad \text{with} \quad \mathrm{D}_a p^{(i)} = \frac{\rho}{a} c_s^2 \Delta_a^{(i)}\,, \tag{4.2}$$

for the $i^{\text{th}} = 1, 2$ order. Applying this relation and setting $\pi_{ab} = \omega_{ab} = q_a = 0$ due to **Assumption 1** - **Assumption 2** the non-linear Eqs. (2.72) and (2.73) simplify to

$$\dot{\Delta}_{\langle a\rangle} = \omega\Theta\Delta_a - (1+\omega)\, Z_a - \sigma_{ab}\Delta^b, \tag{4.3}$$

$$\begin{aligned}\dot{Z}_{\langle a\rangle} = &-\frac{2}{3}\Theta Z_a - \left(1+3c_s^2\right)\frac{\rho}{2}\Delta_a - \frac{c_s^2}{1+\omega}\dot{\Theta}\Delta_a - \frac{c_s^2}{a(1+\omega)}\mathrm{D}_a\Delta - \sigma_{ab}Z^b \\ &- 2a\mathrm{D}_a\sigma^2 + \frac{c_s^4}{a(1+\omega)^2}\mathrm{D}_a\left(\Delta^b\Delta_b\right)\,.\end{aligned} \tag{4.4}$$

Recall that the angled brackets denote projected quantities, or to be more precise $\dot{\Delta}_{\langle a\rangle} := h^b{}_a\dot{\Delta}_b$. Though Δ_a is a projected quantity by itself, it's time derivative can exhibit parts that are locally parallel to the fluid flow lines. Resolving the derivative using the inverse product rule makes this apparent

$$\dot{\Delta}_{\langle a\rangle} = (\dot{h_a^b\Delta_b}) - \dot{h}_a^{\ b}\Delta_b\,. \tag{4.5}$$

However, the spatial projection of a spatial quantity leaves it unchanged $h_a{}^b\Delta_b = \Delta_a$ and furthermore its projection along the velocity vector vanishes $u^a\Delta_a = u^a h_a^{\ b}\nabla_b = 0$. The latter applies to the second term in

$$\dot{h}_a^{\ b}\Delta_b = (u_a A^b + u^b A_a)\Delta_b = u_a A^b\Delta_b\,, \tag{4.6}$$

where we have used the identity for $\dot{h}_{ab}$ given in appendix B.1. In total, the projected time variation of the comoving density gradient becomes

$$\dot{\Delta}_{\langle a\rangle} = \dot{\Delta}_a - u_a A^b\Delta_b\,. \tag{4.7}$$

This result reflects what we would expect. Namely that the total time derivative of the density gradient splits into the temporal variation between the world lines and a contribution along the fluid flow. Using Eq. (4.2), the projected time variation of the density gradient is entirely determined by density gradients

$$\dot{\Delta}_{\langle a\rangle} = \dot{\Delta}_a + u_a \frac{c_s^2}{a(1+\omega)} \Delta^b \Delta_b \,. \tag{4.8}$$

With the same arguments, the time variation of the comoving volume gradient separates in an analog manner

$$\dot{Z}_{\langle a\rangle} = h_a{}^b \dot{Z}_b = \left(h_a{}^b \dot{Z}_b\right) - \dot{h}_a{}^b Z_b = \dot{Z}_a - u_a A^b Z_b \,. \tag{4.9}$$

Replacing the projected time derivatives in Eqs. (4.3) and (4.4) leads us to the first interim result

$$\dot{\Delta}_a + u_a \frac{c_s^2}{a(1+\omega)} \Delta^b \Delta_b = \omega \Theta \Delta_a - (1+\omega) Z_a - \sigma_{ab} \Delta^b, \tag{4.10}$$

$$\begin{aligned} \dot{Z}_a + u_a \frac{c_s^2}{a(1+\omega)} \Delta^b Z_b = &- \frac{2}{3} \Theta Z_a - \left(1 + 3c_s^2\right) \frac{\rho}{2} \Delta_a - \frac{c_s^2}{1+\omega} \dot{\Theta} \Delta_a - \frac{c_s^2}{a(1+\omega)} \mathrm{D}_a \Delta \\ &- \sigma_{ab} Z^b - 2a \mathrm{D}_a \sigma^2 + \frac{c_s^4}{(1+\omega)^2 a} \mathrm{D}_a \left(\Delta^a \Delta_a\right) . \end{aligned} \tag{4.11}$$

4.2. Scalar density variations

We find the scalar density variation from the comoving density gradient by acting with the comoving divergence on the latter $\Delta := a\mathrm{D}^a \Delta_a$. The analog holds true for scalar part of the comoving volume gradient $Z := a\mathrm{D}^a Z_a$. Therefore, in order to convert the equations for the gradients Eqs. (4.10) and (4.11) to scalar equations, we need to apply the comoving divergence to them. We first address Eq. (4.10) and then turn to Eq. (4.11). Each time we go through the equations term by term.

4.2.1. Comoving divergence of the comoving fractional density gradient

The comoving divergence of the first term on the left hand side of Eq. (4.10) has already been calculated in the literature[3]. Quoting the result [135]

$$\begin{aligned} a\mathrm{D}^a \dot{\Delta}_a =& a h^{ab} \nabla_b u^c \nabla_c \Delta_a + a h^{ab} u^c \nabla_b \nabla_c \Delta_a \\ =& \dot{\Delta} + \sigma^{ab} \Delta_{\langle ab\rangle} - \omega^{ab} \Delta_{[ab]} + \frac{1}{3} a \Theta A^a \Delta_a - a A^a \dot{\Delta}_a - a q^a \Delta_a \\ &+ a \left(\sigma^{ab} + \omega^{ab}\right) \Delta_a A_b \,. \end{aligned} \tag{4.12}$$

[3] In general $\mathrm{D}_a \dot{f} = \mathscr{L}_u (\mathrm{D}_a f) - \dot{f} A_a$ [86].

Note that here we made use of the splitting of Δ_a into shear distortions and rotational variations, Eq. (2.71), and that the properties of these components naturally assigns σ_{ab} to $\Delta_{\langle ab\rangle}$ and ω_{ab} to $\Delta_{[ab]}$. Thanks to **Assumption 1** and **Assumption 2** most of the terms on the right hand side vanish. Additionally Eq. (4.2) allows us to replace the acceleration by the density gradient and thus Eq. (4.12) reduces at second order to

$$\begin{aligned} a\mathrm{D}^a\dot{\Delta}_a &= \dot{\Delta} + \sigma^{ab}\Delta_{\langle ab\rangle} - \frac{c_s^2}{3(1+\omega)}\Theta\Delta^a\Delta_a + \frac{c_s^2}{1+\omega}\Delta^a\dot{\Delta}_a + \mathcal{O}(\epsilon^3) \\ &= \dot{\Delta} + \sigma^{ab}\Delta_{\langle ab\rangle} + \frac{c_s^2}{1+\omega}\left[\frac{1}{2}\frac{\mathrm{d}}{\mathrm{d}t} - \frac{1}{3}\Theta\right]\Delta^a\Delta_a\,. \end{aligned} \tag{4.13}$$

Moving on to the second term in Eq. (4.10), we observe that although the product rule generates three terms only the derivative of u_a survives due to $u^a\mathrm{D}_a = 0$ and hence

$$a\mathrm{D}^a u_a \frac{c_s^2}{a(1+\omega)}\Delta^b\Delta_b = \frac{c_s^2}{a(1+\omega)}\Delta^b\Delta_b\, a\mathrm{D}^a u_a = \frac{c_s^2}{(1+\omega)}\Delta^b\Delta_b\Theta\,. \tag{4.14}$$

Turning to the right hand side of Eq. (4.10), we calculate the divergence of the first term to be

$$a\mathrm{D}^a\omega\Theta\Delta_a = \omega(Z^a\Delta_a + \Theta\Delta)\,, \tag{4.15}$$

while the second term becomes

$$-(1+\omega)a\mathrm{D}^a Z_a = -(1+\omega)Z\,. \tag{4.16}$$

Recall that the scalars are defined as $\Delta := a\mathrm{D}^a\Delta_a$ and $Z := a\mathrm{D}^a\Delta_a$. The last term concerns the derivative of the shear tensor. First of all, it should be noted that the coupling $\sigma_{ab}\Delta^b$ is at least of second order due to the fact that the shear as well as the density gradient vanish at zeroth order. The space-like constraint Eq. (2.66) requires that $\mathrm{D}^b\sigma_{ab} \neq 0$ in general and thus the shear would not be transverse. However, since here we only consider gravitational radiation as a source of shear distortions we can demand $\mathrm{D}^b\sigma_{ab} = 0$ in accordance with Ref. [86, 132, 135]. As a result the divergence of the shear-densiy gradient coupling simplifies significantly

$$\begin{aligned} a\mathrm{D}^a(-\sigma_{ab}\Delta^b) &= -(a\underbrace{\mathrm{D}^a\sigma_{ab}}_{=0}\Delta^b + a\,\sigma_{ab}\mathrm{D}^a\Delta^b) \\ &= -\sigma_{ab}\left(\frac{1}{2}\Delta h^{ba} + \Delta^{\langle ba\rangle} + \Delta^{[ba]}\right) \\ &= -\sigma_{ab}\Delta^{\langle ab\rangle}\,. \end{aligned} \tag{4.17}$$

In the second term we have again applied the splitting Eq. (2.71) from which two parts vanish since the shear is tracefree, $\sigma_{ab}h^{ab} = \sigma^a{}_a = 0$, and because the complete contraction of an antisymmetric with a symmetric tensor is zero. Inserting Eqs. (4.14), (4.15), (4.16) and (4.17) into the comoving divergence of Eq. (4.10) leads us to the intermediate result

of this subsection

$$\dot{\Delta} = \omega(Z^a\Delta_a + \Theta\Delta) - (1+\omega)Z - 2\sigma_{ab}\Delta^{\langle ab\rangle} - \frac{c_s^2}{1+\omega}\left(\frac{2}{3}\Theta + \frac{1}{2}\frac{\mathrm{d}}{\mathrm{d}t}\right)\Delta^a\Delta_a\,. \tag{4.18}$$

4.2.2. Comoving divergence of the volume expansion gradient

Similar to the last section, we now calculate the comoving divergence of Eq. (4.11). The first term on the left hand side of the equation behaves identically to Eq. (4.12) and thus we have

$$\begin{aligned} a\mathrm{D}^a\dot{Z}_a &= \dot{Z} + \sigma^{ab}Z_{\langle ab\rangle} + \frac{1}{3}a\Theta A^a Z_a - aA^a\dot{Z}_a \\ &= \dot{Z} + \sigma^{ab}Z_{\langle ab\rangle} - \frac{c_s^2}{3(1+\omega)}\Theta\Delta^a Z_a + \frac{c_s^2}{1+\omega}\Delta^a\dot{Z}_a\,. \end{aligned} \tag{4.19}$$

Likewise, we can adapt Eq. (4.14) to the comoving volume gradient. Recall that $\Theta := \mathrm{D}^a u_a$ was the definition of the volume expansion, enabling us to write

$$a\mathrm{D}^a u_a \frac{c_s^2}{a(1+\omega)}\Delta^b Z_b = \frac{c_s^2}{1+\omega}\Delta^b Z_b\Theta\,. \tag{4.20}$$

We proceed with the first line on the right hand side of Eq. (4.11). The comoving divergence of the first two terms yields either a pure scalar contribution ΘZ and $\rho\Delta$, or a self-coupling $Z^a Z_a$ and $\Delta^a\Delta_a$. Using additionally $a\mathrm{D}_a\rho = \rho\Delta_a$ and $\mathrm{D}^a\mathrm{D}_a = \mathrm{D}^2$, in total we obtain for the terms in that line

$$\begin{aligned} &-\frac{2}{3}\left(Z^a Z_a + \Theta Z\right) - (1+3c_s^2)\frac{1}{2}(\rho\Delta + \rho\Delta^a\Delta_a) \\ &-\frac{c_s^2}{1+\omega}\left(a\Delta_a\mathrm{D}^a\dot{\Theta} + \dot{\Theta}\Delta\right) - \frac{c_s^2}{1+\omega}\mathrm{D}^2\Delta\,. \end{aligned} \tag{4.21}$$

For the moment we keep the $\mathrm{D}^a\dot{\Theta}$-term in its current form and come back to it later. Continuing with the three terms in the second line of Eq. (4.11), we observe that the last two terms become projected Laplacians[4] and the first term obeys the same calculation as performed for the shear Eq. (4.17) in the previous subsection. Thus, taking the comoving divergence of the second line of Eq. (4.11) produces

$$-\sigma_{ab}Z^{\langle ab\rangle} - 2a^2\mathrm{D}^2\sigma^2 + \frac{c_s^4}{(1+\omega)^2}\mathrm{D}^2\left(\Delta^a\Delta_a\right)\,. \tag{4.22}$$

Here, we used the splitting for the volume expansion gradient $a\mathrm{D}_b Z_a = 1/3\, Z h_{ab} + Z_{\langle ab\rangle} + Z_{[ab]}$. All in all, the comoving divergence of Eq. (4.11) leads at second order to the

[4]The operator D^2 is called Laplace-Beltrami operator and applies for a general space-time. For a FLRW space-time it differs from the usual spatial Laplacian for $K \neq 0$.

equation

$$\begin{aligned}\dot{Z} =& -\frac{2}{3}\frac{c_s^2}{1+\omega}\Theta\Delta^a Z_a - \frac{c_s^2}{1+\omega}\Delta^a\dot{Z}_a \\ & -\frac{2}{3}(Z^a Z_a + \Theta Z) - \frac{1}{2}(1+3c_s^2)(\rho\Delta + \rho\Delta^a\Delta_a) \\ & -\frac{c_s^2}{1+\omega}\mathrm{D}^2\Delta - 2\sigma_{ab}Z^{\langle ab\rangle} - 2a^2\mathrm{D}^2\sigma^2 \\ & -\frac{c_s^2}{1+\omega}(\Delta_a a\mathrm{D}^a\dot{\Theta} + \dot{\Theta}\Delta) \\ & +\frac{c_s^4}{(1+\omega)^2}\mathrm{D}^2\left(\Delta^a\Delta_a\right).\end{aligned} \tag{4.23}$$

This equation forms together with Eq. (4.18) a set of coupled equations for the scalar part of the comoving density gradient and the comoving volume expansion gradient. Next, we want to merge them into a single second order differential equation for the scalar density.

4.3. Evolution of second order density perturbations

The two Eqs. (4.18) and (4.23) can be decoupled by taking the time derivative of the former equation and then insert the latter into the result. By doing so, we take **Assumption 4** into account, which demands $\dot{\omega} = \dot{c}_s^2 \approx 0$. Hence, taking the time derivative of Eq. (4.18) yields

$$\begin{aligned}\ddot{\Delta} =& \omega(\dot{Z}_a\Delta^a + Z^a\dot{\Delta}_a + \dot{\Theta}\Delta + \Theta\dot{\Delta}) - (1+\omega)\dot{Z} \\ & -2\frac{\mathrm{d}}{\mathrm{d}t}\left(\sigma_{ab}\Delta^{\langle ab\rangle}\right) - \frac{c_s^2}{1+\omega}\left(\frac{2}{3}\dot{\Theta} + \frac{2}{3}\Theta\frac{\mathrm{d}}{\mathrm{d}t} + \frac{1}{2}\frac{\mathrm{d}^2}{\mathrm{d}t^2}\right)\Delta^a\Delta_a.\end{aligned} \tag{4.24}$$

Due to the occurrence of Z-terms, the equation is still coupled to Eq. (4.23). Our next efforts shall be invested to resolve this dependence and merge both equations into one. This requires several steps. We begin by replacing $\dot{Z}$ with our intermediate result Eq. (4.23) and sort the result such that scalar couplings are aligned in the first line, shear tensors of any form are summarized in the second line, while contractions between gradient quantities are listed in the last two lines,

$$\begin{aligned}\ddot{\Delta} =& \frac{2}{3}(1+\omega)\Theta Z + \omega\Theta\dot{\Delta} + (\omega + c_s^2)\dot{\Theta}\Delta + \frac{(1+\omega)(1+3c_s^2)}{2}\rho\Delta + c_s^2\mathrm{D}^2\Delta \\ & -2\frac{\mathrm{d}}{\mathrm{d}t}\left(\sigma_{ab}\Delta^{\langle ab\rangle}\right) + 2(1+\omega)\sigma_{ab}Z^{\langle ab\rangle} + 2a^2(1+\omega)\mathrm{D}^2\sigma^2 \\ & -\frac{c_s^2}{1+\omega}\left[\frac{2}{3}\dot{\Theta} - \frac{(1+\omega)^2(1+3c_s^2)}{c_s^2}\frac{\rho}{2} + c_s^2\mathrm{D}^2 + \frac{2}{3}\Theta\frac{\mathrm{d}}{\mathrm{d}t} + \frac{1}{2}\frac{\mathrm{d}^2}{\mathrm{d}t^2}\right]\Delta^a\Delta_a \\ & +(\omega + c_s^2)\dot{Z}^a\Delta_a + (\omega\dot{\Delta}_a + \frac{2}{3}c_s^2\Theta\Delta_a + \frac{2}{3}(1+\omega)Z_a)Z^a + c_s^2(\Delta_a a\mathrm{D}^a\dot{\Theta}).\end{aligned} \tag{4.25}$$

The last remaining dependencies on Z left are volume expansion distortion $Z_{\langle ab\rangle}$, the volume expansion gradient Z_a, the scalar Z and derivatives of the volume expansion scalar Θ. In order to eliminate the latter one, we replace it by Raychaudhuri's Eq. (2.63)

$$\dot{\Theta} = -\frac{1}{3}\Theta^2 - \frac{1}{2}(1+3\omega)\rho - 2\sigma^2 - \frac{c_s^2}{a^2(1+\omega)}\Delta + \frac{c_s^4}{a^2(1+\omega)^2}\Delta_a\Delta^a + \Lambda\,. \tag{4.26}$$

The temporal change of the volume expansion experiences also the action of a spatial gradient in the last term of Eq. (4.25). From Eq. (4.26) it can be easily calculated as

$$c_s^2\Delta_a a\mathrm{D}^a\dot{\Theta} = -c_s^2\frac{2}{3}\Theta\Delta_a Z^a - \frac{c_s^2}{2}(1+3\omega)\rho\Delta_a\Delta^a - \frac{c_s^4}{(1+\omega)a}\Delta_a\mathrm{D}^a\Delta\,. \tag{4.27}$$

For the scalar Z we find an equation by rearranging Eq. (4.18) and isolate Z on the left hand side such that

$$Z = -\frac{1}{1+\omega}\left(\dot{\Delta} - \omega Z^a\Delta_a - \omega\Theta\Delta + 2\sigma_{ab}\Delta^{\langle ab\rangle} + \frac{c_s^2}{1+\omega}\left(\frac{2}{3}\Theta + \frac{1}{2}\frac{\mathrm{d}}{\mathrm{d}t}\right)\Delta^a\Delta_a\right)\,. \tag{4.28}$$

With these formlae we can reduce the dependences of Eq. (4.25) on volume expansion variables to the gradient Z_a and the tensor contribution $Z_{\langle ab\rangle}$. So far, scalar part of the comoving fractional density gradient evolves according to

$$\begin{aligned}
&\ddot{\Delta} + \left(\frac{2}{3} - \omega\right)\Theta\dot{\Delta} - \left((\omega - c_s^2)\frac{\Theta^2}{3} + (1 + 2c_s^2 - 3\omega^2)\frac{\rho}{2} + (\omega + c_s^2)\Lambda + c_s^2\mathrm{D}^2\right)\Delta \\
&\quad = -2\left(\frac{2}{3}\Theta + \frac{\mathrm{d}}{\mathrm{d}t}\right)\left(\sigma_{ab}\Delta^{\langle ab\rangle}\right) + 2(1+\omega)\sigma^{ab}Z_{\langle ab\rangle} + 2a^2(1+\omega)\mathrm{D}^2\sigma^2 \\
&\qquad - \frac{c_s^2}{1+\omega}\left[\frac{2}{9}\Theta^2 - \frac{1}{c_s^2}\left((1+\omega)^2 + \left(\frac{8}{3} + 4\omega\right)c_s^2\right)\frac{\rho}{2}\right. \\
&\qquad\qquad \left. + c_s^2\mathrm{D}^2 + \frac{2}{3}\Lambda + \Theta\frac{\mathrm{d}}{\mathrm{d}t} + \frac{1}{2}\frac{\mathrm{d}^2}{\mathrm{d}t^2}\right]\Delta^a\Delta_a \\
&\qquad + (\omega + c_s^2)\dot{Z}^a\Delta_a + \left(\omega\dot{\Delta}_a + \frac{2}{3}\Theta\omega\Delta_a + \frac{2}{3}(1+\omega)Z_a\right)Z^a \\
&\qquad - c_s^2\frac{\omega + c_s^2}{(1+\omega)a^2}\Delta^2 - \frac{c_s^4}{(1+\omega)a}\Delta_a\mathrm{D}^a\Delta\,.
\end{aligned} \tag{4.29}$$

This equation is already quite similar to what we were looking for: A second order differential equation of scalar density perturbations that are coupled to, or sourced by, shear terms. Still, there remain three volume expansion gradient related terms in it, which will be eliminated in the next subsection.

4.3.1. Second order perturbative expansion

Up to here we have stuck to our compact notation in which we compressed the zeroth, first and second order terms in one variable, $f := f^{(0)} + f^{(1)} + f^{(2)}$. To proceed, we now resolve this notation

$$\begin{aligned}
\Delta &\approx \Delta^{(0)} + \Delta^{(1)} + \Delta^{(2)} \equiv \Delta^{(1)} + \Delta^{(2)}\,,\\
Z &\approx Z^{(0)} + Z^{(1)} + Z^{(2)} \equiv Z^{(1)} + Z^{(2)}\,,\\
\sigma &\approx \sigma^{(0)} + \sigma^{(1)} + \sigma^{(2)} \equiv \sigma^{(1)} + \sigma^{(2)}\,,\\
\Theta &\approx \Theta^{(0)} + \Theta^{(1)} + \Theta^{(2)}\,,\\
\rho &\approx \rho^{(0)} + \rho^{(1)} + \rho^{(2)}\,.
\end{aligned} \tag{4.30}$$

Note again that first order gauge invariant variables do not possess a zeroth order term. Furthermore, we observe, that the shear tensor appears only in combination with quantities, which are gauge invariant at first order. Since these variables lack a zeroth order component, only the linear perturbation of the shear can appear in Eq. (4.29) $\sigma \approx \sigma^{(1)}$, if we neglect terms higher than second order. Thus, we can omit the second order perturbation of the shear completely. For the same reason, we do not need to take care of the second order perturbations of the two gauge dependent variables $\rho^{(2)}$ and $\Theta^{(2)}$. Inserting the perturbative expansions into Eq. (4.29) reveals

$$\begin{aligned}
&\ddot{\Delta}^{(2)} + \left(\frac{2}{3} - \omega\right)\Theta^{(0)}\dot{\Delta}^{(2)}\\
&- \left(\frac{1}{3}\,(\omega - c_s^2)\Theta^{(0)\,2} + (1 + 2c_s^2 - 3\omega^2)\frac{\rho^{(0)}}{2} + (\omega + c_s^2)\Lambda + c_s^2\mathrm{D}^2\right)\Delta^{(2)}\\
&\quad = -\left(\frac{2}{3} - \omega\right)\Theta^{(1)}\dot{\Delta}^{(1)} + \left(\frac{2}{3}(\omega - c_s^2)\Theta^{(0)}\Theta^{(1)} + (1 + 2c_s^2 - 3\omega^2)\frac{\rho^{(1)}}{2}\right)\Delta^{(1)}\\
&\quad - 2\left(\frac{2}{3}\Theta^{(0)} + \frac{\mathrm{d}}{\mathrm{d}t}\right)\left(\sigma^{(1)}_{ab}\Delta^{(1)\,\langle ab\rangle}\right) + 2(1+\omega)\sigma^{(1)\,ab}Z^{(1)}_{\langle ab\rangle} + 2a^2(1+\omega)\mathrm{D}^2\sigma^{(1)\,2}\\
&\quad - \frac{c_s^2}{1+\omega}\left[\frac{2}{9}\Theta^{(0)\,2} - \frac{1}{c_s^2}\left((1+\omega)^2 + \left(\frac{8}{3} + 4\omega\right)c_s^2\right)\frac{\rho^{(0)}}{2}\right.\\
&\quad \left. + c_s^2\mathrm{D}^2 + \frac{2}{3}\Lambda + \Theta^{(0)}\frac{\mathrm{d}}{\mathrm{d}t} + \frac{1}{2}\frac{\mathrm{d}^2}{\mathrm{d}t^2}\right]\Delta^{(1)\,a}\Delta^{(1)}_a\\
&\quad + (\omega + c_s^2)\dot{Z}^{(1)\,a}\Delta^{(1)}_a + \left(\omega\dot{\Delta}^{(1)}_a + \frac{2}{3}\Theta^{(0)}\omega\Delta^{(1)}_a + \frac{2}{3}(1+\omega)Z^{(1)}_a\right)Z^{(1)\,a}\\
&\quad - c_s^2\frac{\omega + c_s^2}{(1+\omega)a^2}\Delta^{(1)\,2} - \frac{c_s^4}{(1+\omega)a}\Delta^{(1)}_a\mathrm{D}^a\Delta^{(1)}\,.
\end{aligned} \tag{4.31}$$

To make the structure of the result more apparent, we have organized the equation

above such that second order perturbations are on the left hand side of the equation and first order perturbations are on the right hand side. This shows that we have achieved to get a second order wave equation for the second order density perturbation gradient which is driven by various combinations of first order comoving density gradients and the shear. Apart from them, also the volume expansion gradient $Z_a^{(1)}$ and $Z_{\langle ab\rangle}^{(1)}$ still appear in Eq. (4.31). For $Z_a^{(1)}$ we reorganize Eq. (4.3) such that

$$\begin{aligned} Z_a &= \frac{\omega\Theta\Delta_a - \dot{\Delta}_{\langle a\rangle} - \sigma_{ab}\Delta^b}{1+\omega}\,, \\ \Rightarrow Z_a^{(1)} &= \frac{\omega\Theta^{(0)}\Delta_a^{(1)} - \dot{\Delta}_a^{(1)}}{1+\omega} + \mathcal{O}(\epsilon^2)\,. \end{aligned} \tag{4.32}$$

Inserting this into the second term in the second to last line in Eq. (4.31) generates an equation consisting only of self-contractions of comoving density gradients

$$\begin{aligned} &(\omega\dot{\Delta}_a^{(1)} + \frac{2}{3}\Theta^{(0)}\omega\Delta_a^{(1)} + \frac{2}{3}(1+\omega)Z_a^{(1)})Z^{(1)\,a} = \\ &\quad\frac{\omega-2}{2}\frac{\omega}{1+\omega}\Theta^{(0)}\frac{\mathrm{d}}{\mathrm{d}t}(\Delta^{(1)\,a}\Delta_a^{(1)}) + \frac{\frac{2}{3}-\omega}{1+\omega}\dot{\Delta}^{(1)\,a}\dot{\Delta}_a^{(1)} + \frac{4}{3}\frac{\omega^2}{1+\omega}\Theta^{(0)\,2}\Delta^{(1)\,a}\Delta_a^{(1)}\,. \end{aligned} \tag{4.33}$$

We can replace the time derivative of $Z_a^{(1)}$ occurring in Eq. (4.31) by reorganizing Eq. (4.11) and replace appearing $Z_a^{(1)}$-terms with Eq. (4.32). This gives us the equation

$$\begin{aligned} \dot{Z}_a^{(1)} =& \frac{1}{3}\frac{\Theta^{(0)\,2}}{1+\omega}\left(c_s^2 - 2\omega\right)\Delta_a^{(1)} + \frac{2}{3}\frac{1}{1+\omega}\Theta^{(0)}\dot{\Delta}_a^{(1)} - \frac{c_s^2}{a(1+\omega)}\mathrm{D}^a\Delta^{(1)} \\ &+ \left(\frac{c_s^2}{1+\omega}(1+3\omega) - (1+3c_s^2)\right)\frac{\rho^{(0)}}{2}\Delta_a^{(1)}. \end{aligned} \tag{4.34}$$

With this result at hand we can proceed and finally erase all dependencies on the volume expansion gradients from Eq. (4.31) (only $Z_{\langle ab\rangle}$ remains for reasons that become apparent later on). The first term in the second to last line of the latter becomes

$$\begin{aligned} &(\omega + c_s^2)\dot{Z}^{(1)\,a}\Delta_a^{(1)} = \\ &\quad\frac{1}{3}\frac{\omega+c_s^2}{1+\omega}(c_s^2 - 2\omega)\Theta^{(0)\,2}\Delta_a^{(1)}\Delta^{(1)\,a} + \frac{1}{3}\frac{\omega+c_s^2}{1+\omega}\Theta^{(0)}\frac{\mathrm{d}}{\mathrm{d}t}(\Delta^{(1)\,a}\Delta_a^{(1)}) \\ &\quad - \frac{c_s^2(c_s^2+\omega)}{a(1+\omega)}\Delta_a^{(1)}\mathrm{D}^a\Delta^{(1)} + (\omega+c_s^2)\left(\frac{c_s^2}{1+\omega}(1+3\omega) - (1+3c_s^2)\right)\frac{\rho^{(0)}}{2}\Delta_a^{(1)}\Delta^{(1)\,a}\,. \end{aligned} \tag{4.35}$$

Now, inserting Eqs. (4.32), (4.33), (4.34) and (4.35) into Eq. (4.31) culminates in our final result:

$$
\begin{aligned}
&\ddot{\Delta}^{(2)} + \left(\frac{2}{3} - \omega\right)\Theta^{(0)}\dot{\Delta}^{(2)} \\
&-\left(\frac{1}{3}(\omega - c_s^2)\Theta^{(0)\,2} + (1 + 2c_s^2 - 3\omega^2)\frac{\rho^{(0)}}{2} + (\omega + c_s^2)\Lambda + c_s^2\mathrm{D}^2\right)\Delta^{(2)} \\
&\quad = -\left(\frac{2}{3} - \omega\right)\Theta^{(1)}\dot{\Delta}^{(1)} + \left(\frac{2}{3}(\omega - c_s^2)\Theta^{(0)}\Theta^{(1)} + (1 + 2c_s^2 - 3\omega^2)\frac{\rho^{(1)}}{2}\right)\Delta^{(1)} \\
&\quad - 2\left(\frac{2}{3}\Theta^{(0)} + \frac{\mathrm{d}}{\mathrm{d}t}\right)\left(\sigma_{ab}^{(1)}\Delta^{(1)\,\langle ab\rangle}\right) + 2(1+\omega)\sigma_{ab}^{(1)}Z^{(1)\,\langle ab\rangle} + 2a^2(1+\omega)\mathrm{D}^2\sigma^{(1)\,2} \\
&\quad - \frac{c_s^2}{1+\omega}\left[\left(\frac{2}{3} - \frac{2\omega^2 + c_s^4 - \omega c_s^2}{c_s^2}\right)\frac{\Theta^{(0)\,2}}{3} + \frac{1}{c_s^2}\left(-1 - \omega - \omega c_s^2 - \frac{5}{3}c_s^2 + 2c_s^4\right)\frac{\rho^{(0)}}{2}\right. \\
&\quad \left. + c_s^2\mathrm{D}^2 + \frac{2}{3}\Lambda + \left(\frac{2}{3} + \frac{2\omega}{3c_s^2} - \frac{\omega^2}{2c_s^2}\right)\Theta^{(0)}\frac{\mathrm{d}}{\mathrm{d}t} + \frac{1}{2}\frac{\mathrm{d}^2}{\mathrm{d}t^2}\right]\Delta^{(1)\,a}\Delta_a^{(1)} \\
&\quad + \frac{\frac{2}{3} - \omega}{1+\omega}\dot{\Delta}_a^{(1)}\dot{\Delta}^{(1)\,a} - \frac{c_s^2(c_s^2 + \omega)}{(1+\omega)a^2}\Delta^{(1)\,2} - \frac{c_s^2(2c_s^2 + \omega)}{(1+\omega)a}\Delta_a^{(1)}\mathrm{D}^a\Delta^{(1)}\,. \qquad (4.36)
\end{aligned}
$$

4.4. Second order scalar perturbations in the radiation and matter dominated era

Let us now examine our result in specific epochs. First we fix the background cosmology by making use of **Assumption 5**. By doing so, the zeroth order volume expansion becomes the Hubble constant $\Theta^{(0)} = 3H(t)$. We emphasize that the zeroth order density perturbation only depends on time, $\rho^{(0)} = \rho^{(0)}(t)$. However, this was assumed already in the calculation above. With the Friedmann Eqs. (2.4) and (2.5) for the zeroth order quantities we obtain

$$
\begin{aligned}
&\ddot{\Delta}^{(2)} + 2H\left(1 - \frac{3}{2}\omega\right)\dot{\Delta}^{(2)} \\
&\quad - \left[\frac{3}{2}\left(1 + 2\omega - 3\omega^2\right)H^2 - \frac{1}{2}\left(1 - 2\omega - 3\omega^2\right)\Lambda + \left(1 + 2c_s^2 - 3\omega^2\right)\frac{3K}{2a^2} + c_s^2\mathrm{D}^2\right]\Delta^{(2)} \\
&= -\left(\frac{2}{3} - \omega\right)\Theta^{(1)}\dot{\Delta}^{(1)} + \left(\frac{1}{3}(\omega - c_s^2)6H\Theta^{(1)} + (1 + 2c_s^2 - 3\omega^2)\frac{\rho^{(1)}}{2}\right)\Delta^{(1)} \\
&\quad - 2\left(2H + \frac{\mathrm{d}}{\mathrm{d}t}\right)\sigma^{(1)}_{ab}\Delta^{(1)\,\langle ab\rangle} + 2(1+\omega)\sigma^{(1)}_{ab}Z^{(1)\,\langle ab\rangle} + 2(1+\omega)a^2\mathrm{D}^2\sigma^{(1)\,2} \\
&\quad - \frac{c_s^2}{1+\omega}\left[\left(-1 - \omega + \frac{7}{3}\omega c_s^2 - \frac{5}{3}c_s^2 - 4\omega^2\right)\frac{\rho^{(0)}}{2c_s^2} + c_s^2\mathrm{D}^2 + \left(\omega - 2\frac{\omega^2}{c_s^2} - c_s^2 + \frac{2}{3}\right)\Lambda\right. \\
&\quad \left. + \left(\frac{2}{3} + \frac{2\omega}{3c_s^2} - \frac{\omega^2}{2c_s^2}\right)3H\frac{\mathrm{d}}{\mathrm{d}t} + \frac{1}{2}\frac{\mathrm{d}^2}{\mathrm{d}t^2}\right]\Delta^{(1)\,a}\Delta^{(1)}_a \\
&\quad + \frac{\frac{2}{3} - \omega}{1+\omega}\dot{\Delta}^{(1)}_a\dot{\Delta}^{(1)\,a} - \frac{c_s^2(c_s^2 + \omega)}{(1+\omega)a^2}\Delta^{(1)\,2} - \frac{c_s^2(2c_s^2 + \omega)}{(1+\omega)a}\Delta^{(1)}_a\mathrm{D}^a\Delta^{(1)}\,.
\end{aligned}
\tag{4.37}
$$

Next, we aim to specify this equation in the matter dominated era and the radiation dominated one. While the latter is of special interest to this work, the former enables us to compare our result with the literature [135] in which the calculation has been performed by working in the matter dominated regime right from the beginning. For a better orientation in the equations we reintroduce $\kappa := 8\pi G$.

Matter dominated universe: In Ref. [135] the sourcing of density perturbations from GWs has been considered. The authors proceed in rather different way than we do and assume a FLRW universe in a matter dominated era right away. Also they only study super-horizon modes which considerably simplifies the calculation. However, in this era our results should coincide. In a matter dominated universe the equation of state parameter is $\omega = 0$ and the sound speed vanishes as well $c_s^2 = 0$, if we only consider matter perturbation. In Ref. [135] the result is given in terms of the Ricci tensor, which

emerges when applying the Gauss-Codazzi equation [135]

$$R_{\langle ab\rangle} = -3H\sigma_{ab} - \dot{\sigma}_{ab} \tag{4.38}$$

to the shear tensor. For a matter dominated universe the four-acceleration vanishes (this does not mean $\Delta = 0$! It means that the pressure is zero $p = 0$.) and the relation Eq. (2.73) simplifies substantially

$$\dot{\Delta}_{\langle ab\rangle} = -Z_{\langle ab\rangle} \quad \text{and} \quad \dot{\Delta}_a = -Z_a\,. \tag{4.39}$$

Focusing on super-horizon modes means that the source from which the GWs emerge on sub-horizon scales is irrelevant, $\mathrm{D}^2\sigma^2 = 0$. In a flat universe, $K = 0$, (details see Ref. [135]) our result shown in Eq. (4.37) reduces substantial

$$\begin{aligned}\ddot{\Delta}^{(2)} + 2H\dot{\Delta}^{(2)} - \frac{1}{2}(3H^2 - \Lambda)\Delta^{(2)} =& \frac{3H^2}{2}\kappa\Delta_a^{(1)}\Delta^{(1)\,a} + \frac{2}{3}Z_a^{(1)}Z^{(1)\,a} + 2H\sigma_{ab}^{(1)}\Delta^{(1)\,\langle ab\rangle} \\ &+ 4\sigma_{ab}^{(1)}Z^{(1)\,\langle ab\rangle} + 2R_{\langle ab\rangle}^{(1)}\Delta^{(1)\,\langle ab\rangle} \\ &- \frac{2}{3}\Theta^{(1)}\dot{\Delta}^{(1)} + \frac{1}{2}\rho^{(1)}\Delta^{(1)}\,.\end{aligned} \tag{4.40}$$

This almost reproduces the result in [135] for $\Lambda = 0$. In contrast to the reference, we find two further terms in which the first order perturbations of the gauge dependent variables couple, $-2/3\Theta^{(1)}\dot{\Delta}^{(1)}$ and $\frac{1}{2}\rho^{(1)}\Delta^{(1)}$. The origin of this discrepancy lies in the reduction procedure which is commonly used in the 1+3 covariant theory. In it, the non-linear equations are perturbed by directly taking into account that gauge independent variables only exhibit a first order term while occurring ρ's and Θ's can only appear to zeroth order. This is due to the fact, that they always occur in combination with a gauge invariant variable. While this works perfectly well in the context of first order perturbations, it fails at second order, since the product of a gauge invariant variable and a gauge dependent variable does not uniquely fix the occurring perturbative order anymore. This is why these variables have escaped the calculation in the reference. From the comparison we therefore deduce that our equation can reproduce the result in the literature apart from well justified deviations.

Radiation dominated universe: In this work we want to study FOPT in particle models which typically take place during the early phase of the universe in the era dominated by radiation. In this regime the barotropic equation of state is governed by photon pressure and thus the equation of state parameter is $\omega = 1/3$ and the photon perturbations travel at the speed of sound $c_s^2 = 1/3$. To completely remove the dependence on the comoving volume gradient in Eq. (4.37), we replace the still remaining term $Z_{\langle ab\rangle}^{(1)}$ by acting with the comoving divergence on the equation

$$(1+\omega)Z_a^{(1)} = \omega\Theta\Delta_a^{(1)} - \dot{\Delta}^{(1)} + \mathcal{O}(\epsilon^2)\,. \tag{4.41}$$

Making use of the splitting $a\mathrm{D}_b Z_a = 1/3 h_{ab} Z + Z_{\langle ab\rangle} + Z_{[ab]}$, this equations translates to

$$Z^{(1)}_{\langle ab\rangle} = \frac{\omega\Theta^{(0)}\Delta^{(1)}h_{ab} + \omega\Theta^{(0)}\Delta^{(1)}_{\langle ab\rangle} - \dot{\Delta}^{(1)}_{\langle ab\rangle}}{1+\omega} + \mathcal{O}(\epsilon^2)\,. \tag{4.42}$$

Inserting this into Eq. (4.37) and assuming a flat, $K = 0$, universe without a substantial amount of cosmological constant, $\Lambda = 0$, we finally find

$$\begin{aligned}
&\ddot{\Delta}^{(2)} + H\dot{\Delta}^{(2)} - 2H^2\Delta^{(2)} - \frac{1}{3}\mathrm{D}^2\Delta^{(2)} \\
&\quad = \left.\begin{aligned} &-2\left(H\sigma^{(1)}_{ab}\Delta^{(1)\,\langle ab\rangle} + \dot{\sigma}^{(1)}_{ab}\Delta^{(1)\,\langle ab\rangle} + 2\sigma^{(1)}_{ab}\dot{\Delta}^{(1)\,\langle ab\rangle}\right) \\ &+ \tfrac{8}{3}a^2\mathrm{D}^2\sigma^{(1)\,2} \end{aligned}\right\} \text{GW sources} \\
&\qquad \left.\begin{aligned} &-\tfrac{1}{3}\Theta^{(1)}\dot{\Delta}^{(1)} + \tfrac{2}{3}\rho^{(1)}\Delta^{(1)} \\ &+ \left[\left(2H^2 - \tfrac{1}{12}\mathrm{D}^2\right)\Delta^{(1)}_a - \tfrac{7}{4}H\dot{\Delta}^{(1)}_a - \tfrac{1}{4}\ddot{\Delta}^{(1)}_a\right]\Delta^{(1)\,a} \\ &- \tfrac{1}{6}\tfrac{1}{a^2}\Delta^{(1)\,2} - \tfrac{1}{4}\tfrac{1}{a}\Delta^{(1)}_a\mathrm{D}^a\Delta^{(1)}\,. \end{aligned}\right\} \text{Pure density sources}
\end{aligned} \tag{4.43}$$

This equation is the central result of this chapter. It describes second order density fluctuations sourced by first order density perturbations and the shear tensor. We can understand this equation as implied by the categorization of the source terms on the right hand side. The first category involves the shear-terms, which fall into two subcategories. In the first one are couplings between the shear and primordial tensor modes in the density contrast, while the second one includes only a pure shear term. As we will see in the next chapter, the shear is directly related to GWs and therefore, terms in this first group are seeds set by GWs. The second category involves only couplings of linear density perturbations and the coupling with $\Theta^{(1)}$. These terms are quite complex as they involve various different coupling types. However, if the gravitational radiation is stronger than the linear perturbations, these terms should be suppressed. We will investigate this point in the next chapter, too. Finally, we can see, that the produced density perturbations obey the damped wave equation and thus oscillate.

We now turn to the next chapter, where we discuss this equation in the context of FOPTs and how we can deduce impacts on the matter power spectrum from it.

Chapter 5

Gravitational Wave induced Baryon Acoustic Oscillation

In chapter 4 we have found an equation that governs the evolution of second order density perturbations from shear and linear density fluctuation sources. From that, we determine the first-order phase transition parameters α, r_β and t_* that generate sufficiently strong gravitational waves to affect density perturbations and in turn modify the matter power spectrum. To do so, we isolate the most relevant source term and adapt the equation to the environment and conditions that prevail during generic transitions. The equation is then converted from the 1+3 covariant formulation into familiar quantities from the Bardeen formalism which enable a comfortable way to compare the results with the linear matter power spectrum. The adapted equation is then solved and the result interpret in terms of gravitational wave driven baryon acoustic oscillations. From the solution we deduce the transferfunction and in turn the modifications that the linear matter power spectrum experiences. Demanding that the spectrum may not be altered stronger than cosmic variance allows, we extract limits on the strength and duration of the generated perturbations and translate these bounds to a new constraint on a potential gravitational wave signal today. As for the last chapter the results presented here have been first derived in the authors' Ref. [5] which we closely follow.

5.1. The gravitational wave seed of second order density perturbations

With Eq. (4.43) we have found a relation in which gravitational shear in conjunction with first order density variations drives the production of density perturbations at second order. The next step is to embed this system into the scenario of interest to this work where GWs emerge from a FOPT. Partially, we use slightly different conventions in this subsection for reasons that will become clear later. They are listed in appendix A.

Summarizing from the previous chapters, the physical situation reveals itself as follows: Assume that during the radiation dominated era the dropping temperature of the universe unleashes a FOPT. The adaption of the new VEV proceeds by the formation of bubbles which nucleate at time t_{nuc}. Suppose, the strength of the transition is sufficiently large such that the universe becomes temporarily vacuum dominated, while the bubbles expand. Eventually, the bubbles collide producing GWs at time t_* and reheating the universe back into radiation domination. Via Eq. (4.43) the GWs seed in form of shear distortions the generation of second order density perturbations. If strong enough, these additional perturbations manipulate the linear matter power spectrum and hence may modify the formation of structure.

In order to gain a first impression of the effect, let us for the moment assume that the transition is so strong that it's relict, the shear, constitutes the dominating source in Eq. (4.43) and thus the generation of second order density perturbations is solely governed by the pure shear term

$$\ddot{\Delta}^{(2)} + H\dot{\Delta}^{(2)} - 2H^2\left(1 + \frac{1}{6}\frac{\mathrm{D}^2}{H^2}\right)\Delta^{(2)} = \frac{8}{3}a^2\mathrm{D}^2\sigma^{(1)\,2}\,. \tag{5.1}$$

We shall investigate later the conditions under which this assumption is satisfied. The physical circumstances allow for further simplifications. Recapitulating from chapter 3 we assess that for FOPTs in particle physics the following conditions hold:

- The transitions occur in the radiation dominated era $\omega = 1/3$.
- They take place on sub-horizon scales $k > H_{\mathrm{nuc}}$.
- The transition may complete within a Hubble time $\beta^{-1} \ll H_{\mathrm{nuc}}^{-1}$.
- Strong phase transitions occasionally render the universe vacuum dominated $\Omega_{\mathrm{GW}} \equiv \Omega_{\mathrm{BC}}$. In that case the GW production (percolation) time t_* and the bubble nucleation time t_{nuc} may differ but still $H_* \approx H_{\mathrm{nuc}}$.

Eq. (5.1) already incorporates the assumption that the fluid neither exhibits any vorticity nor relevant remaining anisotropic stresses once the GWs are produced. Furthermore, we consider a spatially flat $K = 0$ universe. Some of these aspects together with a comprehensive view of the described system are illustrated in Fig. 5.1. These properties have the following simplifying implications that reduce the complexity of our equation:

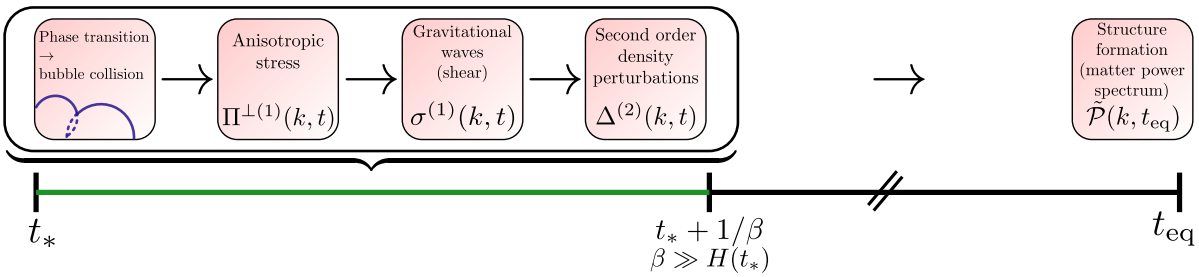

Figure 5.1.: Schematic flow chart of the processes triggered by a FOPT put into chronological perspective as described in the text. The green line marks the duration of the transition since bubble collision. The sequence of processes shown in the chain diagram take place during the whole period of the transition. Adapted from [5].

- On sub-horizon scales the effects of gauge transformations become negligible. Hence the gauge issue becomes unimportant and we do not need to worry about the loss of gauge invariance due to the second order expansion (see, e.g. page 33 in [82].).

- Additionally, on sub-horizon scales and for relatively short phase transitions the Hubble fricition can be omitted $H\dot{\Delta}^{(2)} \approx 0$ and the scale factor as well as the Hubble constant remain almost constant $a(t) \approx a(t_*) \approx a(t_* + \beta^{-1})$ and $H(t) \approx H(t_*) \approx H(t_* + \beta^{-1})$, respectively.

- For sub-horizon modes $k/(a_* H_*) \gg 1$ and hence $(1 - \frac{1}{6}(k/a_* H_*)^2) \approx -\frac{1}{6}(k/a_* H_*)^2$.

Adjusting Eq. (5.1) to the physical situation outlined here and decomposing the variables into Fourier modes[1] $f(\mathbf{x},t) = \int_{\mathbf{k}} f_{\mathbf{k}}\, e^{-i\mathbf{k}\cdot\mathbf{x}}$ leads to

$$\ddot{\Delta}^{(2)}_k - 2H_*^2 \left(1 - \frac{1}{6}\frac{k^2}{a_*^2 H_*^2}\right) \Delta^{(2)}_k = \ddot{\Delta}^{(2)}_k + \frac{1}{3}\frac{k^2}{a_*^2}\Delta^{(2)}_k = -\frac{8}{3}k^2 \left(\sigma^{(1)\,2}\right)_k , \tag{5.2}$$

where we have used $\mathrm{D}^a\mathrm{D}_a = \nabla^2/a^2$. It turns out, that a very transparent way to analyze this equation is to translate the 1+3 variables back to Bardeen's formulation by means of Eqs. (2.89) and (2.91). Let us start with the translation of the shear tensor. In a comoving frame, the transverse part of the shear tensor σ_{ab} converts to it's dual version of the GW tensor $E^T_{\alpha\beta}$ according to Eq. (2.91), see also Ref. [86, 209, 210]. They admit the relation

$$\sigma_{ab} = a^2 \dot{E}^T_{\alpha\beta} \quad \text{and} \quad \sigma^{ab} = a^{-2}\dot{E}^{T\,\alpha\beta} . \tag{5.3}$$

From Eq. (3.27) we recall that the square of the linear, transverse tensor perturbations

[1] Recall that for a flat space-time the generalized harmonic function $\mathcal{Q}_k$ often used in the context of the 1+3 covariant theory become ordinary Fourier-modes, see also appendix B.2. Also note, that $\mathbf{k}$ and $\mathbf{x}$ denote the comoving wave vector and the comoving space vector, respectively.

gives the GW energy density

$$\rho_{\rm GW}(\mathbf{x},t) = \frac{\dot{E}^T_{\alpha\beta}(\mathbf{x},t)\dot{E}^{T\,\alpha\beta}(\mathbf{x},t)}{16\pi G}\,. \tag{5.4}$$

This implies together with Eq. (5.3) that the magnitude of the shear $\sigma^2 := (1/2)\sigma_{ab}\sigma^{ab}$ is

$$\begin{aligned}\rho_{\rm GW}(\mathbf{x},t) &= \frac{1}{8\pi G}\sigma^2(\mathbf{x},t) \quad \text{or}\\ \sigma^2(\mathbf{x},t) &= 3H_*\Omega_{\rm GW}\,,\end{aligned} \tag{5.5}$$

where in the last step we have converted the GW energy density to the GW density parameter $\rho_{\rm GW} = \rho_{\rm tot}\Omega_{\rm GW}$ with the total energy density at the transition time $\rho_{\rm crit} \approx \rho_{\rm tot} = \frac{3H_*^2}{8\pi G}$ (assuming that $\Lambda \approx 0$).

In a similar manner we can deal with the comoving divergence of the fractional density gradient Δ and the density variations δ. In Eq. (2.89) of Sec. 2.2.7 we have already seen that for a spatially flat space-time

$$\Delta(\mathbf{x},t) = \nabla^2\tilde{\delta}(\mathbf{x},t)\,, \tag{5.6}$$

where tilde denoted the gauge invariant version of δ. However, since we work on sub-horizon scales, the gauge issue is not relevant and we can omit the tilde. The definition of the scalar $\Delta := a\mathrm{D}^a(a/\rho\mathrm{D}_a\rho)$ suggests that the same relation also applies for the second order perturbative level[2]. In Fourier space the relations (5.5) and (5.6) read $(\sigma^2)_k = \rho_{\rm GW}(k/a_*,t)$ and $\Delta_k = -k^2\delta(k,t)$, respectively. Applying them to Eq. (5.2) yields

$$\ddot{\delta}^{(2)}_k(t) + \frac{1}{3}\frac{k^2}{a_*^2}\delta^{(2)}_k(t) = 8H_*^2\Omega_{\rm GW}(k/a_*,t) \quad \text{for } t\in[t_*,t_*+1/\beta], \tag{5.7}$$

This equation applies only during the transition. In appendix D we discuss, if the produced GW abundance can also generate significant perturbations after the transition. Here, one has to take into account that the magnitude of the GWs redshifts fast with a^{-4} and the scale factor as well as the Hubble constant change with time. In appendix D we show that this leads to a negligible contribution to the overall production of second order density variations.

5.2. Solution and interpretation

In order to solve Eq. (5.7) we first employ the transformation to dimensionless variables for the time, the wave number and nucleation rate that we have already introduced in

[2]For a second order version of δ see e.g. [211].

Sec. 3.2.2:

$$\tau := H_* t\,, \quad \kappa := \frac{c}{a_* H_*} k \quad \text{and} \quad r_\beta := \frac{\beta}{H_*}\,. \tag{5.8}$$

In the following we denote with primes derivatives with respect to τ. Let us emphasize again that we reintroduced the speed of light c in the definition of κ for better readability. In terms of these dimensionless variables Eq. (5.7) reaches its final form

$$\delta^{(2)\prime\prime}(\kappa,\tau) + \frac{1}{3}\kappa^2 \delta^{(2)}(\kappa,\tau) = 8 \cdot \Omega_{\mathrm{GW}}(\kappa,\tau)\,. \tag{5.9}$$

This equation represents the main result of this work and permits the following interpretation. Recall, that we chose $c_s^2 = 1/3$ which in first order perturbations theory defines perturbations in the radiation fluid. At second order the pressure is approximated as

$$p^{(2)} = c_s^2 \rho^{(2)} + \sigma s^{(2)} + \frac{\partial c_s^2}{\partial \epsilon}\rho^{(1)\,2} + \frac{\partial c_s^2}{\partial s} s^{(1)\,2} + \frac{\partial \sigma}{\partial s} s^{(1)\,2} \approx c_s^2 \rho^{(2)}, \tag{5.10}$$

where $\sigma := \left(\partial p/\partial s\right)$ [212]. For adiabatic perturbations, $s^{(1)} = s^{(2)} = 0$, and constant sound speed, the pressure-energy density relation remains unchanged compared to the first order approximation. Therefore, they obey the same equation as at first order with the same proportionality factor and thus the studied perturbations are identified as variations in the photon plasma $\delta^{(2)} \equiv \delta_\gamma^{(2)}$. Recall, that first order photon perturbations follow Eq. (2.39) which reads in the notation of this chapter

$$\delta_\gamma^{(1)\prime\prime} + \frac{1}{3}\kappa^2 \delta_\gamma^{(1)} = \kappa^2 \Phi = 2\left(\Omega_d^{(0)} \delta_d^{(1)} + \Omega_b^{(0)} \delta_b^{(1)}\right)\,. \tag{5.11}$$

Comparing this equation with Eq. (5.9) we observe that they obey the same logic: Photon perturbations on the left hand side are related to energy abundances of other fluid components on the right hand side. As we have mentioned before, the photon perturbations are tightly coupled to the baryons during radiation domination and thus also the second order photon perturbations we have found will induce acoustic oscillations of baryon perturbations. In contrast to the case of first order Baryon Acoustic Oscillations (BAO)s, these oscillations are induced by inhomogeneities in the GW energy density. Another difference concerns the origin of the initial perturbations. While the initial values of first order perturbations on sub-horizon scales are determined from the perturbations from super-horizon scales in our situation we shall assume that the initial values of the second order perturbations are negligibly small and hence perturbations arise solely from the source term. Therefore, we interpret Eq. (5.9) as second order BAOs driven by inhomogeneities in the GW energy density.

The density parameter of GWs, Ω_{GW}, can be deduced from Eq. (3.28) by simple integration over logarithmic wave number. To account for the sub-horizon nature of the spectrum, we set the lower integration boundary to the size of the horizon at τ_*, which

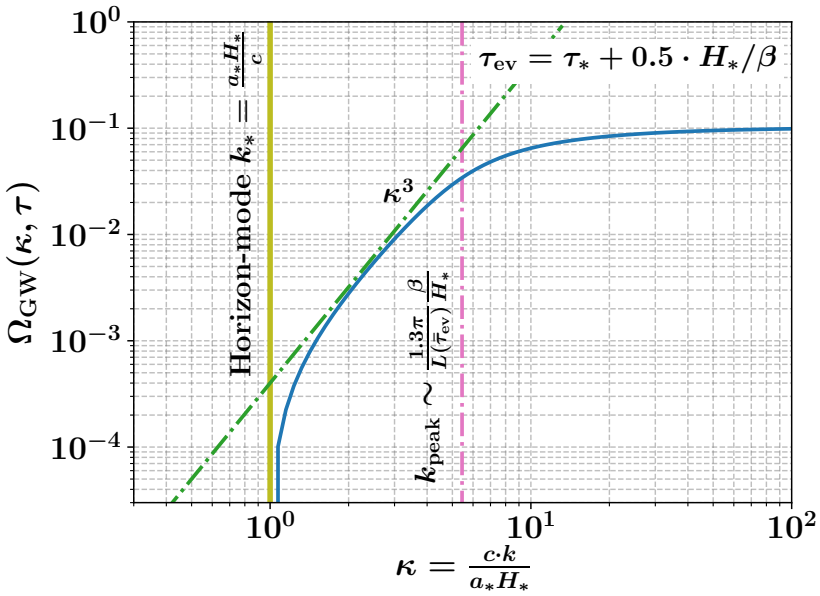

Figure 5.2.: The fractional GW density as a function of dimensionless scale, evaluated in an intermediate stage of the phase transition. The prefactors in Eq. (5.12) are chosen to unity. Shown are also the peak position and asymptotic behavior as two relics of the integrand in Eq. (5.12), the GW energy density per logarithmic frequency. Adapted from [5].

demands $\kappa_* = 1$. The frequency dependent total GW density parameter then reads[3]

$$\Omega_{\rm GW}(\kappa,\tau) = \left(\frac{1}{r_\beta}\right)^2 \left(\frac{\alpha}{1+\alpha}\right)^2 \int_1^\kappa \Delta_{r_\beta}(\kappa',\tau)\,\mathrm{d}\ln\kappa' \,. \tag{5.12}$$

In Fig. 5.2 we show $\Omega_{\rm GW}(\kappa,\tau)$ as a function of wave number for a fixed time and for maximal strength $\alpha \to \infty$ as well as maximal duration $r_\beta = 1$. We observe that $\Omega_{\rm GW}(\kappa,\tau)$ grows until it becomes constant close to peak position $\kappa_{\rm peak}$ of the GW density per logarithmic frequency interval. The function then forms a plateau with magnitude ~ 0.1 which renders the maximal possible fraction of energy stored in GWs.

With this input for the source term we are ready to calculate the perturbations caused by the inhomogeneities in the GW energy spectrum. We insert Eq. (5.12) into Eq. (5.9) and demand that the contribution of primordial second order perturbations is of negligible size. Therefore, we set the initial conditions $\delta^{(2)}(\kappa,\tau_*) = \delta^{(2)\prime}(\kappa,\tau_*) = 0$ to zero. The resulting spectrum at the end of the transition $\delta^{(2)}(\kappa,\tau_* + r_\beta^{-1})$ is presented in Fig. 5.3. We observe that the solution features a prominent peak due to the rise of the GW energy density which is superimposed with a small oscillation pattern originating from

[3]Recall that for transitions which exhibit a long phase of supercooling the bubbles expand with the speed of light $v_w = 1$ into a vacuum dominated universe and hence do not lose energy to the surrounding plasma $\kappa_{\rm eff} = 1$.

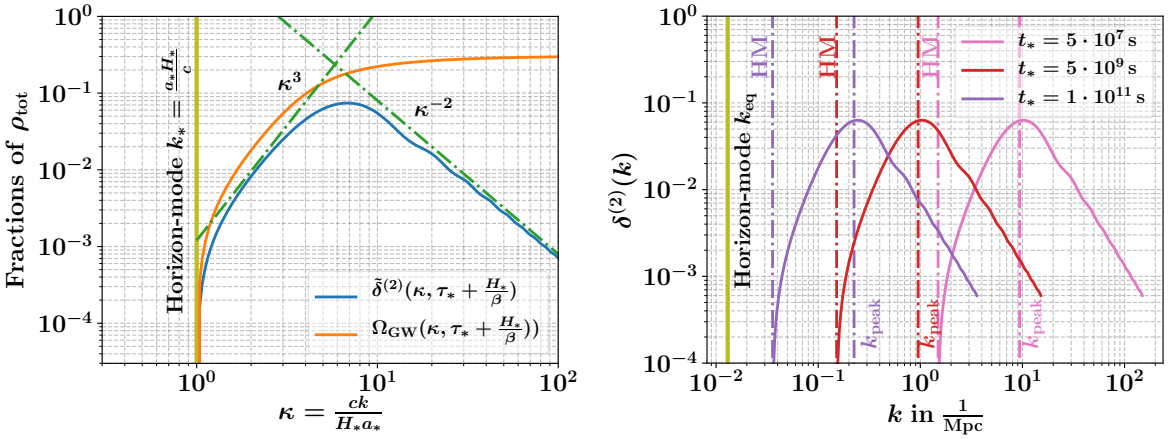

Figure 5.3.: *Left:* The blue line shows the solution of Eq. (5.9) as a function of dimensionless wave number and at the end of the transition. For comparison we also show the source term (orange) and the asymptotic behavior of the flanks. Again, we have put $\alpha \to \infty$ and $r_\beta = 1$. *Right:* The same as the left plot but as a function of comoving wave number. We show the solution exemplary for three different times close to matter-radiation equality together with their peak position and horizon mode. Adapted from [5].

the wave-like form of the equation. The strongest perturbation is generated roughly at the peak position $\kappa_{\rm peak}$ of $\Omega_{\rm GW}^{\rm log}$ which corresponds to the average bubble distance at nucleation. Beyond the peak, the power of the perturbations decreases with κ^{-2}. Besides a numerical solution, we provide in appendix C also analytic solutions for the high and the low wave number regime. Note, that the numerical solution shown in Fig. 5.3 ensures that even for the strongest possible phase transition we can not leave the linear regime $\delta^{(2)} \ll 1$.

Next, let us discuss under which conditions the additional perturbations can alter the linear matter power spectrum. Since their generation is bound to sub-horizon scales they can only impact scales of galaxies and lager when they occur at times that correspond to

$$t : 10^6\,{\rm s} - 10^{12}\,{\rm s} \sim T : (\mathcal{O}(100) - \mathcal{O}(1))\,{\rm eV}\,. \tag{5.13}$$

The upper bound is given by matter-radiation equality $t_{\rm eq} \sim 10^{12}\,{\rm s}$ and is due to our restriction to the radiation dominated era. The scale, at which the peak of the density deviation spectrum occurs, is roughly set by the source term. The latter develops a plateau around the scale where the density parameter per logarithmic frequency exhibits its maximum which lies at (see Sec. 3.2.2)

$$\begin{aligned} k_{\rm peak} &= \frac{2\pi r_\beta H_* a_*}{c}, \quad \text{or} \\ \kappa_{\rm peak} &= 2\pi r_\beta\,. \end{aligned} \tag{5.14}$$

Therefore, the largest impact of the generated density perturbations shown in Fig. 5.3

depends on the production time of GWs (5.13) and the inverse duration of the transition. As shorter the transition as smaller the length-scales which are effected most. In order to compare the time of occurrence and the comoving scale which is affected, we show in Fig. 5.3 the solution of Eq. (5.9) for three different times t_*.

Since we identified our perturbations as perturbations in the baryon-photon plasma, we can also deduce a typical sound horizon of the oscillations. In contrast to the first order perturbations, which immediately start oscillating when they enter the horizon, our oscillations emerge from a single kick. Therefore, we derive the sound horizon for baryon oscillation due to $\delta^{(2)}$ by restricting the integral to the time interval in which the transition proceeds and hence

$$r_s^{\mathrm{GW}} := \int_{t_*}^{t_*+1/\beta} \frac{\mathrm{d}t}{a_*} c_s = \frac{1}{\sqrt{3} a_* \beta} \frac{2\pi}{\sqrt{3}\, k_{\mathrm{peak}}} \,. \tag{5.15}$$

For a transition that occurs around $t_* = 10^{10}\,\mathrm{s}$ this leads to an horizon of size

$$r_s^{\mathrm{GW}} = 3\,\mathrm{Mpc}\,, \tag{5.16}$$

Comparing this to the value of the standard BAOs $r_s = 147\,\mathrm{Mpc}$ [109, 114], we note that a strong phase transition around this time would lead to circular distributions of extra structure on much smaller scales.

In the calculations above we adjusted Eq. (2.7) for the Hubble time such that it holds close to equality where the DM abundance successively takes over

$$H(t) = \frac{\dot{a}}{a} = H_0 \sqrt{\Omega_{m_0}} \frac{\sqrt{a + a_{\mathrm{eq}}}}{a^2} \,. \tag{5.17}$$

For the Hubble time today we used $H_0 \approx 70\,\mathrm{Mpc}/(\mathrm{km\,s}) \approx 2.27 \cdot 10^{-18}\mathrm{s}^{-1}$ and from Planck data we deduced the scale factor at equality as $a_{\mathrm{eq}} = \frac{\Omega_{\gamma_0}}{\Omega_{m_0}} = \frac{8.5 \cdot 10^{-5}}{0.3} = 2.4 \cdot 10^{-4}$ [109]. In order to convert between cosmic time and scale factor we use the implicit relation

$$t \cdot H_0 = \frac{2}{3} \frac{1}{\sqrt{\Omega_{m_0}}} \left[\sqrt{a + a_{\mathrm{eq}}} (a - 2a_{\mathrm{eq}}) + 2a_{\mathrm{eq}}^{3/2} \right] \,, \tag{5.18}$$

which reduces to $a(t) = \sqrt{3 \cdot H_0 \sqrt{\Omega_{\gamma_0}} \cdot t}$ for times long before matter-radiation equality, $a \ll a_{\mathrm{eq}}$.

Before ending this section let us come back to the assumption we made in the beginning, namely that there exist a region in parameter space in which the pure shear term dominates all other source terms. Indeed, with the methods developed above we can estimate this region now. From the relation between the magnitude of the shear and the GW energy density we deduce that roughly $|H_*^{-1}\sigma^{(1)}| \sim \sqrt{3\Omega_{\mathrm{GW}}(\kappa, \tau)}$. The size of the first order scalar fractional density gradient, however, is of order $|\Delta| \sim 10^{-4}$ (see also next section) as suggested by the temperature fluctuations in the Planck data [15]. Therefore, the couplings of shear and $\Delta_{\langle ab \rangle}$ are at most of order $\sqrt{3\Omega_{\mathrm{GW}}(\kappa, \tau)} \times 10^{-4}$. The pure shear

term dominates this and the terms of order $|\Delta|^2$ if $|\sigma^{(1)}| > |\Delta^{(1)}| \sim 10^{-4}$. This turns out to be valid for a rather big set of values. We find that for strong transitions $\alpha \to \infty$ it can proceed as fast as $\beta/H_* \approx 100$ until the maximal value of ρ_{GW} is of order 10^{-4}. Vice versa, for a very long transition $\beta/H_* = 1$, the strength can be as small as $\alpha \approx 0.1$ before being comparable to the magnitude of Δ. This estimation subsequently motivates the ansatz of Eq. (5.1) and confirms that the pure shear term is the most interesting in case of strong phase transitions.

5.3. Imprints on the matter power spectrum

In Sec. 2.1.2 of chapter 2 we have seen that we can account for modifications of the matter power spectrum $\mathcal{P}(k)$ caused by extra perturbations $\delta^{(2)}$ with the help of the transferfunction $T(k)$. Since in our case the additional variations are induced on sub-horizon scales, the transferfunction encodes the relative change they induce on sub-horizon primordial perturbations $\delta_*^{(1)}(k)$ at time t_*. Therefore, we define the transferfunction with the ratio of second order and first order perturbation:

$$T^2_{\delta^{(2)}}(k) := 1 + \left(\frac{\delta^{(2)}(k)}{\delta_*^{(1)}(k)} \right)^2 . \tag{5.19}$$

The information about the altered density fluctuations is then transmitted to the matter power spectrum via the relation

$$\tilde{\mathcal{P}}(k) \sim T^2_{\delta^{(2)}}(k) \mathcal{P}(k) . \tag{5.20}$$

With the perturbations $\delta^{(2)}(k)$ derived in the last section, the function $\delta_*^{(1)}(k)$ remains to be estimated. One possible way is to estimate this function as the standard deviation from the linear matter power spectrum. To do this, we use the fitting formula Eq. (2.36) of the present linear matter power spectrum $\mathcal{P}_0(k)$ and transport it back to the time of the phase transition. Essentially, the spectrum went through two stages since then. First, shape changes during the last part of the radiation dominated era between the occurrence of the phase transition until equality, and secondly mode-independent steady growth in magnitude during matter domination. We accounted for the latter phase by multiplying the spectrum today, $\mathcal{P}_0(k)$, with the linear growth function

$$D_+(a) \approx \frac{5}{2} \frac{a \Omega_{m_0}}{\Omega_{m_0}^{3/4} - \Omega_\Lambda + (1 + \Omega_{m_0}/2)(1 + \Omega_\Lambda/70)} , \tag{5.21}$$

which allows to transport the matter power spectrum back to equality $\tilde{\mathcal{P}}_{\mathrm{eq}}(k) = \mathcal{P}_0(k) D_+^2(a_{\mathrm{eq}})$. With the values for the density parameters of total matter Ω_{m_0} and dark energy Ω_Λ measured by Planck [109] the growth factor evaluates at equality to $D_+(a_{\mathrm{eq}}) \approx 2.5 \cdot 10^{-4}$. Before equality, however, sub-horizon modes remained almost constant in size, but at the time, when the phase transition happened, those modes

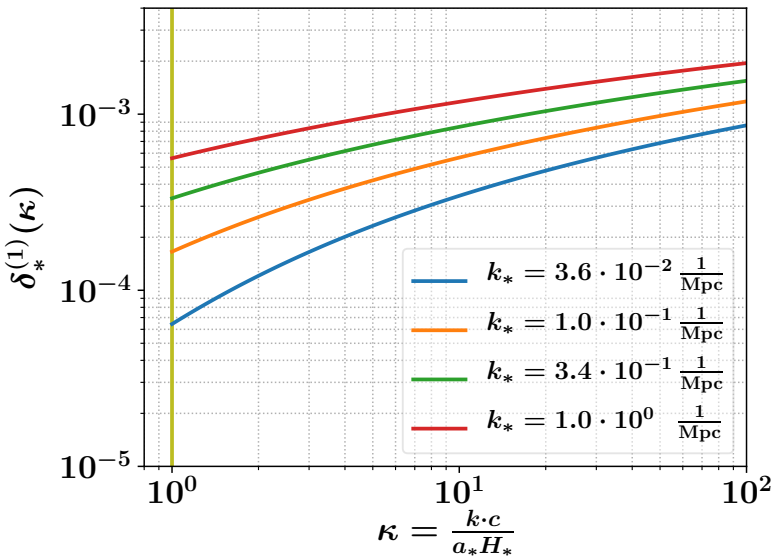

Figure 5.4.: The primordial first order density perturbations estimated from the linear matter power spectrum at sub-horizon scales as a function of the dimensionless wave number κ. Shown are the estimations for four different horizon modes k_*. Adapted from [5].

smaller than k_* had not yet entered the horizon. Thus, we shall restrict ourselves only to modes lager than k_*. Joining these two facts we estimate the primordial modes as

$$\delta^{(1)}_*(k) \cong D_+(a_{\mathrm{eq}}) \sqrt{\int_0^\infty \mathrm{d}\tilde{k} \frac{\tilde{k}^2}{2\pi^2} \mathcal{P}_0(\tilde{k}) W_k^2(\tilde{k})} \quad \text{for} \quad k_* \leq k\,, \tag{5.22}$$

where $W_k(\tilde{k}) := \frac{3}{(\tilde{k}/k)^3}(\sin(\tilde{k}/k) - \tilde{k}/k\cos(\tilde{k}/k))$ is the window function typically used for truncating the spectrum at some scale k. For later use we reformulate $\delta^{(1)}_*(k)$ in terms of the dimensionless wave number $\delta^{(1)}_*(\kappa \cdot k_*)$ and display the result in Fig. 5.4 for different transition times. We observe, that the amplitude of the primordial perturbations is of order 10^{-4} and can even exceed 10^{-3} at high wave numbers.

The resulting form of the transferfunction Eq. (5.19) using Eqs. 5.9 and 5.22 is presented on the left hand side of Figs. 5.6, 5.7, and 5.8 for different choices of percolation times t_*, durations r_β^{-1} and strength α, respectively. As expected, for transitions providing smaller amounts of supercooling and strength the transferfunction approaches unity, while the peak position is determined by the time and duration of the transition. In order to illustrate how these effects modify the matter power spectrum at equality, we adjust it by $T^2_{\delta^{(2)}}$ such that it reads

$$\tilde{\mathcal{P}}_{\mathrm{eq}}(k) = T^2_{\delta^{(2)}}(k) \mathcal{P}_0(k) D^2_+(a_{\mathrm{eq}})\,. \tag{5.23}$$

On the right hand side of Figs. 5.6, 5.7, and 5.8 we show the altered matter power spectra

associated with the transferfunctions on the left hand side. In Fig. 5.5 we have graphically summarized and illustrated the procedure that we conducted to reach Eq. (5.23) for an easier replicability. Next, we aim to derive limits on the transition paramters α and r_β

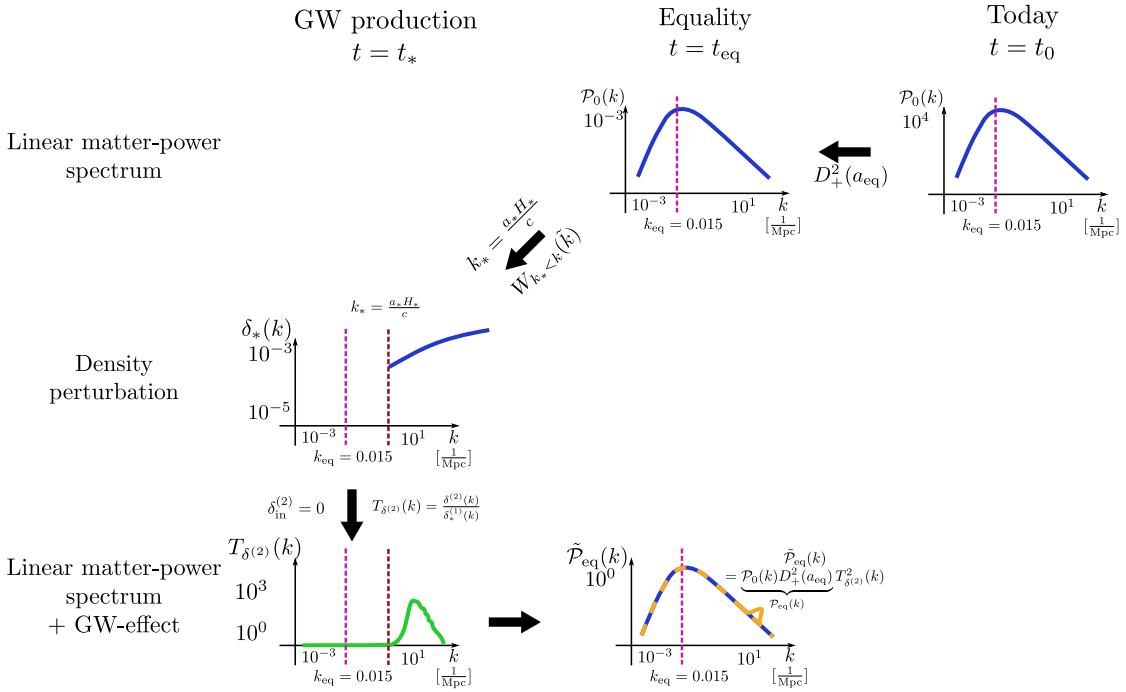

Figure 5.5.: Graphical explanation of our strategy to find the modified linear matter power spectrum. Starting from the upper right, using the growth function we reproduce the amplitude of the matter power spectrum at equality. Then, we estimate the linear perturbations at the scale k_* from it and use the result in order to derive the transfer-function. Finally, we find the modified matter power spectrum. Graphic modified from [5].

for different percolation times t_*. Obviously, the height of the induced peak is mainly controlled by the former two parameters which becomes apparent from the prefactor in Eq. (5.12). As maximally allowed deviation from the linear matter power spectrum we choose to demand that any change to the spectrum should not exceed the limit set by cosmic variance, which constitutes a statistical uncertainty on the precision to which the matter power spectrum can be measured [213]. In the case of Gaussian random fields and an observational volume $V \approx 1(\mathrm{Gpc}/h)^3$, which contains N modes, the cosmic variance of the spectrum is defined as

$$\sigma(k) := \sqrt{\mathrm{cov}(\mathcal{P}_0(k), \mathcal{P}_0(k))} = \mathcal{P}_0(k) \sqrt{\left(\frac{2}{N} + \frac{1}{n}\right)}\,, \tag{5.24}$$

where n is related to the so called band-averaged trispectrum. According to Ref. [214] this spectrum is approximately of size $1/n \approx 0.0079^2\,(\mathrm{Gpc}/h)^3/V$ and the number of modes can be estimated as $2/N = (2\pi)^2/(V \cdot k^2 \Delta k)$, where $\Delta k \sim 0.02 \cdot \log(k\,\mathrm{Mpc})\,(\mathrm{Mpc}/h)^{-1}$

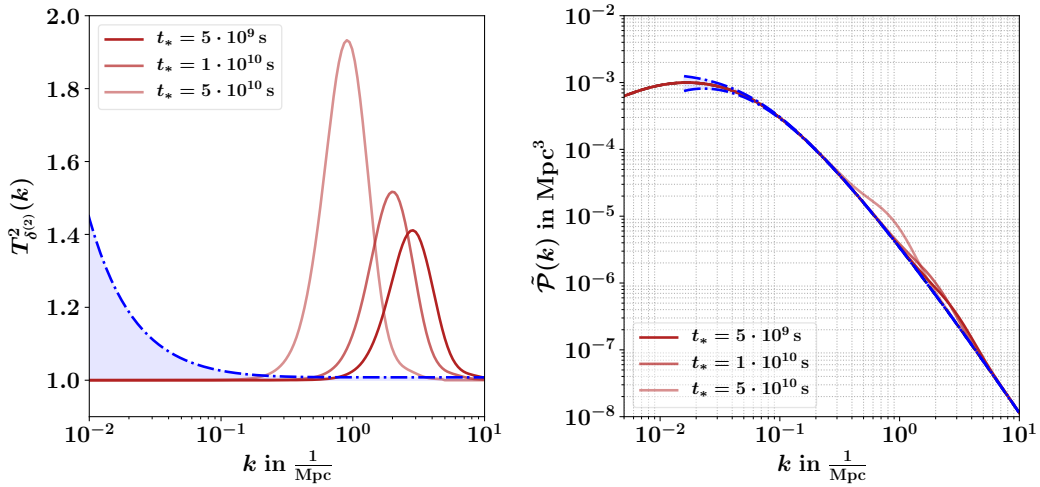

Figure 5.6.: *Left:* The transferfunction for $\delta^{(2)}$ for different times t_* (red shades) and the cosmic variance limit (blue area). *Right:* The modified linear matter power spectrum for different times t_* (red shades). We have set the values for the other parameters to $r_\beta^{-1} = 3$ and $\alpha = 3$. Adapted from [5].

represents the typical distance between galaxies. Imposing this bound upon the modified matter power spectrum $\tilde{\mathcal{P}}(k)$ creates the blue areas in Figs. 5.6, 5.7, and 5.8 which are hardly seen in the right hand side of the plots. Using this, the cosmic variance bound can be translated into exclusion regions on α-β parameter pairs in dependence on the time t_*. In Fig. 5.9 we show a parameter scan in which red shaded regions denote excluded values and white regions denote allowed choices of α and β. As a main result of this work, we can exclude a combination of long $r_\beta < 5 - 6.8$ and very strong $\alpha > 1$ FOPTs to have taken place during these times. The bounds on the parameter triples (α, β, t_*) can be also translated into a new limit on GW signals today. To do so, we use the formula for the logarithmic GW abundance today given by [201]

$$h^2\Omega^{\log}_{\text{GW}_0}(f) = 1.67 \times 10^{-5} \cdot r_\beta^{-2} \cdot \left(\frac{\alpha}{1+\alpha}\right)^2 \left(\frac{100}{g_*}\right)^{\frac{1}{3}} \left(\frac{0.11}{0.42+1}\right) \frac{3.8(f/f_{\text{peak}})^{2.8}}{1+2.8(f/f_{\text{peak}})^{3.8}}\,, \tag{5.25}$$

where the peak frequency f_{peak} today reads

$$f_{\text{peak}} = 16.5 \times 10^{-6}\,\text{Hz} \frac{0.62}{1-0.1+1.8} r_\beta \left(\frac{T_*}{100}\right) \left(\frac{g_*}{100}\right)^{\frac{1}{6}}\,, \tag{5.26}$$

and g_* denotes the number of relativistic degrees of freedom at the time of the transition. Here we take the value of the standard model g_* which is true after the QCD phase transition [215]. However, since we investigate here FOPTs from models beyond the SM this value may change depending on the field content. Therefore, g_* must be adapted to the specific model. During radiation domination the temperature of the plasma at a

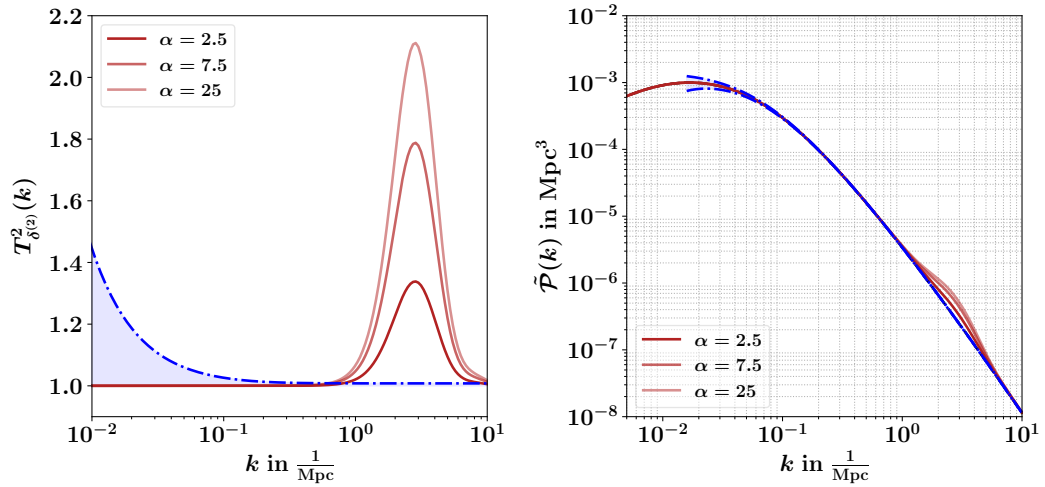

Figure 5.7.: *Left:* The transferfunction for $\delta^{(2)}$ for different values of α (red shades) and the cosmic variance limit (blue area). *Right:* The modified linear matter power spectrum for different values of α (red shades). We have set the values for the other parameters to $r_\beta^{-1} = 3$ and $t_* = 5 \cdot 10^9\,\text{s}$. Adapted from [5].

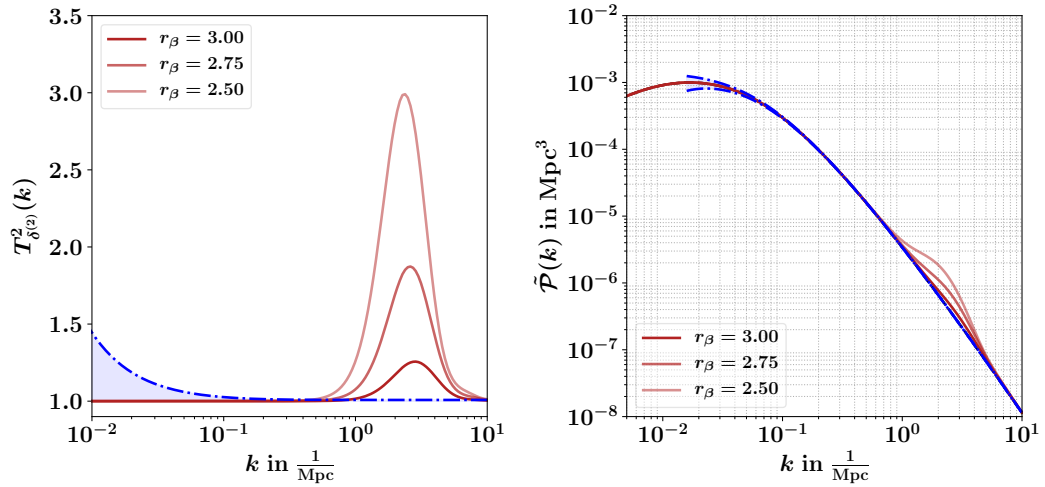

Figure 5.8.: *Left:* The transferfunction for $\delta^{(2)}$ for different times t_* (red shades) and the cosmic variance limit (blue area). *Right:* The modified linear matter power spectrum for different times t_* (red shades). We have set the values for the other parameters to $r_\beta^{-1} = 3$ and $\alpha = 3$. Adapted from [5].

certain time is given by the relation

$$T_* = \frac{30}{\pi^2}\frac{3}{4g_*^3}\left(\frac{1}{8\pi G t_*^2}\right)^{\frac{1}{4}} . \tag{5.27}$$

With this we can convert the bounds on the phase transition parameters due to linear

structure formation to bounds on the maximal magnitude of GW signals. The result is shown in Fig. 5.10 and constitutes the another central result of this work. The frequency band of $f \approx 1.5 \times 10^{-16}\,\mathrm{Hz}$ to $f \approx 1.5 \times 10^{-14}\,\mathrm{Hz}$ in Fig. 5.10 corresponds approximately to the scales on the right flank of the matter power spectrum where our method applies. Also shown are the present and future limits that are or will be set by various experiments. We show here the space-interferometer LISA [45] which is a planned experiment and the timing pulsar arrays [50] NANOGrav [51, 54], PPTA [52] and EPTA [53] which have already set bounds. Additionally we show indirect bounds emerging from the CMB [216–218] which constraints the maximal allowed effective number of neutrino species $N_\nu + \Delta N_\nu$ where $N_\nu = 3$ in the SM. Since these constitute radiation energy, the number can be translated into a bound on the maximal amount of radiation and thus on GWs via [160, 219, 220]

$$h^2 \Omega_{\mathrm{GW}}(f) \leq 5.6 \cdot 10^{-6} \Delta N_\nu \,. \tag{5.28}$$

Besides the CMB also BBN induces a limit to relativistic neutrino species which reads $\Delta N_\nu \leq 0.2$ [221] and is added to Fig. 5.10. We show the abundance of a stochastic GW background as measured today against the frequency f and the comoving wave number k. Note that the bound is other than expected larger for $\alpha = 1$ than for $\alpha \geq 20$. This originates from the fact that for larger α also larger r_β values are excluded, see Fig. 5.9. In turn, for $\alpha = 1$ the inverse duration ratio is smaller, which has much bigger influence on the amplitude of the GW signal than α, see Eq. (5.25). With this result we close this section. In the next part we put our findings into context and conclude.

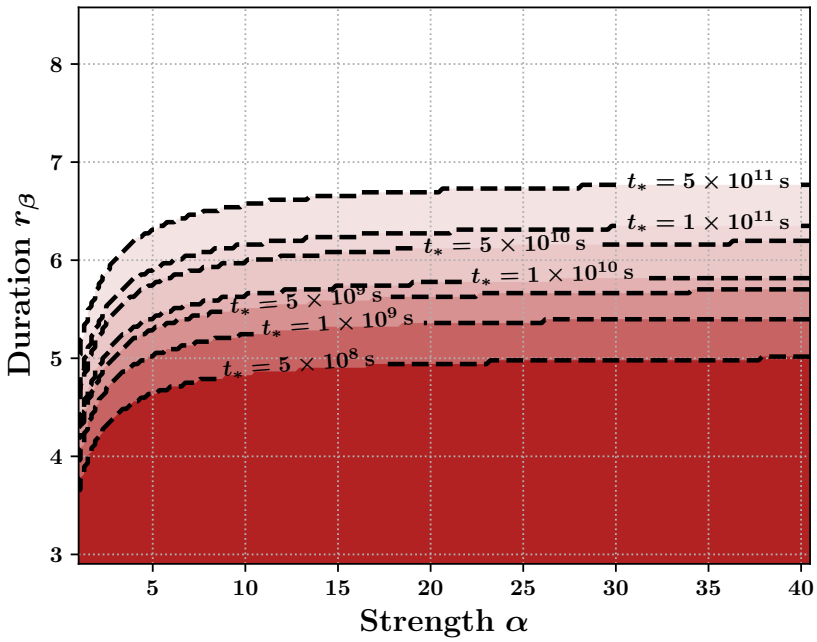

Figure 5.9.: Exclusion parameter region in the α-r_β plane for percolation times t_* which roughly correspond to scales below $k_{\rm eq}$ and above $k = 10\,{\rm Mpc}^{-1}$. The red shaded areas show the constrained values. Taken from [5].

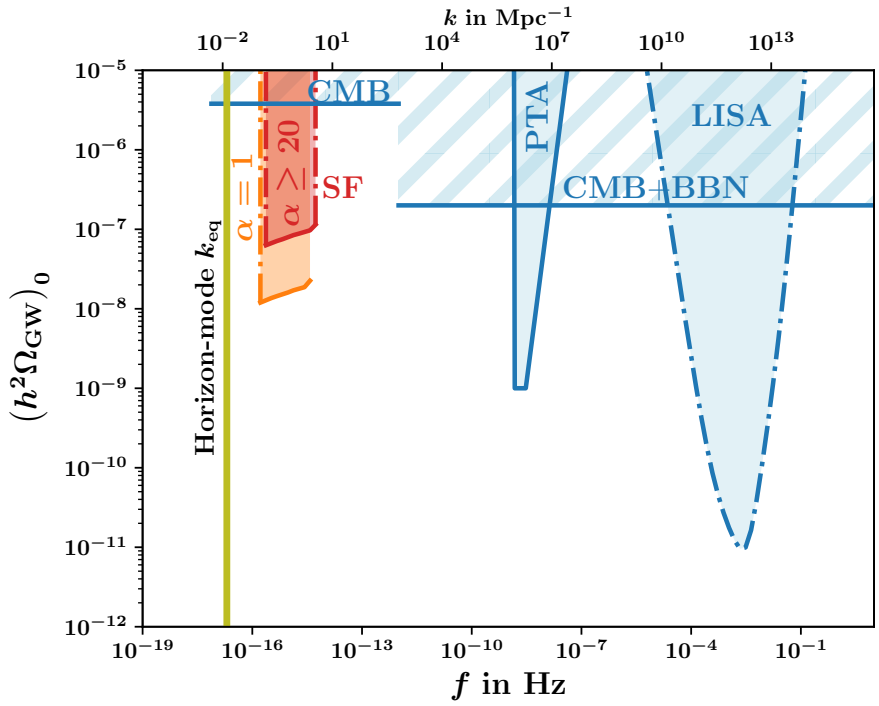

Figure 5.10.: Constraints on the GW abundance today. Next to indirect limits of the CMB and BBN we show the future limit that LISA can set and the one set by timing pulsar arrays. The conversion of the bounds on the phase FOPT parameters that arise from cosmic variance to constraint regions in this plane are shown in red and orange for different α. Taken from [5].

Part III

Final

Chapter 6

Discussion

Let us now turn to the interpretation of our results. First, we put them into context with regards to generic particle models and then generally evaluate our approach to investigate interactions between GWs from FOPTs and density perturbations.

As we have found, to have an impact on the matter power spectrum, the phase transition is required to take place at relatively late times $t_* \gtrsim 10^6\,\mathrm{s}$; much later than for example BBN, taking place at $\sim 10^2\,\mathrm{s}$. This certainly constitutes an untypical time for phase transitions usually considered in particle physics. As depicted in Tabs. 6.1 and 6.2 most models place them at the GeV or TeV scale. However, *late phase transitions* have been considered in the literature in recent years, usually refer to the matter dominated era [222–230]. For the discussion, we want to pay special attention to Ref. [77], which we mentioned already in the introduction. In this paper the generation of density perturbations by a FOPT and the accompanying GWs is considered during the matter dominated phase and at first order, where the extra energy density affects the collapse dynamics of overdensities. This, in turn, changes the amount of enclosed fluctuations in a spherical shell as a function of the transition duration. As a future project, it would be interesting to study if this approach is also viable during radiation domination and if one can connect it to parameters inferred from the underling particle model.

Besides the transition time, we were also able to put stringent limits on the strength and duration, as shown in Fig. 5.9. In Tabs. 6.1 and 6.2 we have listed the corresponding quantites for some exemplary models. Most models, especially those around the EW scale, predict smaller values for the latent heat, $\alpha < 1$, and very fast completion, $r_\beta \sim 100 - 1000$. We observe that especially singlet extensions of the SM modifying the EW phase transition require a huge amount of additional scalars (~ 60) to acquire a latent heat larger than unity. However, in Tab 6.2 we have also listed a model that reaches comparably strong, $\alpha = 0.2$, and long, $r_\beta = 6.42$, transitions in a Higgs portal model. In contrast to the EW scale models, we find the most stringent limit for $\alpha > 1$ on the inverse duration to be $r_\beta \lesssim 6.8$. Due to the low scale behavior of the cosmic variance, which becomes smaller at higher wave numbers, earlier FOPTs are less constrained. Remarkably, such extreme supercooling conditions can be achieved particularly in models that are almost or fully scale invariant[1] [159]. Therefore, *conformal models* are of special

[1] See e.g. the discussion of the Dilaton model in Ref. [159].

Model	Ref.	T_{nuc} (GeV)	α	r_β
Majoron inverse seesaw	[68]	293	0.5	4.9
		183	7.7×10^{-4}	7.2×10^{4}
		77	0.1	231
		122	1.4×10^{-2}	3.1×10^{3}
		92	9.4×10^{-3}	3×10^{4}
SM + 1 scalar	[63]	100	10^{-2}	2×10^{4}
		100	6×10^{-2}	10^{3}
		100	10^{-1}	10^{2}
SM + 4 scalars	[63]	100	2×10^{-2}	4×10^{4}
		100	10^{-1}	10^{3}
		100	4×10^{-1}	10^{2}
SM + 60 scalars	[63]	100	6×10^{-2}	10^{5}
		100	8×10^{-1}	2×10^{3}
		100	2	2×10^{2}
EW with Higgs portal	[159]	56.4	0.20	6.42
2 HDM	[159]	68.71	0.046	2446

Table 6.1.: Benchmark values for phase transition parameters for a selection of models.

interest to the scenario described in this work and certainly require a more detailed investigation in this context. Scale invariance would also allow to place the transition at the scales we characterized as relevant for imprints in the structure. However, it remains to be studied if such a model still can address open issues in the ΛCDM or the SM. Other models exhibiting long lasting phase transitions are for example proposed in the context of Super Symmetry (SUSY) by Ref. [231] ($r_\beta \sim 6.0$) and models with extraordinary strong transitions ($\alpha = 5$) are of Randall-Sundrum type or possible in composite Higgs theories ($\alpha = 10, r_\beta = 3$) [232]. At the moment, we are not aware of models that meet all conditions at once. Namely, taking place around the mentioned scales with the necessary strength and duration. Therefore, with the exclusion regions of Fig. 5.10 we could not yet exclude a specific model.

After having discussed our result in the context of generic particle models, we now address the limitations of our work. Most of them arise from the second order perturbation procedure. In the perturbative expansion we assumed that the fluid is perfect and thus that anisotropic stress contributions vanish, $\pi_{ab} = 0$. However, the gravitational radiation emerges from non-zero anisotropic stress $\Omega(k,t) \sim \Lambda^{ij,mn} T_{ij} T^{*mn} \sim \Pi^2$. In Ref. [77], a similar problem is briefly discussed. Here the author argues that the gravity waves will fill the space uniformly and instantaneously, while the anisotropic stress would remain a localized source. If we would allow in the perturbation calculation for a non-zero, transverse anisotropic stress due to the conservation laws Eqs. (2.61) and (2.62), this would constitute a coupling to the acceleration $A_a^{(1)}$. Since $A_a^{(1)} \sim \mathrm{D}_a p^{(1)}$, which induces a direct connection between the pressure gradient at second order and at first order,

Model	Ref.	T_{nuc} (GeV)	α	r_β
Conformal B-L	[233]	10^3	5×10^4	20
		8×10^3	10^5	18
		10^5	10^8	8
Warped spacetime	[234]	200	5	120
		320	3	250
Dark sector with gauged $U(1)$	[61]	$10^{-2} - 100$	≥ 0.1	≥ 180
DSFZ-Axion	[235]	9×10^6	3.5	150
		6×10^7	10^6	15
General NMSSM	[231]	76.4	0.143	6.0
		112.3	0.037	277
SM + dim. 6 operator	[236]	26	2.3	5
Composite Higgs	[232]	150	≥ 10	~ 3

Table 6.2.: Benchmark values for phase transition parameters for a selection of models.

fluctuations would not propagate independently. As our calculation very much relied on the direct proportionality of acceleration and density gradient, this would significantly complicate the calculation and require additional investigations. Besides this, a coupling $\sim \pi_{ab} A^b$ also appears in the time-dependent evolution of the density gradient in Eqs. (2.72) and (2.73). It is likely that this coupling will not generate large effects similar to the direct coupling of density perturbations and shear stresses. This might also be true for the couplings discussed before.

Another possible limitation originates from the duration of the transition, which lasts almost a Hubble and therefore friction effects could become important. However, we have tested this in our numerical calculations and couldn't find any significant deviations from the solution without the friction term. Moreover, we assumed that the sound speed c_s^2 and the equation of state parameter ω remain constant in time. Close to matter-radiation equality at $t_* \approx 10^{11}\,\text{s}$, we find a mild deviation of the equation of state from a pure radiation fluid with $\omega \approx 0.27$, which do not alter our result significantly. We therefore expect that the equation of state parameter is approximately constant during the short time of a phase transition. Additionally, as we have discussed, at second order the sound speed is in good approximation the relation between pressure and density perturbations, if the sound speed remains constant. For the short transition and in models involving more scalars than fermions this is a reasonable assumption, see Ref. [76].

Further limitations could arise from the fact, that we set $\Lambda = 0$ in our perturbation calculation. However, the FOPTs we focus on generate a strong supercooled phase producing $\Lambda > 0$ during the propagation of bubbles. Since the phase of bubble collision, which turns the universe back to radiation domination, and the production of second order density perturbations coincide, it is difficult to clearly separate the two regimes. Thus, in a more realistic scenario it might be best to account for the reheating time.

Let us emphasize that the scale on which we excluded a stochastic GW background in Fig 5.10 could be further tested by Lyman-α-forest data, see Refs. [12, 237, 238]. Since the cosmic variance is the most conservative bound on the matter power spectrum, using these measurements would exclude a smaller region in the $\alpha - \beta$ plane, which can be tested further in the future[2].

All in all, though we could show that effects of FOPTs transmitted via GWs are possible, we lack models in the found parameter region to compare our result to. Furthermore, perturbing the non-linear equations to second order requires many simplifications that each might be fulfilled better or worse. Nevertheless, based on the acquired results here and in the literature, there is room for future work. We present some possible topics in the next section.

6.1. Outlook

The results we have found in this thesis can be studied further, especially some assumptions and simplifications could be investigated in more depth. From the point of view of cosmological perturbation theory, it would be interesting to redo the second order perturbation analysis in the Bardeen formalism where Einstein's equations are perturbed directly and compare the result with ours. Furthermore, the photon oscillations induced will also be imprinted in higher multipoles of the CMB. Therefore, one could test if this leads to additional constraints.

Certainly, it is also interesting to extend already existing approaches in the future, e.g. Ref. [77] to the case of radiation domination and different particle models. Moreover, one could apply the findings of Schmid et. al. [73, 74] to particle models and effects on primordial perturbations due to a changing speed of sound $c_s^2(t)$ in fermion rich models [76]. The benefit of these approaches is that density perturbations are already affected at first order, which might lead to stronger effects. Furthermore, the linear perturbations could also be altered by the phase of supercooling itself. Since the universe becomes vacuum energy dominated, $\Lambda > 0$ and $\omega = -1$, this changes the equation of motion of $\delta^{(1)}$, see Eq. (2.79).

More direct effects on already existing linear perturbations could also arise in a similar manner as they do for neutrinos. Since the collision of bubbles induces an anisotropic stress to the fluid, it's scalar part Π induces a difference in the Bardeen potentials $\Psi - \Phi \sim \Pi$. By using the CAMB code [239–241] and the analytic results we found in Sec. 3.2.1 one could deduce the effects on the matter power spectrum by this channel. The effect of additional anisotropic stress in the fluid on the CMB has been studied in the past, see e.g. [242].

However, one should always bear in mind that FOPTs are events on sub-horizon scales and therefore the time on which they have to occur to effect structure formation is tightly constrained to late times. Early phase FOPTs could have altered the structure only by the production of primordial black holes at very small scales [243]. In these models the collision of bubbles excites the density fluctuation amplitude to exceed the

[2]We thank Matteo Viel for pointing this out.

critical collapse value and thus black holes form. This has been extensively studied in the literature as a possibility and it would be interesting to see if one can derive general bounds on α and r_β from the bounds on primordial black hole masses.

Lastly, let us mention a recently proposed interaction between density fluctuations and GW in the opposite direction, where the GW signal experiences modifications from density perturbations [244]: Still a lot of interesting work can be done!

Chapter 7

Conclusion

In conclusion we have shown that FOPTs exhibit the ability to imprint a peak-like feature in the matter power spectrum via GWs, if they are strong $\alpha \geq 1$, long lasting $\beta/H_* \lesssim 6.8$ and occur at length-scales of galaxies and larger. The feature is caused by second order fluctuations seeded from inhomogeneities in the GW energy density. The radiation fluid adopts this inhomogeneity and is excited to oscillations, which are dominated by the slope of the GW energy density. Before decoupling, the photons are tightly coupled to the baryons and thus we identify the perturbations as second order baryon acoustic oscillations driven by inhomogeneities in the energy density of GWs, which leads to an enhanced probability to observe structures on Mpc-scales.

We have established these results by perturbing two coupled non-linear equations monitoring the evolution of density gradients in the 1+3 covariant framework. Our calculation culminated into the aforementioned wave-like equation for second order density perturbations where we have singled out the fractional energy density in GWs as the most important source term in presence of a strong FOPT. Therewith, we provide a direct link between GWs and density perturbations. Using this equation we have derived bounds on the maximal allowed duration and strength of the phase transition by comparing the resulting fluctuations altering the matter power spectrum with the bound put by cosmic variance on it. Moreover, these bounds also translate to an exclusion region for a relic stochastic GW background today, which is not reached by planned GW-experiments. However, further research tackling the problem from different perspectives is needed. Especially, a deeper comparison with proposals in which density fluctuations are altered already at the linear level should be addressed next. Beyond cosmological considerations, the investigation of particle models that have the ability to offer solutions to the most prominent problems of the SM, such as the identity of DM, and also exhibit a FOPT at these late times should be carried out.

All in all, this work shows that extracting additional information from different concepts is a promising way to go. The interaction between phase transitions and structure formation is such a way and has the potential to enable insights into the deepest secrets of modern fundamental physics. As it is “[...] a tough time for fundamental physics.” as the recently deceased Steven Weinberg[1] put it [246] and the parameter

[1] *3.5.1933-†23.7.2021 [245].

spaces for many current theories beyond the SM become increasingly under pressure, new, exotic and unexpected paths have to be pursued. The picture of the structure of the universe has evolved a lot since Vincent van Gogh drew his famous painting of a starry night; it is thrilling to await what will be added next on the canvas in the near future and maybe the next new element is the footprint of a first-order phase transition in the large scale structures of our universe.

Part IV

Appendix

Appendix A

Notation and Conventions

Throughout this work we use natural units $c = \hbar = 1$. However, for better readability we restore the light speed c where appropiated. This is mainly done in the figures in chapter 5. Newtons constant is taken as $G = 6.674 \times 10^{-11} \frac{\mathrm{m}^3}{\mathrm{kg\,s}^2}$ and for the slope of the primordial power spectrum we take $n_s \approx 1$. Conformal time is denoted by η and cosmic time by t. Note, that primes on a variable have two different meanings: In the first part of this work primes denote derivatives with respect to conformal time, while in the second part they denote derivatives with respect to the dimensionless cosmic time τ. Sometimes we use the reduced Hubble parameter $H = h \times 100 \frac{\mathrm{km}}{\mathrm{s\,Mpc}}$ whose value today is taken to $h_0 \approx 70$. We use the metric signature $(-+++)$ common in cosmology and relativistic physics.

We distinguish between 3+1 slicing and 1+3 threading of space-time by using opposite letter types for the index. In the 3+1 framework we use Greek indices for four-vectors $\mu, \nu, \dots = 0, 1, 2, 3$ and Latin indices for spatial vectors $i, j = 1, 2, 3$. In the 1+3 splitting, Latin indices denote four-vectors $a, b, \dots = 0, 1, 2, 3$ and Greek indices three-vectors $\alpha\beta, \dots = 1, 2, 3$. Additionally, if we do not refer to the components, but to the full vector, we write spatial vectors in bold letters $\mathbf{V}$.

Transformation into Fourier space are preformed according to

$$f(\mathbf{x}) = \int \mathrm{d}x^3 f(\mathbf{k}) e^{-i\mathbf{k}\cdot\mathbf{x}}\,, \tag{A.1}$$

while the inverse transformation is

$$f(\mathbf{k}) = \frac{1}{(2\pi)^3} \int \mathrm{d}k^3 f(\mathbf{x}) e^{i\mathbf{k}\cdot\mathbf{x}}\,. \tag{A.2}$$

Note, however, that in Sec. 3.2.1 we use a slightly different Fourier convention for transforming from time to frequency space ω in order to be consistent with the respective literature.

Appendix B

Identities and Harmonic Decomposition

B.1. Identities in the 1+3 decomposition of space-time

The behavior of the orthogonal projection operator h_{ab} under the action of the projected gradient and the time derivative fulfills the relations [86, 123]

$$\mathrm{D}_a h_{bc} = 0, \tag{B.1}$$
$$\mathrm{D}^a h_{ab} = u_b \Theta, \tag{B.2}$$
$$\dot{h}_{ab} = u_b A_a + u_a A_b \,. \tag{B.3}$$

The decomposition of the four-velocity with respect to the spatial gradient reads

$$\mathrm{D}_b u_a = \sigma_{ab} + \omega_{ab} + \frac{1}{3}\Theta h_{ab} \,. \tag{B.4}$$

In general, different components of the spatial derivative do not commute. They are non-zero in the presence of vorticity ω_{ab} and of the Riemann tensor in the local rest space of the observer $\mathcal{R}_{abcd}$. For a scalar f, a vector V_a and a tensor S_{ab} the commutation laws are [86]

$$\mathrm{D}_{[a}\mathrm{D}_{b]} f = -\omega_{ab}\dot{f} \,, \tag{B.5}$$
$$\mathrm{D}_{[a}\mathrm{D}_{b]} V_c = -\omega_{ab}\dot{V}_{\langle a\rangle} + \frac{1}{2}\mathcal{R}_{dcba}V^d \,, \tag{B.6}$$
$$\mathrm{D}_{[a}\mathrm{D}_{b]} S_{cd} = -\omega_{ab} h_c{}^e h_d{}^f \dot{S}_{ef} + \frac{1}{2}(\mathcal{R}_{ecba}S^e{}_d + \mathcal{R}_{edba}S_c{}^e) \,. \tag{B.7}$$

In a similar manner the time and the spatial derivative also obey a non-zero commutation law

$$\mathrm{D}_a\dot{f} - h_a{}^b(\dot{\mathrm{D}_b f}) = -\dot{f}A_a + \frac{1}{3}\Theta\mathrm{D}_a f + \mathrm{D}_b f\left(\sigma^b{}_a + \omega^b{}_a\right) \,. \tag{B.8}$$

B.2. Harmonic decomposition

In the presence of non-zero curvature, the mode expansion of scalars, vectors and tensors in terms of harmonic functions does not reduce to a standard Fourier transform. In the covariant formalism one uses general harmonic functions $\mathcal{Q}_{\|}$ to account for this fact. They are defined as eigenfunctions with eigenvalue $-k^2/a^2$ of the orthogonal projected Laplace operator (Laplace-Beltrami operator)

$$\mathrm{D}^2\mathcal{Q}_{k,\{\ ,a,ab\}} = -\frac{k^2}{a^2}\mathcal{Q}_{k,\{\ ,a,ab\}}\,, \tag{B.9}$$

where $\mathcal{Q}_k$ denotes scalar harmonics, $\mathcal{Q}_{k,a}$ denotes vector harmonics and tensor harmonics are denoted by $\mathcal{Q}_{k,ab}$. In a flat space-time, $K = 0$, the harmonic functions have the usual plane wave form and the Laplace-Beltrami operator D^2 becomes the Laplace operator ∇^2/a^2 [92, 247]. Choosing an orthonormal basis, $\mathbf{e}_1$ and $\mathbf{e}_2$, in the plane orthogonal to the wave vector $\mathbf{k}$, the harmonic functions read in flat space

$$\begin{aligned}
\mathcal{Q}_{\mathbf{k}} &= \exp\left(-i\mathbf{k}\cdot\mathbf{x}\right),\\
\mathcal{Q}^{[\pm1]}_{\mathbf{k},\alpha} &= \frac{-i}{\sqrt{2}}(\mathbf{e}_1 \pm i\mathbf{e}_2)_\alpha \exp\left(-i\mathbf{k}\cdot\mathbf{x}\right),\\
\mathcal{Q}^{[\pm2]}_{\mathbf{k},\alpha\beta} &= -\sqrt{\frac{3}{8}}(\mathbf{e}_1 \pm i\mathbf{e}_2)_\alpha(\mathbf{e}_1 \pm i\mathbf{e}_2)_\beta \exp\left(-i\mathbf{k}\cdot\mathbf{x}\right).
\end{aligned}$$

Thus the harmonic decomposition of scalars, vectors and tensors simply becomes the Fourier transform

$$f(\mathbf{x},t) = \int \mathrm{d}k^3\, f_{\mathbf{k}}(t)\mathcal{Q}_{\mathbf{k}}\,, \qquad V_a(\mathbf{x},t) = \int \mathrm{d}k^3 \sum_{m=-1,1} V^{[m]}_{\mathbf{k}}\mathcal{Q}^{[m]}_{\mathbf{k},a}\,, \tag{B.10}$$

$$S_{ab}(\mathbf{x},t) = \int \mathrm{d}k^3 \sum_{m=-2,2} S^{[m]}_{\mathbf{k}}\mathcal{Q}^{[m]}_{\mathbf{k},ab}\,, \tag{B.11}$$

where the sums account for the different polarization states. In both appendices we closely followed [5].

Appendix C

Analytic Solution to the Inhomogeneous Wave Equation

An analytic solution to Eq. (5.9) evaluated at the end of the transition τ_f can be found in the limit of small wave number $\kappa \ll \kappa_{\mathrm{peak}}$ and big wave number $\kappa \gg \kappa_{\mathrm{peak}}$, where $\kappa_{\mathrm{peak}} \approx 2\pi r_\beta$ denotes the position of the maximum of the source term $\Omega_{\mathrm{GW}}^{\mathrm{log}}$ in Eq. (3.45). To do so, we first investigate Ω_{GW} in the two limits and then apply the result to Eq. (5.9). The easiest one is the low κ regime. Expanding $\Omega_{\mathrm{GW}}^{\mathrm{log}}$ around small κ and then performing the logarithmic κ-integration yields

$$\begin{aligned} \Omega_{\mathrm{GW}}^{\mathrm{low}} &= C_{\mathrm{GW}}^{\mathrm{low}}(\kappa - \kappa_{\mathrm{min}})^3(\tau_* - \tau)^4(\tau + \tau_* - 2\tau_f)^2\,, \quad \text{with} \\ C_{\mathrm{GW}}^{\mathrm{low}} &= \frac{1}{3} r_\beta \frac{\alpha^2}{(1+\alpha)^2}\,\epsilon\,. \end{aligned} \tag{C.1}$$

For the high κ case the situation is more complicated, since the integration over κ depends on the small κ behavior. Therefore, we split the integration into two parts with respect to κ_{peak} and find

$$\begin{aligned} \Omega_{\mathrm{GW}}^{\mathrm{high}} &= \int_{\kappa_{\mathrm{min}}}^{\kappa_{\mathrm{peak}}} \left(\Omega_{\mathrm{GW}}^{\mathrm{log}}(\kappa,\tau)\right)^{\mathrm{low}} \mathrm{d}\log\kappa' + \int_{\kappa_{\mathrm{peak}}}^{\kappa} \left(\Omega_{\mathrm{GW}}^{\mathrm{log}}(\kappa,\tau)\right)^{\mathrm{high}} \mathrm{d}\log\kappa' \\ &= C_{\mathrm{GW}}^{\mathrm{low}}(\kappa_{\mathrm{peak}} - \kappa_{\mathrm{min}})^3(\tau_* - \tau)^4(\tau + \tau_* - 2\tau_f)^2 \\ &\quad + C_{\mathrm{GW}}^{\mathrm{high}} \frac{\kappa - \kappa_{\mathrm{min}}}{\kappa\kappa_{\mathrm{min}}} \frac{1}{(\tau + \tau_* - 2\tau_f)^2}\,, \end{aligned} \tag{C.2}$$

where we have introduced the coefficient in the high κ regime $C_{\mathrm{GW}}^{\mathrm{high}} = \frac{81}{r_\beta^3}\frac{\alpha^2}{(1+\alpha)^2}\,\epsilon$. Note that the source terms are only defined within the interval $\tau_* < \tau < \tau_f$.

The analytic solution of Eq. (5.9) in the two limits can now be deduced by using the variation of parameter method. Solving first the homogeneous equation $\delta^{(2)\prime\prime}(\kappa,\tau) + \frac{1}{3}\kappa^2\delta^{(2)}(\kappa,\tau) = 0$ yields the solution

$$\delta_h^{(2)}(\kappa,\tau) = A_\kappa \cos\left(\frac{\kappa}{\sqrt{3}}\tau\right) + B_\kappa \sin\left(\frac{\kappa}{\sqrt{3}}\tau\right)\,, \tag{C.3}$$

where A_κ and B_κ are constants, which need to be specified by the initial conditions[1]. With this, the general inhomogeneous solution is then given by

$$\begin{aligned}\delta^{(2)}(\kappa,\tau) = \delta_h^{(2)}(\kappa,\tau) + \frac{8\sqrt{3}}{\kappa}\Bigg[&\sin\left(\frac{\kappa}{\sqrt{3}}\tau\right)\int_{\tau_*}^{\tau_f}\cos\left(\frac{\kappa}{\sqrt{3}}\tilde{\tau}\right)\Omega_{\mathrm{GW}}(\tilde{\tau},\kappa)\,\mathrm{d}\tilde{\tau}\\ &-\cos\left(\frac{\kappa}{\sqrt{3}}\tau\right)\int_{\tau_*}^{\tau_f}\sin\left(\frac{\kappa}{\sqrt{3}}\tilde{\tau}\right)\Omega_{\mathrm{GW}}(\tilde{\tau},\kappa)\,\mathrm{d}\tilde{\tau}\Bigg]\,.\end{aligned} \tag{C.4}$$

The time integrations can now be solved in the high or low wave number regime by inserting Eq. (C.2) or Eq. (C.1), respectively. The low-κ solution $\delta^{(2)\,\mathrm{low}}$ becomes

$$\delta^{(2)\,\mathrm{low}}(\kappa,\tau) = \left(A_\kappa + A^{\mathrm{low}}_{\mathrm{GW}\kappa}\right)\cos\left(\frac{\kappa\tau}{\sqrt{3}}\right) + \left(B_\kappa + B^{\mathrm{low}}_{\mathrm{GW}\kappa}\right)\sin\left(\frac{\kappa\tau}{\sqrt{3}}\right)\,, \tag{C.5}$$

where the modified coefficients $A^{\mathrm{low}}_{\mathrm{GW}\kappa}$ and $B^{\mathrm{low}}_{\mathrm{GW}\kappa}$ read

$$\begin{aligned}A^{\mathrm{low}}_{\mathrm{GW}\kappa} = &-\frac{24C^{\mathrm{low}}_{\mathrm{GW}}\left(\kappa^3-\kappa^3_{\mathrm{min}}\right)}{\kappa^8}\\ &\Bigg[2\sqrt{3}r_\beta^{-1}\kappa\left(2160\sin\left(\frac{\kappa\tau_*}{\sqrt{3}}\right)+\left(1080+36r_\beta^{-2}\kappa^2+r_\beta^{-4}\kappa^4\right)\sin\left(\frac{\kappa\tau_f}{\sqrt{3}}\right)\right)\\ &+\left(19440+216r_\beta^{-2}\kappa^2-6r_\beta^{-4}\kappa^4-r_\beta^{-6}\kappa^6\right)\cos\left(\frac{\kappa\tau_f}{\sqrt{3}}\right)\\ &+432\left(2r_\beta^{-2}\kappa^2-45\right)\cos\left(\frac{\kappa\tau_*}{\sqrt{3}}\right)\Bigg]\end{aligned} \tag{C.6}$$

and

$$\begin{aligned}B_{\mathrm{GW}\kappa^{\mathrm{low}}} = &\frac{24C^{\mathrm{low}}_{\mathrm{GW}}\left(\kappa^3-\kappa^3_{\mathrm{min}}\right)}{\kappa^8}\\ &\Bigg[2\sqrt{3}r_\beta^{-1}\left(2160\kappa\cos\left(\frac{\kappa\tau_*}{\sqrt{3}}\right)+\kappa\left(1080+36r_\beta^{-2}\kappa^2+r_\beta^{-4}\right)\cos\left(\frac{\kappa\tau_f}{\sqrt{3}}\right)\right)\\ &+\left(-19440-216r_\beta^{-2}\kappa^2+6r_\beta^{-4}\kappa^4+r_\beta^{-6}\kappa^6\right)\sin\left(\frac{\kappa\tau_f}{\sqrt{3}}\right)\\ &+432\left(45-2r_\beta^{-2}\kappa^2\right)\sin\left(\frac{\kappa\tau_*}{\sqrt{3}}\right)\Bigg]\,.\end{aligned} \tag{C.7}$$

In the same manner we derive the analytic solution for high dimensionless wave numbers.

[1] In this work we assumed no preexisting second order density perturbations and therefore zero initial conditions.

The general inhomogeneous solution is

$$\delta^{(2)\,\mathrm{high}}(\kappa,\tau) = \left(A_\kappa + A^{\mathrm{high}}_{\mathrm{GW}\kappa}\right)\cos\left(\frac{\kappa\tau}{\sqrt{3}}\right) + \left(B_\kappa + B^{\mathrm{high}}_{\mathrm{GW}\kappa}\right)\sin\left(\frac{\kappa\tau}{\sqrt{3}}\right), \tag{C.8}$$

where the modified coefficients $A^{\mathrm{high}}_{\mathrm{GW}\kappa}$ and $B^{\mathrm{high}}_{\mathrm{GW}\kappa}$ are given by

$$\begin{aligned} A^{\mathrm{high}}_{\mathrm{GW}} =& A^{\mathrm{low}}_{\mathrm{GW}\kappa_{\mathrm{peak}}} - \frac{4C^{\mathrm{high}}_{\mathrm{GW}}(\kappa-\kappa_{\mathrm{peak}})}{3\sqrt{3}\kappa^2\kappa_{\mathrm{peak}}}\left[6r_\beta\sin\left(\frac{\kappa\tau_f}{\sqrt{3}}\right) - 3r_\beta\sin\left(\frac{\kappa\tau_*}{\sqrt{3}}\right) + \right. \\ & 2\sqrt{3}\kappa\left(\left(\mathrm{Ci}\left(\frac{\kappa}{\sqrt{3}r_\beta}\right) - \mathrm{Ci}\left(\frac{2\kappa}{\sqrt{3}r_\beta}\right)\right)\cos\left(\frac{\kappa(2\tau_f-\tau_*)}{\sqrt{3}}\right) + \\ & \left.\left.\left(\mathrm{Si}\left(\frac{\kappa}{\sqrt{3}r_\beta}\right) - \mathrm{Si}\left(\frac{2\kappa}{\sqrt{3}r_\beta}\right)\right)\sin\left(\frac{\kappa(2\tau_f-\tau_*)}{\sqrt{3}}\right)\right)\right] \end{aligned} \tag{C.9}$$

and

$$\begin{aligned} B^{\mathrm{high}}_{\mathrm{GW}} =& B^{\mathrm{low}}_{\mathrm{GW}\kappa_{\mathrm{peak}}} - \frac{4C^{\mathrm{high}}_{\mathrm{GW}}(\kappa-\kappa_{\mathrm{peak}})}{3\sqrt{3}\kappa^2\kappa_{\mathrm{peak}}}\left[6r_\beta\cos\left(\frac{\kappa\tau_f}{\sqrt{3}}\right) - 3r_\beta\cos\left(\frac{\kappa\tau_*}{\sqrt{3}}\right) + \right. \\ & 2\sqrt{3}\kappa\left(\left(\mathrm{Ci}\left(\frac{2\kappa}{\sqrt{3}r_\beta}\right) - \mathrm{Ci}\left(\frac{\kappa}{\sqrt{3}r_\beta}\right)\right)\sin\left(\frac{\kappa(2\tau_f-\tau_*)}{\sqrt{3}}\right) + \\ & \left.\left.\left(\mathrm{Si}\left(\frac{\kappa}{\sqrt{3}r_\beta}\right) - \mathrm{Si}\left(\frac{2\kappa}{\sqrt{3}r_\beta}\right)\right)\cos\left(\frac{\kappa(2\tau_f-\tau_*)}{\sqrt{3}}\right)\right)\right]. \end{aligned} \tag{C.10}$$

The functions $\mathrm{Ci}(x)$ and $\mathrm{Si}(x)$ denote the trigenemetric integrals defined by $\mathrm{Ci}(x) := \int_0^x \frac{\cos t}{t}\,\mathrm{d}t$ and $\mathrm{Si}(x) := \int_0^x \frac{\sin t}{t}\,\mathrm{d}t$, respectively.

We evaluate the analytic solutions Eqs. (C.5) and (C.8) at the end of the transition $\tau = \tau_f$ with zero initial conditions and compare the result with the numerical solution in Fig. 5.3. While we observe a very good agreement of the low wave number approximation with the numerical solution, we find a small phase shift in the oscillation pattern of the high-κ solution. This might be due to the use of κ_{peak} for splitting the integrals, which we took as constant but in fact also changes with time. Nevertheless, the overall slope of the numerical and analytical solutions do coincide perfectly. This appendix is based on Ref. [5].

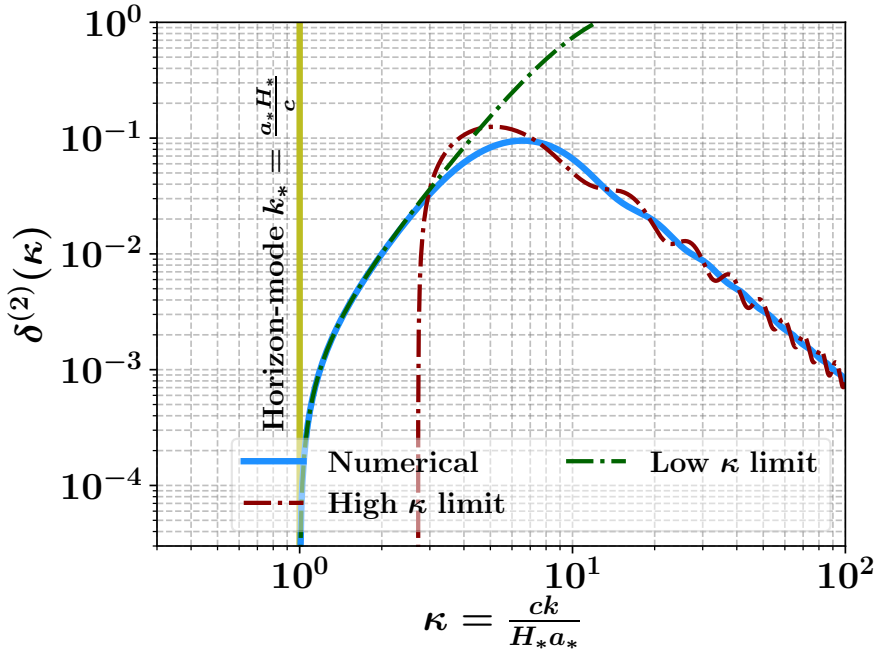

Figure C.1.: Comparison of the analytic solutions in the high (red) and low wave number (green) regime with the numerical solution of Eq. (5.9) (blue). For demonstration reasons we choose $r_\beta = 1$ and $\alpha \to \infty$. Adapted from Ref. [5].

Appendix D

Post Transition generated Second Order Perturbations

After the FOPT is completed, space is filled with gravitational radiation and hence the source term of Eq. (5.9) remains active. However, due to the expansion of the universe, the amplitude of density parameter is redshifted with $\sim a^{-4}(t)$. In the following we show that this justifies to assume that no further second order perturbations are produced from $\Omega_{\mathrm{GW}}(\kappa)$ after the transition has ended and therefore to put the right hand side in Eq. (5.7) to zero.

After the transition Eq. (5.9) reads

$$\delta''(\kappa,\tau)+\frac{a(t)'}{a(t)}\delta'(\kappa,\tau)+\frac{1}{3}\frac{a_*^2}{a(\tau)^2}\kappa^2\delta(\kappa,\tau)=8\frac{H(\tau)^2}{H_*^2}\frac{a_*^4}{a(\tau)^4}\cdot\Omega_{\mathrm{GW}}\left(\kappa\left(\frac{a_*}{a(\tau)}\right),\tau\right). \tag{D.1}$$

Since all bubbles are collided, there is no further source of GWs and therefore the amplitude of the GW density parameter only changes due to redshift. Thus the amplitude of the bare parameter is constant in time $\Omega_{\mathrm{GW}}(\kappa,\tau_f)=\Omega_{\mathrm{GW}}(\kappa)$. We here omit the redshift $\left(\frac{a_*}{a(\tau)}\right)$ in κ, since it does not alter the amplitude. We split the calculation into two parts. First, we solve the homogeneous differential equation and use as initial conditions the amplitudes of second order density perturbations at the end of the phase transition, which we have derived in the result part of this work. Then, we deduce the inhomogeneous solution and compare it's amplitude with the one of the homogeneous solution. The homogeneous solution of Eq. (D.1) for a general $a(\tau)$ yields

$$\delta_h(\kappa,\tau>\tau_f)=C_\kappa\cos\left[\frac{a_*\kappa}{\sqrt{3}}\int_{\tau_f}^{\tau}\frac{1}{a(\tilde{\tau})}\,\mathrm{d}\tilde{\tau}\right]+D_\kappa\sin\left[\frac{a_*\kappa}{\sqrt{3}}\int_{\tau_f}^{\tau}\frac{1}{a(\tilde{\tau})}\,\mathrm{d}\tilde{\tau}\right], \tag{D.2}$$

where C_κ and D_κ are integration constants. In a radiation dominated universe the scale factor and the Hubble parameter evolve as

$$a(\tau)=a_*\sqrt{\frac{\tau}{\tau_*}}\quad\text{and}\qquad H(\tau)=H_*\frac{1}{2\tau}, \tag{D.3}$$

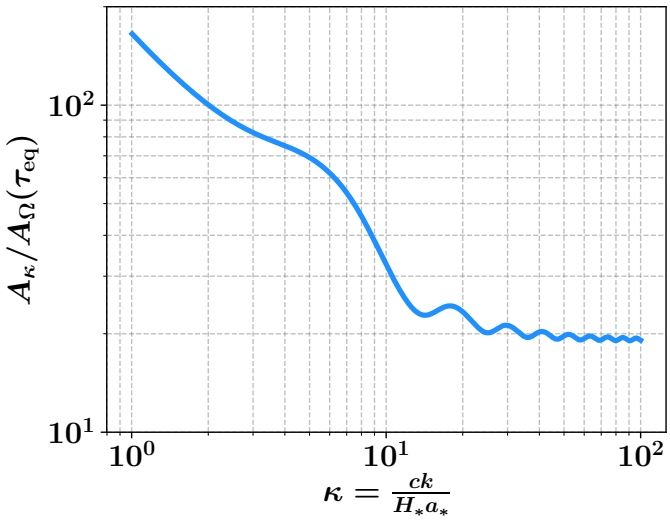

Figure D.1.: Relative amplitudes of second order perturbations sourced during the FOPT and afterwards by the GW density parameter. The amplitude of perturbations that the relic GWs produce until matter-radiation equality is much smaller than the amplitudes produced during the transition. As benchmark value we have used $t_* = 10^{10}\,\mathrm{s}$. Adapted from Ref. [5].

respectively. Plugging these into Eq. (D.2) we can perform the integration

$$\delta_h(\kappa, \tau > \tau_f) = C_\kappa \cos\left[\frac{2\tau_*\kappa}{\sqrt{3}}\left(\sqrt{\tau} - \sqrt{\tau_f}\right)\right] + D_\kappa \sin\left[\frac{2\tau_*\kappa}{\sqrt{3}}\left(\sqrt{\tau} - \sqrt{\tau_f}\right)\right]. \tag{D.4}$$

Applying the variation of parameter method to the differential equation yields the inhomogeneous solution

$$\begin{aligned}\delta_{\rm nh}(\kappa, \tau > \tau_f) = \\ C_\Omega(\kappa,\tau)\cos\left[\frac{2\sqrt{\tau_*}\kappa}{\sqrt{3}}\left(\sqrt{\tau} - \sqrt{\tau_f}\right)\right] + D_\Omega(\kappa,\tau)\sin\left[\frac{2\sqrt{\tau_*}\kappa}{\sqrt{3}}\left(\sqrt{\tau} - \sqrt{\tau_f}\right)\right],\end{aligned} \tag{D.5}$$

with coefficients

$$C_\Omega(\kappa,\tau) = -\int_{\tau_f}^{\tau} \frac{\sqrt{3}8\frac{H(\tilde\tau)^2}{H_*^2}\frac{a_*^4}{a(\tilde\tau)^4}\cdot\Omega_{\rm GW}(\kappa)\sqrt{\frac{\tilde\tau}{\tau_*}}\sin\left(\frac{2\kappa\sqrt{\tau_*}\left(\sqrt{\tilde\tau}-\sqrt{\tau_f}\right)}{\sqrt{3}}\right)}{\kappa}\,\mathrm{d}\tilde\tau \tag{D.6}$$

and

$$D_\Omega(\kappa,\tau) = \int_{\tau_f}^{\tau} \frac{\sqrt{3}8\frac{H(\tilde\tau)^2}{H_*^2}\frac{a_*^4}{a(\tilde\tau)^4}\cdot\Omega_{\rm GW}(\kappa)\sqrt{\frac{\tilde\tau}{\tau_*}}\cos\left(\frac{2\kappa\sqrt{\tau_*}\left(\sqrt{\tilde\tau}-\sqrt{\tau_f}\right)}{\sqrt{3}}\right)}{\kappa}\,\mathrm{d}\tilde\tau\,. \tag{D.7}$$

We simplify Eqs. (D.4) and (D.5) by using the trigonometric identity

$$C\cos x + D\sin x = A\sin(x+\phi)\,, \tag{D.8}$$

where the combined amplitude A and the phase ϕ are defined as $A := \sqrt{C^2+D^2}$ and $\phi := \arctan\frac{C}{D}$, respectively. The homogeneous and inhomogeneous solution then read

$$\delta_h(\kappa,\tau>\tau_f) = A_\kappa \sin\left[\frac{2\tau_*\kappa}{\sqrt{3}}\left(\sqrt{\tau}-\sqrt{\tau_f}\right)+\phi_\kappa\right]\,, \tag{D.9}$$

$$\delta_{\rm nh}(\kappa,\tau>\tau_f) = A_\Omega(\kappa,\tau) \sin\left[\frac{2\sqrt{\tau_*}\kappa}{\sqrt{3}}\left(\sqrt{\tau}-\sqrt{\tau_f}\right)+\phi_\Omega\right]\,. \tag{D.10}$$

In Fig. (D.1) we have plotted the ratio of the amplitude of the perturbations generated during the transition A_κ and the perturbations generated after the transition $A_\Omega(\kappa,\tau_{\rm eq})$ until matter-radiation equality. We have ignored changes in the scale factor and the Hubble rate close to equality here for simplicity. We observe, that the amplitude of the perturbations produced after the transition is much smaller than the amplitude of the fluctuations produced after the transition. This rough estimate justifies to set the right hand side in Eq. (5.7) to zero in good approximation. This appendix is based on Ref. [5].

Bibliography

[7] V. van Gogh, "The starry night — Wikipedia, the free encyclopedia." https://en.wikipedia.org/wiki/File:Van_Gogh_-_Starry_Night_-_Google_Art_Project.jpg, 1889. [Online; accessed 15-July-2021]; Original version: oil on canvas, 73 x 92 cm, Museum of Modern Art, New York.

[8] "Claude monet — Wikipedia, the free encyclopedia." https://de.wikipedia.org/wiki/Claude_Monet. [Online; accessed 14-August-2021].

[9] "Vincent van gogh — Wikipedia, the free encyclopedia." https://en.wikipedia.org/wiki/Vincent_van_Gogh. [Online; accessed 29-July-2021].

[10] M. Colless *et al.*, *The 2dF Galaxy Redshift Survey: spectra and redshifts*, Monthly Notices of the Royal Astronomical Society **328** no. 4, (Dec., 2001) 1039–1063, arXiv:astro-ph/0106498 [astro-ph].

[11] **SDSS** Collaboration, M. R. Blanton *et al.*, *The Galaxy luminosity function and luminosity density at redshift $z = 0.1$*, Astrophys. J. **592** (2003) 819–838, arXiv:astro-ph/0210215.

[12] M. Tegmark and M. Zaldarriaga, *Separating the early universe from the late universe: Cosmological parameter estimation beyond the black box*, Phys. Rev. D **66** (2002) 103508, arXiv:astro-ph/0207047.

[13] T. S. H. C. of Theoretical Cosmology, University of Camebridge, "The origins of the universe: the big beng." http://www.ctc.cam.ac.uk/outreach/origins/big_bang_three.php. [Online; accessed 13-August-2021].

[14] T. E. S. Agency, "Planck history of universe." https://www.esa.int/ESA_Multimedia/Images/2013/03/Planck_history_of_Universe. [Online; accessed 13-August-2021].

[15] **Planck** Collaboration, N. Aghanim *et al.*, *Planck 2018 results. VI. Cosmological parameters*, Astron. Astrophys. **641** (2020) A6, arXiv:1807.06209 [astro-ph.CO].

[16] V. Springel, "The millennium simulation project." https://wwwmpa.mpa-garching.mpg.de/galform/virgo/millennium/. [Online; accessed 29-July-2021].

[17] V. Springel, S. D. M. White, A. Jenkins, C. S. Frenk, N. Yoshida, L. Gao, J. Navarro, R. Thacker, D. Croton, J. Helly, J. A. Peacock, S. Cole, P. Thomas, H. Couchman, A. Evrard, J. Colberg, and F. Pearce, *Simulations of the formation, evolution and clustering of galaxies and quasars*, Nature **435** no. 7042, (June, 2005) 629–636, arXiv:astro-ph/0504097 [astro-ph].

[18] P. W. Higgs, *Broken Symmetries and the Masses of Gauge Bosons*, Phys. Rev. Lett. **13** (Oct, 1964) 508–509. https://link.aps.org/doi/10.1103/PhysRevLett.13.508.

[19] **CMS** Collaboration, S. Chatrchyan *et al.*, *Observation of a New Boson at a Mass of 125 GeV with the CMS Experiment at the LHC*, Phys. Lett. B **716** (2012) 30–61, arXiv:1207.7235 [hep-ex].

[20] **ATLAS** Collaboration, G. Aad *et al.*, *Observation of a new particle in the search for the Standard Model Higgs boson with the ATLAS detector at the LHC*, Phys. Lett. B **716** (2012) 1–29, arXiv:1207.7214 [hep-ex].

[21] S. Weinberg, *A Model of Leptons*, Phys. Rev. Lett. **19** (Nov, 1967) 1264–1266. https://link.aps.org/doi/10.1103/PhysRevLett.19.1264.

[22] S. L. Glashow, *Partial-symmetries of weak interactions*, Nuclear Physics **22** no. 4, (1961) 579–588. https://www.sciencedirect.com/science/article/pii/0029558261904692.

[23] A. Salam, *Weak and Electromagnetic Interactions*, Conf. Proc. C **680519** (1968) 367–377.

[24] G. F. Smoot *et al.*, *Structure in the COBE Differential Microwave Radiometer First-Year Maps*, Astrophys. J. Suppl. **396** (Sept., 1992) L1.

[25] **WMAP** Collaboration, D. N. Spergel *et al.*, *First year Wilkinson Microwave Anisotropy Probe (WMAP) observations: Determination of cosmological parameters*, Astrophys. J. Suppl. **148** (2003) 175–194, arXiv:astro-ph/0302209.

[26] C. L. Bennett *et al.*, *Nine-year Wilkinson Microwave Anisotropy Probe (WMAP) Observations: Final Maps and Results*, Astrophys. J. Suppl. **208** no. 2, (Oct., 2013) 20, arXiv:1212.5225 [astro-ph.CO].

[27] **Planck** Collaboration, P. A. R. Ade *et al.*, *Planck 2013 results. XVI. Cosmological parameters*, Astron. Astrophys. **571** (2014) A16, arXiv:1303.5076 [astro-ph.CO].

[28] V. Springel *et al.*, *Simulating the joint evolution of quasars, galaxies and their large-scale distribution*, Nature **435** (2005) 629–636, arXiv:astro-ph/0504097.

[29] V. Springel, C. S. Frenk, and S. D. M. White, *The large-scale structure of the Universe*, Nature **440** (2006) 1137, arXiv:astro-ph/0604561.

[30] **XENON** Collaboration, E. Aprile *et al.*, *Dark Matter Search Results from a One Ton-Year Exposure of XENON1T*, Phys. Rev. Lett. **121** no. 11, (2018) 111302, arXiv:1805.12562 [astro-ph.CO].

[31] F. Zwicky, *Die Rotverschiebung von extragalaktischen Nebeln*, Helvetica Physica Acta **6** (Jan., 1933) 110–127.

[32] V. C. Rubin and J. Ford, W. Kent, *Rotation of the Andromeda Nebula from a Spectroscopic Survey of Emission Regions*, TheAstrophysicalJournal **159** (Feb., 1970) 379.

[33] D. Clowe, M. Bradac, A. H. Gonzalez, M. Markevitch, S. W. Randall, C. Jones, and D. Zaritsky, *A direct empirical proof of the existence of dark matter*, Astrophys. J. Lett. **648** (2006) L109–L113, arXiv:astro-ph/0608407.

[34] R. H. Cyburt, B. D. Fields, K. A. Olive, and T.-H. Yeh, *Big bang nucleosynthesis: Present status*, Rev. Mod. Phys. **88** (Feb, 2016) 015004. https://link.aps.org/doi/10.1103/RevModPhys.88.015004.

[35] K. Olive, *Review of Particle Physics*, Chinese Physics C **40** no. 10, (Oct, 2016) 100001. https://doi.org/10.1088/1674-1137/40/10/100001.

[36] P. J. E. Peebles and B. Ratra, *The Cosmological Constant and Dark Energy*, Rev. Mod. Phys. **75** (2003) 559–606, arXiv:astro-ph/0207347.

[37] **Supernova Search Team** Collaboration, A. G. Riess *et al.*, *Observational evidence from supernovae for an accelerating universe and a cosmological constant*, Astron. J. **116** (1998) 1009–1038, arXiv:astro-ph/9805201.

[38] **Supernova Cosmology Project** Collaboration, S. Perlmutter *et al.*, *Measurements of Ω and Λ from 42 high redshift supernovae*, Astrophys. J. **517** (1999) 565–586, arXiv:astro-ph/9812133.

[39] J. Aasi *et al.*, *Advanced LIGO*, Classical and Quantum Gravity **32** no. 7, (Mar, 2015) 074001. https://doi.org/10.1088/0264-9381/32/7/074001.

[40] T. Accadia *et al.*, *Status of the Virgo project*, Classical and Quantum Gravity **28** no. 11, (June, 2011) 114002.

[41] **LIGO Scientific, Virgo** Collaboration, B. Abbott *et al.*, *Binary Black Hole Mergers in the first Advanced LIGO Observing Run*, Phys. Rev. X **6** no. 4, (2016) 041015, arXiv:1606.04856 [gr-qc]. [Erratum: Phys.Rev.X 8, 039903 (2018)].

[42] J. H. Taylor and J. M. Weisberg, *A new test of general relativity - Gravitational radiation and the binary pulsar PSR 1913+16*, The Astrophysical Journal **253** (Feb., 1982) 908–920.

[43] **LIGO Scientific, Virgo** Collaboration, B. P. Abbott *et al.*, *GW170817: Observation of Gravitational Waves from a Binary Neutron Star Inspiral*, Phys. Rev. Lett. **119** no. 16, (2017) 161101, arXiv:1710.05832 [gr-qc].

[44] **LIGO Scientific, Virgo, Fermi GBM, INTEGRAL, IceCube, AstroSat Cadmium Zinc Telluride Imager Team, IPN, Insight-Hxmt, ANTARES, Swift, AGILE Team, 1M2H Team, Dark Energy Camera GW-EM, DES, DLT40, GRAWITA, Fermi-LAT, ATCA, ASKAP, Las Cumbres Observatory Group, OzGrav, DWF (Deeper Wider Faster Program), AST3, CAASTRO, VINROUGE, MASTER, J-GEM, GROWTH, JAGWAR, CaltechNRAO, TTU-NRAO, NuSTAR, Pan-STARRS, MAXI Team, TZAC Consortium, KU, Nordic Optical Telescope, ePESSTO, GROND, Texas Tech University, SALT Group, TOROS, BOOTES, MWA, CALET, IKI-GW Follow-up, H.E.S.S., LOFAR, LWA, HAWC, Pierre Auger, ALMA, Euro VLBI Team, Pi of Sky, Chandra Team at McGill University, DFN, ATLAS Telescopes, High Time Resolution Universe Survey, RIMAS, RATIR, SKA South Africa/MeerKAT** Collaboration, B. P. Abbott *et al.*, *Multi-messenger Observations of a Binary Neutron Star Merger*, Astrophys. J. Lett. **848** no. 2, (2017) L12, arXiv:1710.05833 [astro-ph.HE].

[45] P. A.-S. et al., *Laser Interferometer Space Antenna*, 2017.

[46] M. Punturo *et al.*, *The Einstein Telescope: A third-generation gravitational wave observatory*, Class. Quant. Grav. **27** (2010) 194002.

[47] B. Sathyaprakash *et al.*, *Scientific Objectives of Einstein Telescope*, Class. Quant. Grav. **29** (2012) 124013, arXiv:1206.0331 [gr-qc]. [Erratum: Class.Quant.Grav. 30, 079501 (2013)].

[48] S. Kawamura *et al.*, *The Japanese space gravitational wave antenna: DECIGO*, Classical and Quantum Gravity **28** no. 9, (Apr, 2011) 094011. https://doi.org/10.1088/0264-9381/28/9/094011.

[49] V. Corbin and N. J. Cornish, *Detecting the cosmic gravitational wave background with the big bang observer*, Class. Quant. Grav. **23** (2006) 2435–2446, arXiv:gr-qc/0512039.

[50] S. Burke-Spolaor *et al.*, *The Astrophysics of Nanohertz Gravitational Waves*, Astron. Astrophys. Rev. **27** no. 1, (2019) 5, arXiv:1811.08826 [astro-ph.HE].

[51] M. A. McLaughlin, *The North American Nanohertz Observatory for Gravitational Waves*, Class. Quant. Grav. **30** (2013) 224008, arXiv:1310.0758 [astro-ph.IM].

[52] R. N. Manchester ed al., *The Parkes Pulsar Timing Array Project*, Publications of the Astronomical Society of Australia **30** (Jan., 2013) e017, arXiv:1210.6130 [astro-ph.IM].

[53] L. Lentati *et al.*, *European Pulsar Timing Array Limits On An Isotropic Stochastic Gravitational-Wave Background*, Mon. Not. Roy. Astron. Soc. **453** no. 3, (2015) 2576–2598, arXiv:1504.03692 [astro-ph.CO].

[54] **NANOGrav** Collaboration, Z. Arzoumanian *et al.*, *The NANOGrav 12.5 yr Data Set: Search for an Isotropic Stochastic Gravitational-wave Background*, Astrophys. J. Lett. **905** no. 2, (2020) L34, arXiv:2009.04496 [astro-ph.HE].

[55] L. F. Abbott and M. B. Wise, *Constraints on generalized inflationary cosmologies*, Nuclear Physics B **244** no. 2, (1984) 541–548.

[56] M. S. Turner and F. Wilczek, *Relic gravitational waves and extended inflation*, Phys. Rev. Lett. **65** (Dec, 1990) 3080–3083. https://link.aps.org/doi/10.1103/PhysRevLett.65.3080.

[57] D. Baumann, P. J. Steinhardt, K. Takahashi, and K. Ichiki, *Gravitational Wave Spectrum Induced by Primordial Scalar Perturbations*, Phys. Rev. D **76** (2007) 084019, arXiv:hep-th/0703290.

[58] M. C. Guzzetti, N. Bartolo, M. Liguori, and S. Matarrese, *Gravitational waves from inflation*, Riv. Nuovo Cim. **39** no. 9, (2016) 399–495, arXiv:1605.01615 [astro-ph.CO].

[59] J. N. Guenther, *Overview of the QCD phase diagram: Recent progress from the lattice*, Eur. Phys. J. A **57** no. 4, (2021) 136, arXiv:2010.15503 [hep-lat].

[60] S. Profumo, M. J. Ramsey-Musolf, and G. Shaughnessy, *Singlet Higgs phenomenology and the electroweak phase transition*, JHEP **08** (2007) 010, arXiv:0705.2425 [hep-ph].

[61] J. Jaeckel, V. V. Khoze, and M. Spannowsky, *Hearing the signal of dark sectors with gravitational wave detectors*, Phys. Rev. D **94** no. 10, (2016) 103519, arXiv:1602.03901 [hep-ph].

[62] P. Schwaller, *Gravitational Waves from a Dark Phase Transition*, Phys. Rev. Lett. **115** no. 18, (2015) 181101, arXiv:1504.07263 [hep-ph].

[63] M. Kakizaki, S. Kanemura, and T. Matsui, *Gravitational waves as a probe of extended scalar sectors with the first order electroweak phase transition*, Phys. Rev. D **92** no. 11, (2015) 115007, arXiv:1509.08394 [hep-ph].

[64] M. Chala, G. Nardini, and I. Sobolev, *Unified explanation for dark matter and electroweak baryogenesis with direct detection and gravitational wave signatures*, Phys. Rev. D **94** no. 5, (2016) 055006, arXiv:1605.08663 [hep-ph].

[65] V. Brdar, A. J. Helmboldt, and J. Kubo, *Gravitational Waves from First-Order Phase Transitions: LIGO as a Window to Unexplored Seesaw Scales*, JCAP **02** (2019) 021, arXiv:1810.12306 [hep-ph].

[66] A. J. Helmboldt, J. Kubo, and S. van der Woude, *Observational prospects for gravitational waves from hidden or dark chiral phase transitions*, Phys. Rev. D **100** no. 5, (2019) 055025, arXiv:1904.07891 [hep-ph].

[67] V. Brdar, L. Graf, A. J. Helmboldt, and X.-J. Xu, *Gravitational Waves as a Probe of Left-Right Symmetry Breaking*, JCAP **12** (2019) 027, arXiv:1909.02018 [hep-ph].

[68] A. Addazi, A. Marcianò, A. P. Morais, R. Pasechnik, R. Srivastava, and J. W. Valle, *Gravitational footprints of massive neutrinos and lepton number breaking*, Phys. Lett. B **807** (2020) 135577, arXiv:1909.09740 [hep-ph].

[69] B. Laurent, J. M. Cline, A. Friedlander, D.-M. He, K. Kainulainen, and D. Tucker-Smith, *Baryogenesis and gravity waves from a UV-completed electroweak phase transition*, arXiv:2102.12490 [hep-ph].

[70] A. D. Sakharov, *Violation of CP Invariance, C asymmetry, and baryon asymmetry of the universe*, Pisma Zh. Eksp. Teor. Fiz. **5** (1967) 32–35.

[71] D. E. Morrissey and M. J. Ramsey-Musolf, *Electroweak baryogenesis*, New J. Phys. **14** (2012) 125003, arXiv:1206.2942 [hep-ph].

[72] D. J. Weir, *Gravitational waves from a first order electroweak phase transition: a brief review*, Phil. Trans. Roy. Soc. Lond. A **376** no. 2114, (2018) 20170126, arXiv:1705.01783 [hep-ph].

[73] C. Schmid, D. J. Schwarz, and P. Widerin, *Peaks above the Harrison-Zel'dovich spectrum due to the quark - gluon to hadron transition*, Phys. Rev. Lett. **78** (1997) 791–794, arXiv:astro-ph/9606125.

[74] C. Schmid, D. J. Schwarz, and P. Widerin, *Amplification of cosmological inhomogeneities from the QCD transition*, Phys. Rev. D **59** (1999) 043517, arXiv:astro-ph/9807257.

[75] Schwarz, Dominik J., *Evolution of gravitational waves through cosmological transitions*, Mod. Phys. Lett. A **13** (1998) 2771–2778, arXiv:gr-qc/9709027.

[76] F. Giese, T. Konstandin, K. Schmitz, and J. Van De Vis, *Model-independent energy budget for LISA*, JCAP **01** (2021) 072, arXiv:2010.09744 [astro-ph.CO].

[77] I. Wasserman, *Late Phase Transitions and the Spontaneous Generation of Cosmological Density Perturbations*, Phys. Rev. Lett. **57** (1986) 2234–2236.

[78] G. Van Rossum and F. L. Drake Jr, *Python reference manual*. Centrum voor Wiskunde en Informatica Amsterdam, 1995.

[79] W. R. Inc., "Mathematica, Version 12.3.1." Https://www.wolfram.com/mathematica. Champaign, IL, 2021.

[80] Inkscape Project, "Inkscape." Https://inkscape.org.

[81] J. M. Bardeen, *Gauge-invariant cosmological perturbations*, Phys. Rev. D **22** (Oct, 1980) 1882–1905. https://link.aps.org/doi/10.1103/PhysRevD.22.1882.

[82] H. Kurki-Suonio, *Cosmological Perturbation Theory, part 1*, March, 2020. https://www.mv.helsinki.fi/home/hkurkisu/CosPer.pdf. Lecture notes for a course ofcosmological perturbation theory given at the university of Helsinki.

[83] C. Knobel, *An Introduction into the Theory of Cosmological Structure Formation*, arXiv e-prints (Aug., 2012) arXiv:1208.5931, arXiv:1208.5931 [astro-ph.CO].

[84] B. Ryden, *Introduction to cosmology*. Cambridge University Press, 2017.

[85] G. F. R. Ellis and H. van Elst, *Cosmological models: Cargese lectures 1998*, NATO Sci. Ser. C **541** (1999) 1–116, arXiv:gr-qc/9812046.

[86] C. G. Tsagas, A. Challinor, and R. Maartens, *Relativistic cosmology and large-scale structure*, Phys. Rept. **465** (2008) 61–147, arXiv:0705.4397 [astro-ph].

[87] S. Weinberg, *Cosmology*. 2008.

[88] P. J. E. Peebles, *The large-scale structure of the universe*. 1980.

[89] **SDSS** Collaboration, D. G. York *et al.*, *The Sloan Digital Sky Survey: Technical Summary*, Astron. J. **120** (2000) 1579–1587, arXiv:astro-ph/0006396.

[90] K. K. S. Wu, O. Lahav, and M. J. Rees, *The large-scale smoothness of the Universe*, Nature **397** (1999) 225–230, arXiv:astro-ph/9804062.

[91] D. W. Hogg, D. J. Eisenstein, M. R. Blanton, N. A. Bahcall, J. Brinkmann, J. E. Gunn, and D. P. Schneider, *Cosmic homogeneity demonstrated with luminous red galaxies*, Astrophys. J. **624** (2005) 54–58, arXiv:astro-ph/0411197.

[92] R. Durrer, *The Cosmic Microwave Background*. Cambridge University Press, Cambridge, 2008.

[93] S. M. Carroll, *Spacetime and Geometry*. Cambridge University Press, 7, 2019.

[94] A. Friedmann, *Über die Krümmung des Raumes*, Zeitschrift fur Physik **10** (Jan., 1922) 377–386.

[95] G. Lemaître, *Un Univers homogène de masse constante et de rayon croissant rendant compte de la vitesse radiale des n'ebuleuses extra-galactiques*, Annales de la Société Scientifique de Bruxelles **47** (Jan., 1927) 49–59.

[96] H. P. Robertson, *Kinematics and World-Structure*, Astrophysical Journal **82** (Nov., 1935) 284.

[97] A. G. Walker, *On Milne's Theory of World-Structure**, Proceedings of the London Mathematical Society **s2-42** no. 1, (1937) 90–127, https://londmathsoc.onlinelibrary.wiley.com/doi/pdf/10.1112/plms/s2-42.1.90. https://londmathsoc.onlinelibrary.wiley.com/doi/abs/10.1112/plms/s2-42.1.90.

[98] A. Einstein, *Zur Allgemeinen Relativitätstheorie*, Sitzungsber. Preuss. Akad. Wiss. Berlin (Math. Phys.) **1915** (1915) 778–786. [Addendum: Sitzungsber.Preuss.Akad.Wiss.Berlin (Math.Phys.) 1915, 799–801 (1915)].

[99] A. Einstein, *The Foundation of the General Theory of Relativity*, Annalen Phys. **49** no. 7, (1916) 769–822.

[100] E. W. Kolb and M. S. Turner, *The Early Universe*, vol. 69. 1990.

[101] A. Friedmann, *Über die Möglichkeit einer Welt mit konstanter negativer Krümmung des Raumes*, Zeitschrift fur Physik **21** no. 1, (Dec., 1924) 326–332.

[102] V. Mukhanov, *Physical Foundations of Cosmology*. Cambridge University Press, Oxford, 2005.

[103] E. Lifshitz, *Republication of: On the gravitational stability of the expanding universe*, J. Phys. (USSR) **10** no. 2, (1946) 116.

[104] G. F. R. Ellis and M. Bruni, *Covariant and gauge-invariant approach to cosmological density fluctuations*, Phys. Rev. D **40** (Sep, 1989) 1804–1818. https://link.aps.org/doi/10.1103/PhysRevD.40.1804.

[105] H. Kodama and M. Sasaki, *Cosmological Perturbation Theory*, Progress of Theoretical Physics Supplement **78** (Jan., 1984) 1.

[106] R. J. Adler, *The geometry of random fields*. SIAM, 2010.

[107] P. Watts and P. Coles, *Statistical cosmology with quadratic density fields*, Mon. Not. Roy. Astron. Soc. **338** (2003) 806, arXiv:astro-ph/0208295.

[108] J. M. Bardeen, J. R. Bond, N. Kaiser, and A. S. Szalay, *The Statistics of Peaks of Gaussian Random Fields*, Astrophys. J. **304** (1986) 15–61.

[109] **Planck** Collaboration, N. Aghanim *et al.*, *Planck 2018 results. VI. Cosmological parameters*, Astron. Astrophys. **641** (2020) A6, arXiv:1807.06209 [astro-ph.CO].

[110] "The nist reference on constants, units, and unvertainty." https://physics.nist.gov/cgi-bin/cuu/Value?sigmae. [Online; accessed 2-August-2021].

[111] P. J. E. Peebles and J. T. Yu, *Primeval adiabatic perturbation in an expanding universe*, Astrophys. J. **162** (1970) 815–836.

[112] E. Komatsu, "Some basics of the expansion of the universe,cosmic microwave background, and large-scale structure of the universe." https://wwwmpa.mpa-garching.mpg.de/~komatsu/cmb/lecture_cosmo_iucaa_2011.pdf, 2011. [Online; accessed 23-June-2021].

[113] D. J. Eisenstein and W. Hu, *Baryonic features in the matter transfer function*, Astrophys. J. **496** (1998) 605, arXiv:astro-ph/9709112.

[114] **BOSS** Collaboration, S. Alam *et al.*, *The clustering of galaxies in the completed SDSS-III Baryon Oscillation Spectroscopic Survey: cosmological analysis of the DR12 galaxy sample*, Mon. Not. Roy. Astron. Soc. **470** no. 3, (2017) 2617–2652, arXiv:1607.03155 [astro-ph.CO].

[115] J. Lesgourgues and S. Pastor, *Massive neutrinos and cosmology*, Phys. Rept. **429** (2006) 307–379, arXiv:astro-ph/0603494.

[116] S. Agarwal and H. A. Feldman, *The effect of massive neutrinos on the matter power spectrum*, Monthly Notices of the Royal Astronomical Society **410** no. 3, (Jan., 2011) 1647–1654, arXiv:1006.0689 [astro-ph.CO].

[117] S. Boersma and T. Dray, *Slicing, threading \& parametric manifolds*, Gen. Rel. Grav. **27** (1995) 319–339, arXiv:gr-qc/9407020.

[118] O. Heckmann and E. Schücking, *Bemerkungen zur Newtonschen Kosmologie. I. Mit 3 Textabbildungen in 8 Einzeldarstellungen*, Zeitschrift für Astrophysik **38** (Jan., 1955) 95.

[119] J. Ehlers, *Contributions to the relativistic mechanics of continuous media*, Abh. Akad. Wiss. Lit. Mainz. Nat. Kl. **11** (1961) 793–837.

[120] A. Raychaudhuri, *Relativistic and Newtonian Cosmology*, Zeitschrift für Astrophysik **43** (Jan., 1957) 161.

[121] S. W. Hawking, *Perturbations of an Expanding Universe*, APJ **145** (Aug., 1966) 544.

[122] E. Hubble, *A relation between distance and radial velocity among extra-galactic nebulae*, Proc. Nat. Acad. Sci. **15** (1929) 168–173.

[123] M. Bruni, P. K. Dunsby, and G. F. Ellis, *Cosmological perturbations and the physical meaning of gauge invariant variables*, Astrophys. J. **395** (1992) 34–53.

[124] J. M. Stewart and M. Walker, *Perturbations of space-times in general relativity*, Proc. R. Soc. Lond. **A 341** no. 49, (1974) .

[125] G. F. R. Ellis, J. Hwang, and M. Bruni, *Covariant and gauge-independent perfect-fluid Robertson-Walker perturbations*, Phys. Rev. D **40** (Sep, 1989) 1819–1826. https://link.aps.org/doi/10.1103/PhysRevD.40.1819.

[126] G. F. R. Ellis, M. Bruni, and J. Hwang, *Density-gradient-vorticity relation in perfect-fluid Robertson-Walker perturbations*, Phys. Rev. D **42** (Aug, 1990) 1035–1046. https://link.aps.org/doi/10.1103/PhysRevD.42.1035.

[127] P. K. S. Dunsby, M. Bruni, and G. F. R. Ellis, *Covariant Perturbations in a multifluid cosmological medium*, Astrophys. J. **395** (1992) 54–73.

[128] P. K. S. Dunsby, B. A. C. C. Bassett, and G. F. R. Ellis, *Covariant analysis of gravitational waves in a cosmological context*, Class. Quant. Grav. **14** (1997) 1215–1222, arXiv:gr-qc/9811092.

[129] R. Maartens, *Linearization instability of gravity waves?*, Phys. Rev. D **55** (1997) 463–467, arXiv:astro-ph/9609198.

[130] S. W. Hawking and G. F. R. Ellis, *The Large Scale Structure of Space-Time*. Cambridge Monographs on Mathematical Physics. Cambridge University Press, 1973.

[131] R. Maartens, T. Gebbie, and G. F. R. Ellis, *Cosmic microwave background anisotropies: Nonlinear dynamics*, Phys. Rev. D **59** (Mar, 1999) 083506. https://link.aps.org/doi/10.1103/PhysRevD.59.083506.

[132] A. Challinor, *Microwave background anisotropies from gravitational waves: the 1 + 3 covariant approach*, Classical and Quantum Gravity **17** no. 4, (Jan, 2000) 871–889. https://doi.org/10.1088%2F0264-9381%2F17%2F4%2F309.

[133] P. K. Dunsby, B. A. Bassett, and G. F. Ellis, *Covariant analysis of gravitational waves in a cosmological context*, Class. Quant. Grav. **14** (1997) 1215–1222, arXiv:gr-qc/9811092.

[134] B. Leong, P. Dunsby, A. Challinor, and A. Lasenby, *(1+3) covariant dynamics of scalar perturbations in brane worlds*, Phys. Rev. D **65** (2002) 104012, arXiv:gr-qc/0111033.

[135] D. Pazouli and C. G. Tsagas, *Gravitational-wave implications for structure formation: A second-order approach*, Phys. Rev. **D93** no. 6, (2016) 063520, arXiv:1512.02932 [gr-qc].

[136] S. W. Goode, *Analysis of spatially inhomogeneous perturbations of the FRW cosmologies*, Phys. Rev. D; (United States) . https://www.osti.gov/biblio/6141791.

[137] M. Laine and A. Vuorinen, *Basics of Thermal Field Theory*, vol. 925. Springer, 2016. arXiv:1701.01554 [hep-ph].

[138] A. Kosowsky, M. S. Turner, and R. Watkins, *Gravitational radiation from colliding vacuum bubbles*, Phys. Rev. D **45** (Jun, 1992) 4514–4535. https://link.aps.org/doi/10.1103/PhysRevD.45.4514.

[139] A. Kosowsky and M. S. Turner, *Gravitational radiation from colliding vacuum bubbles: Envelope approximation to many-bubble collisions*, Phys. Rev. D **47** (May, 1993) 4372–4391. https://link.aps.org/doi/10.1103/PhysRevD.47.4372.

[140] C. Caprini, R. Durrer, T. Konstandin, and G. Servant, *General Properties of the Gravitational Wave Spectrum from Phase Transitions*, Phys. Rev. D **79** (2009) 083519, arXiv:0901.1661 [astro-ph.CO].

[141] K. Binder, *Theory of first-order phase transitions*, Reports on Progress in Physics **50** no. 7, (Jul, 1987) 783–859. https://doi.org/10.1088/0034-4885/50/7/001.

[142] P. Ehrenfest, *Phasenumwandlungen im ueblichen und erweiterten Sinn, classifiziert nach dementsprechenden Singularitaeten des thermodynamischen Potentiales.*, Verhandlingen der Koninklijke Akademie van Wetenschappen(Amsterdam) **36** (1933) 153–157. https://www.dwc.knaw.nl/DL/publications/PU00016385.pdf. [Online; accessed 7-July-2021].

[143] E. Witten, *Cosmic separation of phases*, Phys. Rev. D **30** (Jul, 1984) 272–285. https://link.aps.org/doi/10.1103/PhysRevD.30.272.

[144] C. J. Hogan, *Gravitational radiation from cosmological phase transitions*, Monthly Notices of the Royal Astronomical Society **218** no. 4, (02, 1986) 629–636, https://academic.oup.com/mnras/article-pdf/218/4/629/3299141/mnras218-0629.pdf. https://doi.org/10.1093/mnras/218.4.629.

[145] M. Laine, *Thermal phase transitions in cosmology*, in *5th International Conference on Particle Physics and the Early Universe*. 11, 2001. arXiv:hep-ph/0111349.

[146] *Symmetry behavior in gauge theories*, Annals of Physics **101** no. 1, (1976) 195–238. https://www.sciencedirect.com/science/article/pii/0003491676902797.

[147] D. Kirzhnits and A. Linde, *Macroscopic consequences of the Weinberg model*, Physics Letters B **42** no. 4, (1972) 471–474. https://www.sciencedirect.com/science/article/pii/0370269372901098.

[148] S. Weinberg, *Gauge and global symmetries at high temperature*, Phys. Rev. D **9** (Jun, 1974) 3357–3378. https://link.aps.org/doi/10.1103/PhysRevD.9.3357.

[149] M. D'Onofrio and K. Rummukainen, *Standard model cross-over on the lattice*, Phys. Rev. D **93** no. 2, (2016) 025003, arXiv:1508.07161 [hep-ph].

[150] P. D. Group, P. A. Zyla, *et al.*, *Review of Particle Physics*, Progress of Theoretical and Experimental Physics **2020** no. 8, (08, 2020) , https://academic.oup.com/ptep/article-pdf/2020/8/083C01/34673722/ptaa104.pdf https://doi.org/10.1093/ptep/ptaa104. 083C01.

[151] K. Kajantie, M. Laine, K. Rummukainen, and M. E. Shaposhnikov, *The Electroweak phase transition: A Nonperturbative analysis*, Nucl. Phys. B **466** (1996) 189–258, arXiv:hep-lat/9510020.

[152] F. Csikor, Z. Fodor, and J. Heitger, *Endpoint of the hot electroweak phase transition*, Phys. Rev. Lett. **82** (1999) 21–24, arXiv:hep-ph/9809291.

[153] M. A. Stephanov, *QCD phase diagram: An Overview*, PoS **LAT2006** (2006) 024, arXiv:hep-lat/0701002.

[154] O. Kaczmarek, F. Karsch, A. Lahiri, L. Mazur, and C. Schmidt, *QCD phase transition in the chiral limit*, 3, 2020. arXiv:2003.07920 [hep-lat].

[155] K. Fukushima and T. Hatsuda, *The phase diagram of dense QCD*, Rept. Prog. Phys. **74** (2011) 014001, arXiv:1005.4814 [hep-ph].

[156] R. Apreda, M. Maggiore, A. Nicolis, and A. Riotto, *Gravitational waves from electroweak phase transitions*, Nucl. Phys. B **631** (2002) 342–368, arXiv:gr-qc/0107033.

[157] M. Maggiore, *Gravitational wave experiments and early universe cosmology*, Phys. Rept. **331** (2000) 283–367, arXiv:gr-qc/9909001.

[158] N. Christensen, *Stochastic Gravitational Wave Backgrounds*, Rept. Prog. Phys. **82** no. 1, (2019) 016903, arXiv:1811.08797 [gr-qc].

[159] C. Caprini *et al.*, *Science with the space-based interferometer eLISA. II: Gravitational waves from cosmological phase transitions*, JCAP **04** (2016) 001, arXiv:1512.06239 [astro-ph.CO].

[160] C. Caprini and D. G. Figueroa, *Cosmological Backgrounds of Gravitational Waves*, Class. Quant. Grav. **35** no. 16, (2018) 163001, arXiv:1801.04268 [astro-ph.CO].

[161] M. B. Hindmarsh, M. Lüben, J. Lumma, and M. Pauly, *Phase transitions in the early universe*, SciPost Phys. Lect. Notes **24** (2021) 1, arXiv:2008.09136 [astro-ph.CO].

[162] G. Ballesteros, J. Redondo, A. Ringwald, and C. Tamarit, *Standard Model-axion-seesaw-Higgs portal inflation. Five problems of particle physics and cosmology solved in one stroke*, JCAP **08** (2017) 001, arXiv:1610.01639 [hep-ph].

[163] S. Coleman and E. Weinberg, *Radiative Corrections as the Origin of Spontaneous Symmetry Breaking*, Phys. Rev. D **7** (Mar, 1973) 1888–1910. https://link.aps.org/doi/10.1103/PhysRevD.7.1888.

[164] L. Dolan and R. Jackiw, *Symmetry behavior at finite temperature*, Phys. Rev. D **9** (Jun, 1974) 3320–3341. https://link.aps.org/doi/10.1103/PhysRevD.9.3320.

[165] J. R. Espinosa, T. Konstandin, and F. Riva, *Strong Electroweak Phase Transitions in the Standard Model with a Singlet*, Nucl. Phys. B **854** (2012) 592–630, arXiv:1107.5441 [hep-ph].

[166] C. Delaunay, C. Grojean, and J. D. Wells, *Dynamics of Non-renormalizable Electroweak Symmetry Breaking*, JHEP **04** (2008) 029, arXiv:0711.2511 [hep-ph].

[167] M. E. Carrington, *Effective potential at finite temperature in the standard model*, Phys. Rev. D **45** (Apr, 1992) 2933–2944. https://link.aps.org/doi/10.1103/PhysRevD.45.2933.

[168] U. Kraemmer and A. Rebhan, *Advances in perturbative thermal field theory*, Rept. Prog. Phys. **67** (2004) 351, arXiv:hep-ph/0310337.

[169] D. Curtin, P. Meade, and H. Ramani, *Thermal Resummation and Phase Transitions*, Eur. Phys. J. C **78** no. 9, (2018) 787, arXiv:1612.00466 [hep-ph].

[170] J. S. Langer, *Statistical theory of the decay of metastable states*, Annals Phys. **54** (1969) 258–275.

[171] I. Y. Kobzarev, L. B. Okun, and M. B. Voloshin, *Bubbles in Metastable Vacuum*, Yad. Fiz. **20** (1974) 1229–1234.

[172] S. R. Coleman, *The Fate of the False Vacuum. 1. Semiclassical Theory*, Phys. Rev. **D15** (1977) 2929–2936. [Erratum: Phys. Rev.D16,1248(1977)].

[173] A. Linde, *Decay of the false vacuum at finite temperature*, Nuclear Physics B **216** no. 2, (1983) 421–445. https://www.sciencedirect.com/science/article/pii/0550321383902936.

[174] M. Dine, R. G. Leigh, P. Y. Huet, A. D. Linde, and D. A. Linde, *Towards the theory of the electroweak phase transition*, Phys. Rev. D **46** (1992) 550–571, arXiv:hep-ph/9203203.

[175] M. Quiros, *Finite temperature field theory and phase transitions*, in *ICTP Summer School in High-Energy Physics and Cosmology*. 1, 1999. arXiv:hep-ph/9901312.

[176] B. Imtiaz, Y.-F. Cai, and Y. Wan, *Two-field cosmological phase transitions and gravitational waves in the singlet Majoron model*, Eur. Phys. J. C **79** no. 1, (2019) 25, arXiv:1804.05835 [hep-ph].

[177] G. Kurup and M. Perelstein, *Dynamics of Electroweak Phase Transition In Singlet-Scalar Extension of the Standard Model*, Phys. Rev. D **96** no. 1, (2017) 015036, arXiv:1704.03381 [hep-ph].

[178] A. Linde, *On the vacuum instability and the Higgs meson mass*, Physics Letters B **70** no. 3, (1977) 306–308. https://www.sciencedirect.com/science/article/pii/0370269377906645.

[179] S. R. Coleman and F. De Luccia, *Gravitational Effects on and of Vacuum Decay*, Phys. Rev. **D21** (1980) 3305.

[180] M. Shaposhnikov, *Baryon asymmetry of the universe in standard electroweak theory*, Nuclear Physics B **287** (1987) 757–775. https://www.sciencedirect.com/science/article/pii/0550321387901271.

[181] V. Kuzmin, V. Rubakov, and M. Shaposhnikov, *On anomalous electroweak baryon-number non-conservation in the early universe*, Physics Letters B **155** no. 1, (1985) 36–42. https://www.sciencedirect.com/science/article/pii/0370269385910287.

[182] A. G. Cohen, D. B. Kaplan, and A. E. Nelson, *Progress in electroweak baryogenesis*, Ann. Rev. Nucl. Part. Sci. **43** (1993) 27–70, arXiv:hep-ph/9302210.

[183] V. A. Rubakov and M. E. Shaposhnikov, *Electroweak baryon number nonconservation in the early universe and in high-energy collisions*, Usp. Fiz. Nauk **166** (1996) 493–537, arXiv:hep-ph/9603208.

[184] A. Einstein, *Näherungsweise Integration der Feldgleichungen der Gravitation*, Sitzungsberichte der Königlich Preußischen Akademie der Wissenschaften (Berlin (Jan., 1916) 688–696.

[185] A. Einstein, *Über Gravitationswellen*, Sitzungsberichte der Königlich Preußischen Akademie der Wissenschaften (Berlin (Jan., 1918) 154–167.

[186] C. Caprini, R. Durrer, and G. Servant, *Gravitational wave generation from bubble collisions in first-order phase transitions: An analytic approach*, Phys. Rev. D **77** (2008) 124015, arXiv:0711.2593 [astro-ph].

[187] R. Jinno and M. Takimoto, *Gravitational waves from bubble collisions: An analytic derivation*, Phys. Rev. **D95** no. 2, (2017) 024009, arXiv:1605.01403 [astro-ph.CO].

[188] A. Kosowsky, A. Mack, and T. Kahniashvili, *Gravitational radiation from cosmological turbulence*, Phys. Rev. D **66** (2002) 024030, arXiv:astro-ph/0111483.

[189] A. D. Dolgov, D. Grasso, and A. Nicolis, *Relic backgrounds of gravitational waves from cosmic turbulence*, Phys. Rev. D **66** (2002) 103505, arXiv:astro-ph/0206461.

[190] M. Hindmarsh, S. J. Huber, K. Rummukainen, and D. J. Weir, *Gravitational waves from the sound of a first order phase transition*, Phys. Rev. Lett. **112** (2014) 041301, arXiv:1304.2433 [hep-ph].

[191] J. T. Giblin, Jr. and J. B. Mertens, *Vacuum Bubbles in the Presence of a Relativistic Fluid*, JHEP **12** (2013) 042, arXiv:1310.2948 [hep-th].

[192] M. Hindmarsh, S. J. Huber, K. Rummukainen, and D. J. Weir, *Numerical simulations of acoustically generated gravitational waves at a first order phase transition*, Phys. Rev. D **92** no. 12, (2015) 123009, arXiv:1504.03291 [astro-ph.CO].

[193] C. Caprini, R. Durrer, and G. Servant, *The stochastic gravitational wave background from turbulence and magnetic fields generated by a first-order phase transition*, JCAP **12** (2009) 024, arXiv:0909.0622 [astro-ph.CO].

[194] L. Kisslinger and T. Kahniashvili, *Polarized Gravitational Waves from Cosmological Phase Transitions*, Phys. Rev. D **92** no. 4, (2015) 043006, arXiv:1505.03680 [astro-ph.CO].

[195] D. Bodeker and G. D. Moore, *Can electroweak bubble walls run away?*, JCAP **05** (2009) 009, arXiv:0903.4099 [hep-ph].

[196] D. Cutting, M. Hindmarsh, and D. J. Weir, *Gravitational waves from vacuum first-order phase transitions: from the envelope to the lattice*, Phys. Rev. D **97** no. 12, (2018) 123513, arXiv:1802.05712 [astro-ph.CO].

[197] D. Cutting, M. Hindmarsh, and D. J. Weir, *Vorticity, kinetic energy, and suppressed gravitational wave production in strong first order phase transitions*, Phys. Rev. Lett. **125** no. 2, (2020) 021302, arXiv:1906.00480 [hep-ph].

[198] R. Jinno, T. Konstandin, and H. Rubira, *A hybrid simulation of gravitational wave production in first-order phase transitions*, 10, 2020.

[199] A. Kosowsky and M. S. Turner, *Gravitational radiation from colliding vacuum bubbles: envelope approximation to many bubble collisions*, Phys. Rev. D **47** (1993) 4372–4391, arXiv:astro-ph/9211004.

[200] M. Kamionkowski, A. Kosowsky, and M. S. Turner, *Gravitational radiation from first order phase transitions*, Phys. Rev. D **49** (1994) 2837–2851, arXiv:astro-ph/9310044.

[201] S. J. Huber and T. Konstandin, *Gravitational Wave Production by Collisions: More Bubbles*, JCAP **09** (2008) 022, arXiv:0806.1828 [hep-ph].

[202] A. Kosowsky, M. S. Turner, and R. Watkins, *Gravitational waves from first-order cosmological phase transitions*, Phys. Rev. Lett. **69** (Oct, 1992) 2026–2029. https://link.aps.org/doi/10.1103/PhysRevLett.69.2026.

[203] L. A. Boyle and P. J. Steinhardt, *Probing the early universe with inflationary gravitational waves*, Phys. Rev. D **77** (2008) 063504, arXiv:astro-ph/0512014.

[204] V. De Luca, G. Franciolini, A. Kehagias, and A. Riotto, *On the Gauge Invariance of Cosmological Gravitational Waves*, JCAP **03** (2020) 014, arXiv:1911.09689 [gr-qc].

[205] L. Pilo, A. Riotto, and A. Zaffaroni, *On the amount of gravitational waves from inflation*, Phys. Rev. Lett. **92** (2004) 201303, arXiv:astro-ph/0401302.

[206] G. Ellis, M. Bruni, and J. Hwang, *Density Gradient - Vorticity Relation in Perfect Fluid {Robertson-Walker} Perturbations*, Phys. Rev. D **42** (1990) 1035–1046.

[207] M. Bruni, S. Matarrese, S. Mollerach, and S. Sonego, *Perturbations of space-time: Gauge transformations and gauge invariance at second order and beyond*, Class. Quant. Grav. **14** (1997) 2585–2606, arXiv:gr-qc/9609040.

[208] K. Nakamura, *Second-order Gauge-invariant Cosmological Perturbation Theory: Current Status updated in 2019*, arXiv:1912.12805 [gr-qc].

[209] C. Caprini and R. Durrer, *Gravitational wave production: A Strong constraint on primordial magnetic fields*, Phys. Rev. D **65** (2001) 023517, arXiv:astro-ph/0106244.

[210] C. G. Tsagas, *Gravitational waves and cosmic magnetism: A Cosmological approach*, Class. Quant. Grav. **19** (2002) 3709–3722, arXiv:gr-qc/0202095.

[211] C. Uggla and J. Wainwright, *Dynamics of cosmological perturbations at first and second order*, Phys. Rev. D **98** no. 10, (2018) 103534, arXiv:1808.03200 [gr-qc].

[212] K. Nakamura, *Second-order Gauge-invariant Cosmological Perturbation Theory: Current Status updated in 2019*, arXiv:1912.12805 [gr-qc].

[213] R. Scoccimarro, M. Zaldarriaga, and L. Hui, *Power spectrum correlations induced by nonlinear clustering*, Astrophys. J. **527** (1999) 1, arXiv:astro-ph/9901099.

[214] I. Mohammed and U. Seljak, *Analytic model for the matter power spectrum, its covariance matrix, and baryonic effects*, Mon. Not. Roy. Astron. Soc. **445** no. 4, (2014) 3382–3400, arXiv:1407.0060 [astro-ph.CO].

[215] M. Laine and M. Meyer, *Standard Model thermodynamics across the electroweak crossover*, JCAP **07** (2015) 035, arXiv:1503.04935 [hep-ph].

[216] T. L. Smith, E. Pierpaoli, and M. Kamionkowski, *A new cosmic microwave background constraint to primordial gravitational waves*, Phys. Rev. Lett. **97** (2006) 021301, arXiv:astro-ph/0603144.

[217] I. Sendra and T. L. Smith, *Improved limits on short-wavelength gravitational waves from the cosmic microwave background*, Phys. Rev. D **85** (2012) 123002, arXiv:1203.4232 [astro-ph.CO].

[218] L. Pagano, L. Salvati, and A. Melchiorri, *New constraints on primordial gravitational waves from Planck 2015*, Phys. Lett. B **760** (2016) 823–825, arXiv:1508.02393 [astro-ph.CO].

[219] P. D. Lasky *et al.*, *Gravitational-wave cosmology across 29 decades in frequency*, Phys. Rev. X **6** no. 1, (2016) 011035, arXiv:1511.05994 [astro-ph.CO].

[220] S. Henrot-Versille *et al.*, *Improved constraint on the primordial gravitational-wave density using recent cosmological data and its impact on cosmic string models*, Class. Quant. Grav. **32** no. 4, (2015) 045003, arXiv:1408.5299 [astro-ph.CO].

[221] R. H. Cyburt, B. D. Fields, K. A. Olive, and E. Skillman, *New BBN limits on physics beyond the standard model from ^4He*, Astropart. Phys. **23** (2005) 313–323, arXiv:astro-ph/0408033.

[222] J. R. Primack and M. A. Sher, *PHOTON MASS AT LOW TEMPERATURE?*, Nature **288** (1980) 680–681.

[223] C. T. Hill, D. N. Schramm, and J. N. Fry, *Cosmological Structure Formation from Soft Topological Defects*, Comments Nucl. Part. Phys. **19** no. 1, (1989) 25–39.

[224] W. H. Press, B. S. Ryden, and D. N. Spergel, *Single Mechanism for Generating Large Scale Structure and Providing Dark Missing Matter*, Phys. Rev. Lett. **64** (1990) 1084.

[225] G. M. Fuller and D. N. Schramm, *Neutrino flypaper and the formation of structure in the universe*, Phys. Rev. D **45** (1992) 2595–2600.

[226] J. A. Frieman, C. T. Hill, and R. Watkins, *Late time cosmological phase transitions. 1. Particle physics models and cosmic evolution*, Phys. Rev. D **46** (1992) 1226–1238.

[227] E. W. Kolb and Y. Wang, *Domain wall formation in late time phase transitions*, Phys. Rev. D **45** (1992) 4421–4427.

[228] X.-c. Luo and D. N. Schramm, *The Phenomenological status of late time phase transition models after COBE*, Astrophys. J. **421** (1994) 393–399.

[229] S. Dutta, S. D. Hsu, D. Reeb, and R. J. Scherrer, *Dark radiation as a signature of dark energy*, Phys. Rev. D **79** (2009) 103504, arXiv:0902.4699 [astro-ph.CO].

[230] A. V. Patwardhan and G. M. Fuller, *Late-time vacuum phase transitions: Connecting sub-eV scale physics with cosmological structure formation*, Phys. Rev. D **90** no. 6, (2014) 063009, arXiv:1401.1923 [astro-ph.CO].

[231] S. J. Huber, T. Konstandin, G. Nardini, and I. Rues, *Detectable Gravitational Waves from Very Strong Phase Transitions in the General NMSSM*, JCAP **03** (2016) 036, arXiv:1512.06357 [hep-ph].

[232] C. Caprini *et al.*, *Detecting gravitational waves from cosmological phase transitions with LISA: an update*, JCAP **03** (2020) 024, arXiv:1910.13125 [astro-ph.CO].

[233] K. Hashino, R. Jinno, M. Kakizaki, S. Kanemura, T. Takahashi, and M. Takimoto, *Selecting models of first-order phase transitions using the synergy between collider and gravitational-wave experiments*, Phys. Rev. D **99** no. 7, (2019) 075011, arXiv:1809.04994 [hep-ph].

[234] L. Randall and G. Servant, *Gravitational waves from warped spacetime*, JHEP **05** (2007) 054, arXiv:hep-ph/0607158.

[235] B. Von Harling, A. Pomarol, O. Pujolàs, and F. Rompineve, *Peccei-Quinn Phase Transition at LIGO*, JHEP **04** (2020) 195, arXiv:1912.07587 [hep-ph].

[236] S. J. Huber and T. Konstandin, *Production of gravitational waves in the nMSSM*, JCAP **05** (2008) 017, arXiv:0709.2091 [hep-ph].

[237] R. A. C. Croft, D. H. Weinberg, M. Bolte, S. Burles, L. Hernquist, N. Katz, D. Kirkman, and D. Tytler, *Towards a precise measurement of matter clustering: Lyman alpha forest data at redshifts 2-4*, Astrophys. J. **581** (2002) 20–52, arXiv:astro-ph/0012324.

[238] N. Y. Gnedin and A. J. S. Hamilton, *Matter power spectrum from the Lyman-alpha forest: Myth or reality?*, Mon. Not. Roy. Astron. Soc. **334** (2002) 107–116, arXiv:astro-ph/0111194.

[239] A. Lewis and S. Bridle, *Cosmological parameters from CMB and other data: A Monte Carlo approach*, Phys. Rev. D **66** (2002) 103511, arXiv:astro-ph/0205436 [astro-ph].

[240] A. Lewis, *Efficient sampling of fast and slow cosmological parameters*, Phys. Rev. D **87** (2013) 103529, arXiv:1304.4473 [astro-ph.CO].

[241] A. Lewis, *GetDist: a Python package for analysing Monte Carlo samples*, arXiv:1910.13970 [astro-ph.IM]. https://getdist.readthedocs.io.

[242] K. Kojima, T. Kajino, and G. J. Mathews, *Generation of curvature perturbations with extra anisotropic stress*, JCAP **2010** no. 2, (Feb., 2010) 018, arXiv:0910.1976 [astro-ph.CO].

[243] M. J. Baker, M. Breitbach, J. Kopp, and L. Mittnacht, *Primordial Black Holes from First-Order Cosmological Phase Transitions*, arXiv:2105.07481 [astro-ph.CO].

[244] V. Domcke, R. Jinno, and H. Rubira, *Deformation of the gravitational wave spectrum by density perturbations*, JCAP **06** (2020) 046, arXiv:2002.11083 [astro-ph.CO].

[245] "Steven weinberg — Wikipedia, the free encyclopedia." https://de.wikipedia.org/wiki/Steven_Weinberg. [Online; accessed 22-August-2021].

[246] woit, "Steven weinberg 1933-2021." https://www.math.columbia.edu/~woit/wordpress/?p=12413, Jul, 2021. [Online; accessed 18-August-2021].

[247] O. F. Piattella, *Lecture Notes in Cosmology*. UNITEXT for Physics. Springer, Cham, 2018. arXiv:1803.00070 [astro-ph.CO].

Ich versichere, die Arbeit selbstständig angefertigt und dazu nur die im Literaturverzeichnis angegebenen Quellen benutzt zu haben.

Heidelberg, den 20ten September, 2021

Christian Döring